

UNIVERSIDADE FEDERAL DE SÃO CARLOS  
CENTRO DE CIÊNCIAS EXATAS E DE TECNOLOGIA  
DEPARTAMENTO DE QUÍMICA  
PROGRAMA DE PÓS-GRADUAÇÃO EM QUÍMICA

**“METAL SULFIDES: PHOTOLUMINESCENCE AND  
PHOTOCATALYTIC PROPERTIES”**

**Cristiane Wienke Raubach Ratmann\***

Tese apresentada como parte dos requisitos  
para obtenção do título de DOUTOR EM  
CIÊNCIAS, área de concentração: QUÍMICA.

**Orientador: Prof. Dr. Elson Longo**

**\* bolsista: FAPESP**

**São Carlos - SP**  
Agosto, 2013

**Ficha catalográfica elaborada pelo DePT da  
Biblioteca Comunitária/UFSCar**

R236ms

Ratmann, Cristiane Wienke Raubach.

Metal sulfides : photoluminescence and photocatalytic properties / Cristiane Wienke Raubach Ratmann. -- São Carlos : UFSCar, 2013.

73 f.

Tese (Doutorado) -- Universidade Federal de São Carlos, 2013.

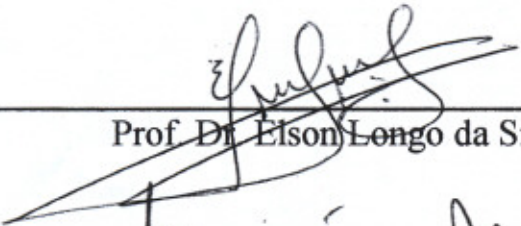
1. Fotocatálise. 2. Sulfetos. 3. Microondas. 4. Fotoluminescência. I. Título.

CDD: 541.395 (20<sup>a</sup>)

**UNIVERSIDADE FEDERAL DE SÃO CARLOS**  
*Centro de Ciências Exatas e de Tecnologia*  
*Departamento de Química*  
**PROGRAMA DE PÓS-GRADUAÇÃO EM QUÍMICA**  
**Curso de Doutorado**

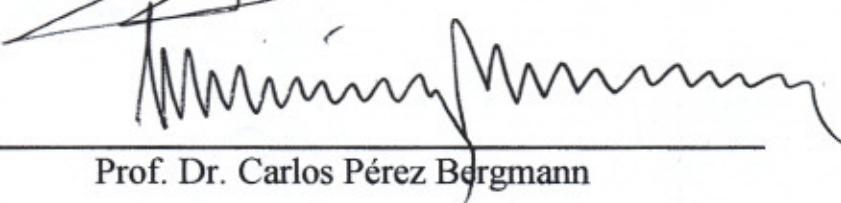
---

*Assinaturas dos membros da comissão examinadora que avaliou e aprovou a defesa de tese de doutorado da candidata **Cristiane Wienke Raubach Ratmann**, realizada em 30 de agosto de 2013:*



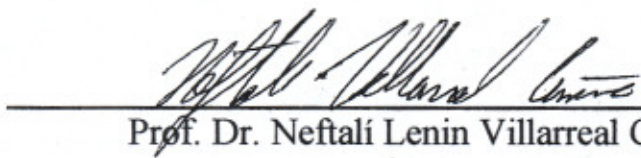
---

Prof. Dr. Elson Longo da Silva



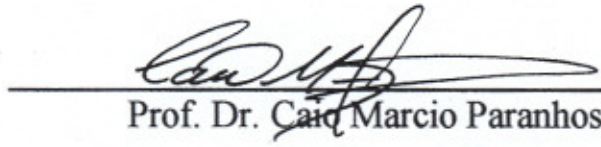
---

Prof. Dr. Carlos Pérez Bergmann



---

Prof. Dr. Neftalí Lenin Villarreal Carreño



---

Prof. Dr. Carlo Marcio Paranhos da Silva



---

Dra. Elaine Cristina Paris

## DEDICATION

Dedicado este trabalho aos meus pais, Edgar e Leda Raubach e ao meu marido Ezequiel Ratmann, os quais estiveram sempre ao meu lado me apoiando.

## ACKNOWLEDGEMENT

Agradeço em primeiro lugar a Deus, por ter me dado força em todos os momentos desta jornada, iluminando o meu caminho e dos meus familiares, nunca permitindo a interrupção deste projeto.

Agradeço ao professor Dr. Elson Longo, meu orientador, pelo tempo, dedicação, paciência, colaboração e esforços despendidos em prol da construção deste trabalho e conseqüentemente ao meu crescimento profissional.

A FAPESP (processo: 2010/19484-0) e, CNPq (processo: 149945/2010-8) pelas bolsas concedidas e a CAPES pelo apoio financeiro.

Aos colegas de jornada: Yuri, Mateus, Mário, Amanda, Rafaela, Tatiana, Leilane, Paula, Içamira, Elídia, Luiz, entre tantos outros. Em especial, aos meus colegas Yuri e Mateus, pela paciência e pelo companheirismo de sempre. Também quero agradecer a minha amiga e colega Rafaela que sempre esteve do meu lado e me apoiou em todos os momentos, bons e ruins, que é mais que uma colega de trabalho é uma amiga que levarei sempre no meu coração. Agradeço também aos meus amigos Mário e Priscila que me apoiaram desde o começo, me abrigaram e me auxiliaram em tudo que precisei. Sou grata a Dani, ao Ismael, ao Rori, a Madalena, ao Ricardo, a Luma, a Priscila, e ao Tiago pelo suporte técnico e administrativo durante todo este tempo de trabalho. Ao grupo de modelagem e simulação molecular, INCTMN da UNESP de Bauru, Prof. Dr. Júlio Sambrano e Prof. Dr. Priscila Buzolin.

Gostaria de deixar também meus agradecimentos aos membros da banca que aceitaram participar de minha avaliação e com isto contribuir para a finalização deste trabalho. Quero agradecer aos meus pais, Edgar e Leda Raubach, por terem me proporcionado essa oportunidade, porque sem eles nada disso seria possível. Agradeço ao meu marido, Ezequiel Ratmann, pelo amor, pela paciência e pelo companheirismo das horas boas e ruins. Sem o apoio dele, essa jornada não teria um final.

A todos aqueles que de alguma maneira contribuíram para a realização deste trabalho.

## LIST OF ABBREVIATIONS

ZnS – Zinc sulfide

CdS – Cadmium sulfide

PL – Photoluminescence

NPs – Nanoparticles

XRD – X-Ray Diffraction

TEM – Transmission Electron Microscopy

EG – Ethylene glycol

HRTEM – High resolution transmission electron microscopy

$E_{\text{gap}}$  – Optical band gap

$E_{\text{Fe}}$  – Electron Fermi level

$E_{\text{Fh}}$  – Hole Fermi level

CCCT – Cluster to cluster charge transfer

MAS – Microwave assisted solvothermal

RhB – Rhodamine B

JCPDS – Joint Committee on Powder Diffraction Standards

DOS – Density of states

VB – Valence band

VC – Conduction band

DFT – Density functional theory

TMAH – Tetramethylammonium hydroxide

FEG-SEM – Field emission scanning electron microscopy

CS – crystallite size

FWHM – Full width at half maximum

CaS – Calcium sulfide

AES – Alkaline earth sulfide

ICSD – Inorganic Crystal Structure Data

CIF – Crystallographic information file

TDOS – Total density of states

PDOS – Partial density of states

## LIST OF TABLES

### **Paper 1:**

**Table 1** – Experimental and theoretical band Gap energy and Fermi energy of ordered (o) and disordered (d) CdS and ZnS periodic models.

### **Paper 2:**

**Table 1** – Mulliken charge distribution ( $|e|$ ) for CdS<sub>o</sub> and ZnS<sub>d</sub> models

### **Paper 3:**

**TABLE I** – Comparison among synthesis methods.

### **Paper 4:**

**Table 1** – Lattice parameters, Unit cell volume, R values obtained by Rietveld Refinement Data for the CaS crystals.

**Table 2** – Calculated and experimental band gap values (eV) for CaS.



## LIST OF FIGURES

### Paper 1:

**Figure 1** – (a) TEM image of SAM03 (CdS@ZnS); (b) HRTEM image of region A; (c) HRTEM image of region B.

**Figure 2** – PL emission spectrum of ZnS, CdS and CdS@ZnS core-shell.

**Figure 3** – (a) Electronic models of CdS@ZnS core-shell interface before the photon arrival (b) illustration of model of CdS@ZnS core-shell.

### Paper 2:

**Fig. 1** – (a) XRD patterns of sulfide samples and (b) UV-Vis spectrum of the CdS pure, ZnS pure and CdS@ZnS decorated system synthesized at 453 K for 32 min in MAS.

**Fig. 2** – (a) Kinetics of photocatalytic degradation of RhB with the synthesized CdS, ZnS pure and CdS@ZnS decorated system and (b) mechanism of the photodegradation for the CdS@ZnS sample.

**Fig. 3** – Density of states (DOS) for CdS<sub>o</sub>.

**Fig. 4** – Density of states (DOS) for ZnS<sub>d</sub>.

**Fig. 5** – Projected spin density map of the CdS ordered and ZnS disordered.

**Fig. 6** – Mechanism models of the CdS@ZnS decorated system interface in the photodegradation process.

### Paper 3:

**FIG. 1** – The XRD patterns of ZnS powders processed in a microwave-solvothermal system at 413 K for different times; (a) capped ZnS, and (b) ZnS. The vertical dashed lines indicate the position and relative intensity of JCPDS card 36-1450.

**FIG. 2** – The FEG-SEM image of 1 min uncapped ZnS.

**FIG. 3** – The FEG-TEM images of 1 min capped ZnS. (a) The crystallites agglomerated, (b) crystallite with amorphous edges, (c) crystallites with cubic and hexagonal phases, (d) hexagonal phase FFT, and (e) cubic phase FFT.

**FIG. 4** – The UV-vis spectrum of ZnS powders; (a) capped ZnS and (b) Uncapped ZnS.

**FIG. 5** – The PL spectrum of ZnS powders at room temperature.

**FIG. 6** – Wide-band model, indicating the intermediary levels in the forbidden area.

**FIG. 7** – Band structures for (a) o-ZnS, and (b) d-ZnS.

**FIG. 8** – Total and p-DOS calculation on S atoms for (a) o-ZnS, and (b) d-ZnS models.

**FIG. 9** – Total and p-DOS calculation on Zn atoms for (a) and (b) o-ZnS and (c) and (d) d-ZnS models.

**Paper 4:**

**Figure 1** – Arrangement of calcium and sulfur atoms in the CaS structure.

**Figure 2** – XRD patterns of CaS crystals synthesized by MAS for different times. The vertical lines indicate the position and relative intensity of the ICSD card n° 41956 for the cubic CaS phase.

**Figure 3** – Rietveld refinement plot of CaS crystals prepared by MAS for (a) 4, (b) 8, (c) 16, (d) 32 and (e) 64 min.

**Figure 4** – P-DOS and T-DOS projected in: o-CaS (a), d-CaS: (b) (0.0 0.0 0.1), (c) (0.0 0.0 0.3) and (d) (0.0 0.0 0.5).

**Figure 5** – The FEG-SEM image of CaS synthesized MAS of the (a) 4 (b) 8 (c) 16 (d) 32 and (e) 64 min.

**Figure 6** – PL emission spectrum of CaS synthesized by MAS for different times.

**Figure 7** – (a) wide band model to illustrate the three steps of PL emissions and (b) theoretical model indicating the intermediary levels in the forbidden area.

**Figure 8** – Electron density maps for the CaS crystal with vertical plane in the [100] direction: o-CaS (a), d-CaS: (b) (0.0 0.0 0.1), (c) (0.0 0.0 0.3) and (d) (0.0 0.0 0.5).

**Figure 9** – Deconvoluted PL bands in three curves, centered in 443 nm, 490 nm and 550 nm, and their contributions.

## PAPERS

- × **Raubach, Cristiane W.** ; Krolow, Matheus Z.; Mesko, Marcia F.; Cava, Sergio; Moreira, Mario L.; Longo, Elson; Carreño., Neftalí L. V.. Interfacial photoluminescence emission properties of core/shell Al<sub>2</sub>O<sub>3</sub>/ZrO<sub>2</sub>. *CrystEngComm* (Cambridge. Online), v. 1, p. 1-5, (2012).
  
- × **Raubach, Cristiane W.** ; Buzolin, Prescila G.C.; de Santana, Yuri V.B.; Longo, Elson; Longo, Valéria M.; Varela, José A.; Avansi, Waldir; Ferrer, Mateus M.; Sambrano, Júlio R.. Structural and optical approach of CdS@ZnS core shell system. *Chemical Physics Letters* (Print), v. 536, p. 96-99, (2012).
  
- × Mateus M. Ferrer, Yuri V. B. de Santana, **Cristiane W. Raubach**, Julio R. Sambrano and Elson Longo. “Experimental and Theoretical Studies of Photoluminescence in ZnS Obtained by Microwave-Assisted Solvothermal Method”. *Current Physical Chemistry*, 2013, 3, 000-000.
  
- × **Cristiane W. Raubach**, Yuri V. B. De Santana, Mateus M. Ferrer, Prescila G. C. Buzolin, Júlio R. Sambrano and Elson Longo. “Photocatalytic activity of semiconductor sulfide heterostructures”. *Dalton Transactions*. DOI: 10.1039/C3DT50374G. (2013).
  
- × La Porta, Felipe A.; Ferrer, Mateus M.; De Santana, Yuri V.B.; **Raubach, Cristiane W.**; Longo, Valéria M.; Sambrano, Júlio R.; Longo, Elson; Andrés, Juan; Li, Máximo S.; Varela, José A. “Synthesis of wurtzite ZnS nanoparticles using the microwave assisted solvothermal method”. *Journal of Alloys and Componds*. 556, 153-159, (2013).
  
- × DELBRÜCKE, TIAGO; GOUVÊA, ROGÉRIO A.; MOREIRA, MÁRIO L.; **Raubach, Cristiane W.**; VARELA, JOSÉ A.; Longo, Elson; GONÇALVES, MARGARETE R. F.; CAVA, S.; CAVA, SERGIO. “Sintering of porous alumina obtained by biotemplate fibers for low thermal conductivity applications”. *Journal of the European Ceramic Society*, v. 33, p. 1087-1092, (2013).

- × Carreño, N. L. V.; OLIVEIRA, T. C. S.; PIVA, E.; LEAL, F. B.; LIMA, G. S.; MONCKS, M. D.; **Raubach, Cristiane W.**; OGLIARI, F. A.. “YbF<sub>3</sub>/SiO<sub>2</sub> Fillers as Radiopacifiers in a Dental Adhesive Resin”. *Nano-Micro Letters*, v.4, p. 189-196, (2012).
  
- × De Santana, Yuri V. B.; **Raubach, Cristiane W.**; Ferrer, Mateus M.; La Porta, Felipe; Sambrano, Julio R.; Longo, Valeria M.; Leite, Edson R.; Longo, Elson; Raubach, Cristiane W.. “Experimental and theoretical studies on the enhanced photoluminescence activity of zinc sulfide with a capping agent”. *Journal of Applied Physics*, v. 110, p. 123507, (2011).
  
- × La Porta, Felipe; Ferrer, Mateus M.; De Santana, Yuri V.B.; **Raubach, C. W.** ; Sambrano, Júlio R.; Longo, Valéria M.; Li, Máximo S.; Varela, José A.; Longo, Elson. “Towards an Understanding on the Role of Precursor in the Synthesis”. *Current Physical Chemistry*, (2013).
  
- × Capítulo de Livro: 1) M.Z. Krolow, C.A. Hartwig, G.C. Link, **C.W. Raubach**, J.S.F. Pereira, R.S. Picoloto, M.R.F. Gonçalves, N.L.V. Carreño, M.F. Mesko. “Synthesis and Characterisation of Carbon Nanocomposites”. *NanoCarbon 2011*. (2013), p. 33-47.

## RESUMO

“SULFETOS METÁLICOS: PROPRIEDADES FOTOLUMINESCENTES E FOTOCATALÍTICAS”. Neste trabalho relata-se um estudo teórico e experimental da atividade fotoluminescente (FL) e fotocatalítica de sulfetos metálicos puros e em sistemas decorados preparados por intermédio do método solvotérmico assistido por micro-ondas. O modelo teórico do sistema decorado foi criado de forma a analisar a transição eletrônica, principalmente nas suas interfaces. Os resultados mostram que a interface do sistema decorado (*core-shell*) produz uma transferência de carga do elétron do sulfeto de cádmio (CdS) para os buracos do sulfeto de zinco (ZnS), o que ajuda a aumentar a atividade fotoluminescente e fotocatalítica do sistema. Para os sistemas puros, observou-se a eficácia do método de síntese empregado, sendo verificado que o processo de obtenção do ZnS e sulfeto de cálcio (CaS) foi de extrema importância. Por intermédio dos modelos teóricos foi possível avaliar a influência causada pelo método. A variação nos parâmetros de síntese mostra uma influência direta nas propriedades FL dos sulfetos obtidos que pode ser atribuída a organização estrutural. O modelo teórico mostra como essa ordem e desordem do sistema podem afetar essas propriedades dos materiais obtidos.

## ABSTRACT

“METAL SULFIDES: PHOTOLUMINESCENCE AND PHOTOCATALYTIC PROPERTIES”. In this work we report an experimental and theoretical study of photoluminescence (PL) and photocatalytic activity of pure metal sulfides and systems furnished prepared by microwave assisted solvothermal (MAS) method. The theoretical model of the decorated system was created in order to analyze the electronic transition, especially in their interfaces. The results show that the system interface decorated (core-shell) produces an electron charge transfer of holes from cadmium sulfide (CdS) to zinc sulfide (ZnS), which helps increase the PL and photocatalytic activity of the system. For the pure systems, was observed the efficacy of the method synthesis employed verified that the process for obtaining the ZnS and calcium sulfide (CaS) was extremely important. Through the theoretical models was possible to evaluate the influence caused by the solvothermal influence caused by the MAS method. The variation in the synthesis parameters shows a direct influence on the PL properties of sulfides obtained which can be attributed to structural organization. The theoretical results how this order and disorder of the system can affect these properties of the obtained materials.

## SUMMARY

DEDICATION .....	ii
ACKNOWLEDGMENT .....	iii
LIST OF ABBREVIATIONS .....	iv
LIST OF TABLES .....	vi
LIST OF FIGURES.....	viii
PAPERS.....	ix
RESUMO.....	xii
ABSTRACT.....	xii
1. INTRODUCTION .....	1
2. PAPERS .....	8
2.1. PAPER 1 .....	8
Introduction.....	9
Methods .....	10
Results and discussion .....	11
Conclusions .....	17
Acknowledgements.....	17
References .....	17
2.2. PAPER 2.....	19
Introduction.....	20
Methods .....	21
Results and discussion .....	23
Conclusions .....	31
Acknowledgements .....	32
References .....	32
2.3. PAPER 3.....	34
INTRODUCTION .....	35
EXPERIMENT .....	36
RESULTS AND DISCUSSION .....	38
CONCLUSION.....	49
ACKNOWLEDGMENTS.....	49
REFERENCES .....	49

<b>2.4. PAPER 4</b> .....	<b>52</b>
<b>Introduction</b> .....	<b>53</b>
<b>Methods</b> .....	<b>54</b>
<b>Results and discussion</b> .....	<b>56</b>
<b>Conclusions</b> .....	<b>66</b>
<b>Acknowledgements</b> .....	<b>67</b>
<b>References</b> .....	<b>67</b>
<b>3. GENERAL CONCLUSIONS</b> .....	<b>70</b>
<b>4. REFERENCES</b> .....	<b>71</b>



# 1. INTRODUCTION

In recent decades, nanostructured materials have been the focus of attention of researchers. The synthesis, characterization and applications of nanoparticles are among the most important sections in nanotechnology. The transition from microparticles to nanoparticles can lead to significant changes in physical and chemical properties. Some of the important characteristics of these materials are: the small size of the particles, which leads to a atoms surface area of the nanoparticles (the increase in the surface area relative to volume) and as a result, the prevalence of quantum effects. This is mainly happen, due to the excess energy stored in the interfaces which are regions with high density of defects. This fact allows the preparation of a new range of materials with different properties. However, no technological application is possible if these factors are not well controlled in order to allow reproducibility [1-3].

In a quite comprehensively way the synthesis of these particles may be prepared according to a bottom-up approach (smallest to highest), which consists in producing nanoparticles from individual molecules or through the top-down procedure (highest to lowest), which consists in producing nano material from the coarse and fine scale. The top-down procedure has the main problem the surface imperfections in the structure and, beyond that, it is common to have a low particle size homogeneity. These imperfections can cause significant differences in the physical properties and the surface of the nanomaterial. But the bottom-up method is shown a route where there produce particles smaller than the top-down route [4-5].

Inside the class of materials, semiconductors are known to possess electrical properties which are intermediate between the electrical conductors and insulators. These materials allow the initiation of integrated circuits that revolutionized electronic devices like the computer industry. Semiconductors are known to have empty states adjacent to the valence band partially unavailable. The electrons, therefore, need to cross a gap separating the valence band to the conduction band to produce conduction. For this it is necessary to provide the electron energy difference between these two states is approximately equal to the energy spacing between the

bands [6]. The importance of these semiconductor materials is precisely by fact of their electrical conductivity can be changed by external stimuli such as magnetic field and electromagnetic field.

Among these materials, semiconductor nanostructures have attracted considerable interest over the last few years due to its properties are different materials micrometer. Among these properties, the modification of the gap's energy is the most interesting for semiconductors. Controlling this energy (through the shape, structural defects, etc.) can be observed different properties of the same material. These types of semiconductors have a large number of applications such as flat screen displays, optical sensors, electroluminescent devices, lasers and catalysts [7-8].

Zinc sulfide (ZnS) and cadmium sulfide (CdS) were among the oldest semiconductors studied. These present materials fundamental properties and remarkable versatility. The ZnS has always been widely used in photoluminescent, electroluminescent and catodoluminescent devices thanks to its better stability compared with other chalcogenides [9]. Member of the group semiconductor II-VI, the ZnS has two main forms, Cubic (also known as zinc blende, or sphalerite) and hexagonal phase (known as the less stable wurtzite and cubic). The transition from cubic to hexagonal phase occurs around 1017°C (bulk). The two phases exhibit an energy gap of 3.72 eV for the cubic phase and 3.77 eV for the hexagonal phase at 27°C in bulks [10-11]. In both cases the coordination sphere is equal to 4.

Through many work with different methods of synthesis of zinc sulfide nanocrystals, it can be found a wide variety of morphologies. These nanostructures have attracted much interest due to their fascinating properties correlated with these differences. Therefore, different methods can produce different ZnS particles, both in respect of their shape, size and density of defects which can cause large differences in material properties [10, 12-14].

Among the many synthesis methods ZnS, it is very common to use agents to control the size and shape of the particles, called leveling agents capped or size. These agents act in order to prevent agglomeration and coalescence between

primary particles so electrostatic or steric impediment. Electrostatic stabilization involves the creation of an electrical double layer due to ions adsorbed on the surface thus generating repulsion between particles of the same charge. Already steric hindrance is caused due to approximation by preventing the large particles adsorbed on the surface [13-14].

Sulfides from II family elements are considered excellent phosphorescent materials. According to the literature calcium sulfide has four crystalline phases. Three such phases assigned to the zinc blende phase and wurtzite phase (B1, B2, B3 - zinc blende) and (B4 - wurtzite) [15-17]. Luo et. al. [17] performed an experimental study on the structural and electronic properties of CaS. The authors analyzed the phase transformations of the compound diffraction measurements using X-ray energy dispersive. The results show the existence of more than one phase to CaS. The temperature CaS crystallized NaCl structure, however, under pressure up to 40 GPa, CaS undergoes a change in structure to the CsCl type phase [17]. Recently Chen and colleagues studied theoretically the electronic and structural properties of CaS considering the four phases of the compound. Their studies showed that single phase B2 of CaS has an indirect band gap, while the other stages have a direct band gap [15]. In two other studies, the authors performed experimental studies using optical absorption spectra indicated that the B1 phase as having with indirect band gap between 4.43 [18] eV and 4,52 eV [16]. The calcium sulfide exhibits luminescence in different wavelengths, ultraviolet and visible light. The calcium sulfide exhibits luminescence in different wavelengths, ultraviolet and visible light. The preparation of these sulfides requires some care. The calcium sulfide, for example, is unstable in water and require precautions during preparation [19]. The calcium sulfide is hard to be prepared in aqueous solutions due to their hydrolysis therefore the commercial calcium sulfide is prepared at high temperatures (~ 1200 ° C).

Several methods have been used to overcome the problem such as synthesis stream [19], solvothermal [20], alkoxides [21], sol-gel [22]. Recently Wu et al synthesized calcium sulfide doped with iron by means of co-precipitation method [23]. Adhikary et al synthesized CaS solid diffusion method, and verified the

thermoluminescent properties [24]. The sulfides formed by the members of the family of alkaline earth metal are known as semiconductor with high band gap (for example, CaS 3.4 to 4.4 eV [25], MgS 5,2 – 5,4 eV [26] and SrS 4,3 eV [27]).

Among the aforementioned methods for obtaining the calcium sulfide, solvothermal method has proven to be a very versatile method for the synthesis of nanomaterials. It is similar to hydrothermal method the only difference being the solvent used. For the hydrothermal system the solvent is water, while for the solvothermal system has the versatility to use different solvents (ethylene glycol, ethanol etc.). The reactions solvothermal have indicated advantages for the synthesis of crystals, for example, obtaining pure phase at low temperatures, in addition to precise control of several factors involved in the synthesis as cation concentrations, pH, temperature, heating rate and counter ions present in the reaction. Moreover, in most cases has relatively long time for obtaining the pure material. This disadvantage of slow kinetics of the reaction was resolved using microwaves as the heating source system.

Microwaves are electromagnetic waves comprising a range of wavelengths from 1mm to 1m. The most common operating range is 12 cm corresponding to 2.45 GHz frequency, used in household appliances. The use of new synthetic methods, and among these new methodologies, the microwave-assisted hydrothermal method (Microwave Assisted Hydrothermal or MAH) has been highlighted. In 1986 Fischer [28] employed the combination microwave and hydrothermal techniques to solubilize certain types of geological materials (minerals and rocks) for chemical analysis. Komaeneni et al [29] were pioneers in studies of the effect on crystallization kinetics using this method. These authors analyzed several parameters in hydrothermal reactions assisted by microwave (MAH) such as the concentration of chemical species, temperature and time of crystallization, which resulted in obtaining various oxides.

The effect of the microwave synthesis of materials is still controversial and not well understood. This is due to the fact that the phenomena involved are difficult to be clearly defined and explained. One of the primary aspects is the ability of the compound (solvent or reagent) to absorb the energy of microwave radiation

and convert it into heat. In general, this effect arises from the direct coupling of molecules of solvent with the electromagnetic field in the region of microwaves of 2.45 GHz. Therefore, microwave irradiation induces a rotation due to molecular dipole alignment of solvent (polar) with the external oscillating electric field [30-32].

The dielectric constant of the medium as well as the dielectric loss factor shows the efficiency of the interaction of microwaves and heat through. This is based on energy absorption per unit volume, Equation (1):

$$P = \sigma|E|^2 = 2\pi f \varepsilon_0 \varepsilon_{eff}'' |E|^2 = 2\pi f \varepsilon_0 \varepsilon_r' \tan \delta |E|^2 \quad 1.1$$

where E is the magnitude of the internal magnetic field,  $\varepsilon_{eff}''$  is the factor electric field relative,  $\varepsilon_0$  is the electric permittivity in vacuum, f is the microwave frequency,  $\sigma$  is the total effect of conductivity,  $\varepsilon_r'$  is the relative dielectric constant, and  $\tan \delta$  is the loss of power required to provide a given amount of energy. In this equation, the dielectric properties assume an important role in the degree of energy absorbed by the material. The majority of the microwave energy absorbed is converted into heat within the material as shown in Equation (2):

$$\frac{\Delta T}{\Delta t} = 2\pi f \varepsilon_0 \varepsilon_{eff}'' |E|^2 / \rho C_p \quad 1.2$$

where T is the temperature, t is the time,  $\rho$  is the density,  $C_p$  is the heat capacity. Note that there are no structural parameters (atomic, structural or otherwise) in this equation. Structural features that are assumed to charges in dielectric properties ( $\varepsilon_{eff}''$ ,  $\varepsilon_r'$  e  $\tan \delta$ ) [31-32].

Different from conventional thermal processing, where the energy is transferred to the material by convection, conduction and radiation to heat the surface of the material, the microwave energy is transmitted directly to the material through molecular interactions with the electromagnetic field. Thus, the energy transfer does not depend on diffusion of heat through the surface of the material being possible to achieve quick heating and even in thick materials.

As previously mentioned, nanostructured materials can exhibit various properties, for example, optical and catalytic properties. Optical phenomena able to

convert some types of energy in electromagnetic radiation always have been extensively studied. This type of phenomenon when has electromagnetic radiation emission in the visible region, is called "luminescence". This ability of materials in emit light arouses great interest worldwide. Furthermore, the luminescence is a great tool for the study of structural materials, it is directly related to their atomic structures and electronic states [33].

The luminescence is classified according to the type of excitation energy used. Some types of excitement possible generate chemiluminescence, cathodoluminescence, electroluminescence and photoluminescence. Chemiluminescence is produced when a chemical reaction provides an electronically excited species that emits light when it returns to the ground state, or transfers its energy to other species, which then produces emissions, the cathodoluminescence results from a beam of high energy electrons or Cathode ray, the electroluminescence is caused by a voltage applied to the luminescent substance, and the photoluminescence is characterized as photons visible or ultraviolet light is used for excitation [34].

The phenomenon "photoluminescence" includes fluorescence and phosphorescence. The fluorescence of phosphorescence differs in the fact that the electronic transitions responsible for the fluorescence energy do not involve a change in electron spin. As a result, the fluorescence decay time is short, ceasing almost immediately ( $<10^{-5}$ s). In contrast, a change in electron spin accompanying phosphorescent emissions making radiation which is able to last for a long easily time detected after the end of irradiation, often several seconds or more [34].

Photocatalytic materials use light energy to catalyze a chemical reaction. Photocatalytic applications include decomposition of water into hydrogen and oxygen and the complete oxidation of organic contaminants in aqueous environments. Most studies of photocatalysis using  $\text{TiO}_2$  as a photocatalyst synthetic or commercial. In recent years, many catalysts such as  $\text{TiO}_2$ ,  $\text{WO}_3$ ,  $\text{ZrO}_2$ ,  $\text{CdS}$ ,  $\text{ZnS}$  and other has been employed for the oxidation of environmental contaminants in water [35]. Composite materials have recently attracted much attention, especially in the coating structure on a nanometer scale, where the coating is simply the act of

decorating a material at the nanoscale, on the other hand. Studies of surfaces and interfaces are expanding the areas of scientific research and technological innovation. Accordingly, the development of new heterostructure is still a difficult subject. Continuous research suggest that semiconductor/semiconductor (heterostructures) nanocrystals have a significant impact on photocatalytic properties due to the elimination of surface defects nonradiative recombination [36-38]. There are studies with particles decorated with metallic sulfides which show improvements in their optical properties and photocatalytic [39-42].

Within this context in this paper it is reported a theoretical and experimental study of photoluminescence and photocatalytic activity of pure metal sulfides and systems furnished prepared by solvothermal method assisted by microwave. The theoretical model of the decorated system was created in order to analyze the electronic transition, especially in their interfaces.

## 2. PAPERS

### 2.1. PAPER 1 – Chemical Physics Letters



Contents lists available at [SciVerse ScienceDirect](http://SciVerse ScienceDirect) – Chemical Physics Letters  
journal homepage: [www.elsevier.com/locate/cplett](http://www.elsevier.com/locate/cplett)

### Structural and optical approach of CdS@ZnS core–shell system

Cristiane W. Raubach <sup>a,†</sup>, Yuri V.B. de Santana<sup>a</sup>, Mateus M. Ferrer<sup>a</sup>,  
Valéria M. Longo<sup>b</sup>, José A. Varela<sup>b</sup>, Waldir Avansi Jr.<sup>b</sup>, Prescila G.C.  
Buzolin<sup>c</sup>, Júlio R. Sambrano<sup>c</sup>, Elson Longo<sup>b</sup>

<sup>a</sup> INCTMN-UFSCar, Universidade Federal de São Carlos, P.O. Box 676, 13565-905 São Carlos, SP, Brazil

<sup>b</sup> INCTMN-UNESP, Universidade Estadual Paulista, P.O. Box 355, 14801-907 Araraquara, SP, Brazil

<sup>c</sup> INCTMN-UNESP, Universidade Estadual Paulista, P.O. Box 473, 17033-360 Bauru, SP, Brazil

† Corresponding author: E-mail address: [cristiane@liec.ufscar.br](mailto:cristiane@liec.ufscar.br) (C.W. Raubach).

#### article info

##### Article history:

Received 27

January 2012

In final form 22

March 2012

Available online 3

April 2012

#### abstract

An intense red-green photoluminescence (PL) emission was observed, at room temperature, in a CdS@ZnS core–shell system. The PL intensity emission of CdS@ZnS core–shell was strongly superior from that observed in individual CdS and ZnS nanoparticles. In this sense, we reported a comprehensive experimental and theoretical study of the optical behavior of CdS and ZnS nanoparticles (NPs), and CdS@ZnS core–shell system in the light the structural order–disorder conception. We also propose a model were the core and shell interface leads to favorable condition that triggers PL emission in CdS@ZnS core–shell.

2012 Elsevier B.V. All rights reserved.



## Introduction

Wurtzite, CdS and ZnS, are a direct band gap semiconductors with gap energy of 2.42 and 3.7 eV at 300 K, respectively. CdS and ZnS, were one of the first discovered semiconductors [1] and has promising applications in photochemical catalysis [2], gas sensor [3], and optical material [4,5]. The synthesis of CdS and ZnS NPs semiconductors has been the focus of recent scientific research due to their important nonlinear optical properties, luminescent properties, quantum size effect and other important physical and chemical properties [6,7]. These NPs bridge the gap between CdS and ZnS, there by offering the opportunity to study the evolution of interface properties [8,9]. Continuous researches suggest that semiconductor/semiconductor (called as heterostructures) nanocrystals confer a noticeable enhancement in the luminescence and conductive properties due to elimination of surface non-radiative recombination defects [5,10]. Therefore, the design and preparation of composite materials, such as CdSe/ZnS, CdSe/CdS, ZnO/ZnS and CdS/ZnS have been attracted much more research interests [1,5,11]. The study of surfaces and interfaces are expanding areas of scientific studies and technological innovations. In this sense, the development of new heterostructures is still a challenging subject [12]. In the case of this work, the modulation of the properties by tailoring the nucleation of one phase on the surface of other is a critical step. Studies in nanostructured materials indicate that the PL property is not only derived from the bulk structure but also controlled by the surface chemical bonds and optical transition in the surface/interface region [13–15]. Several studies performed by our group pointed out the effect of structural order–disorder in the modulation of the PL emission [16–18].

The surface modification of a wide band gap semiconducting shell around a narrow band gap core can alter the charge, functionality, and reactivity of the materials and consequently enhance the functional properties due to localization of the electron–hole pairs [1,19,20]. In this Letter, we report a comprehensive experimental and theoretical study of the PL emission of CdS or ZnS nanocrystals and CdS@ZnS core–shell system. Experimentally, the samples were characterized by X-ray Diffraction (XRD), UV–Vis spectra, Transmission Electron Microscopy (TEM)

and PL spectroscopy. Theoretically, first principle calculations were used in sense to investigate the interface between CdS and ZnS that renders the enhanced PL emission. In the light of these results a model of electronic charge and whole transference between the interfaces of CdS@ZnS system is proposed.

## Methods

CdS and ZnS samples (denoted as SAM01 and SAM02, respectively), were synthesized using microwave-assisted solvothermal method, at 453 K during 32 min as described previously [20]. CdS@ZnS (SAM03) core-shell was synthesized using 0.017 mol of CdS powders dispersed in 25 ml of Ethylene Glycol (EG) (solution 01). Separately 0.017 mol zinc ions and 0.03 mol of thiourea were dissolved in 75 ml of EG (solution 02). Then solutions 01 and 02 were mixture in a 120 ml Teflon autoclave and put in the microwave system during 32 min at 453 K. The resulting solution was washed with ethanol several times to neutralize the solution pH (7), and the precipitates were finally collected, and dried at 373 K (5 h). The powders obtained were characterized by XRD collected from  $10^\circ$  to  $70^\circ$  in the  $2\theta$  range using Cu Ka radiation (Rigaku-Max/2500PC) and TEM JEOL JEM 2100 microscopy, operating at 200 KV. UV-Vis spectra were taken using a spectrophotometer of Varian, model Cary 5G (USA) in diffuse reflection mode. PL spectra were collected with a Thermal Jarrel Ash Monospec monochromator and a Hamamatsu R446 Photomultiplier. The 350.7 nm (2.57 eV) exciting wavelength of a krypton ion laser (Coherent Innova) was used with the output of the laser kept at 200 mW. All measurements were taken at room temperature.

## Results and discussion

XRD patterns were collected for each sample to check the crystalline phase. The XRD (see Supporting Information – S.I.) patterns for the SAM01 could be indexed to CdS crystalline hexagonal in agreement with the respective JCPDS card 65-3414. For the SAM02, the crystalline phase of the as obtained powder could be indexed to ZnS crystalline hexagonal in agreement with the respective JCPDS card 32-1450 [21], The existence of a cubic ZnS phase from XRD patterns alone cannot be excluded due to the large similarity between cubic and hexagonal ZnS structures. Thus, these results indicate that ZnS powders processed in a microwave

solvothermal system are crystalline, pure and ordered at long range. Interest to note, that for the SAM03 the mainly peak diffractions observed was related to CdS crystalline phase. Wurtzite has space group P63mc, where each Zn or Cd atom is surrounded by four S atoms at the corners of tetrahedron. Periodic DFT calculations with the B3LYP hybrid functional [22], were performed using the CRYSTAL09 computer code [23]. The atomic centers have been described by an all electron basis set Zn\_86-411d31G [24], for Zn and S\_86-311G S [25]. For CdS, the atomic centers have been described by Gaussian basis sets of double zeta valence polarized (DZVP) [26]. It was modified to be used in CRYSTAL09 code (see S.I.).

As a first step, the optimization of the exponents for the outer- most sp and d shells was carried out to minimize the total energy of the structure at experimental parameters. The optimized external exponents are  $\alpha_{sp}(\text{Zn}) = 0.14349998$ ,  $\alpha_d(\text{Zn}) = 0.73000001$  and  $\alpha_{sp}(\text{S}) = 0.38000002$ . The Powel algorithm [27], method was used to perform all basis sets of the optimization procedure. From these optimized exponents, a new optimization procedure of lattice parameters a, c and  $u = (1/3)*(a/c)^2 + (1/4)$  was performed. The calculated and experimental values (given in parentheses) are  $a = 4.30$  (4.14) Å,  $c = 6.96$  (6.71) Å [28] and  $u = 0.377$  (0.376) for CdS and  $a = 3.84$  (3.85) Å,  $c = 6.26$  (6.29) Å and  $u = 0.379$  (0.375) for ZnS. Our results are in good agreement with other theoretical and experimental data [29].

Two periodic models were built from these optimized parameters to represent the ordered ZnS\_o or CdS\_o models and disordered ZnS\_d or CdS\_d models, displacing the Zn or Cd atom, 0.3 Å, in the z-direction, respectively. These models can be useful to represent different degrees of order–disorder in the material, as well as structural defects resulting from Zn to Cd displacements.

Figure 1 presents the TEM images of SAM03. In fact, an expanded image of regions A, in Figure 1a, shows that the SAM03 was formed by a polycrystalline core, Figure 1b. Analyzing an expanded view of region A, inset of Figure 1b, is possible to observe the presence of lattice parameter with about 0.32 nm. This distance is consistent with the (101) plane of the CdS structure, in good agreement with XRD patterns. Additionally, Figure 1c presents an expanded view of

region B in Figure 1a suggesting that the observed layer covering the polycrystalline core can be attributed to amorphous ZnS particles, since XRD for SAM03 presents only the CdS crystalline phase (see S.I.).

PL spectra recorded with a 350.7 nm excitation wavelength for the as obtained samples are shown in Figure 2. The PL spectrum of the SAM01 (CdS) shows a red maximum emission around 655 nm and a greenish maximum emission for SAM02 (ZnS) around 532 nm. The PL spectrum of for the SAM03 presents the maximum emission around 590 nm. The blue shift observed for the SAM03 compared to SAM01 could be explained for the possible presence of the ZnS disordered shell coated on the surface CdS core, as observed by XRD (see S.I.) and HRTEM images, Figure 1b and c. [30]. Another interesting effect in PL spectra is the enhancement in the emission for the SAM03, that can be associated with an inter-band connection between the interface of CdS core and ZnS disordered shell, where ZnS confines the photogenerated electron–hole pairs to the CdS core interface whose is modified by the quantum confinement effect, leading to the passivation of non-radiative transitions, thus enhancing the luminescence intensity [13,19,31]. Thus, the core–shell interface can be monitored directly by PL.

It is well known that the physical and chemical properties of materials are strongly correlated with some structural factors, mainly, the structural order (o) disorder (d) in the lattice. The materials can be described in terms of the packing of the constituent clusters of the atoms which can be considered the structural motifs. In a typical semiconductor, the intercluster (intermediary range) and intracluster (local range) interaction can occurs as a consequence of tree different sources: orientation, induction and dispersion interactions [32]. The orientation interaction results from the correlation between the rotation motion of the permanent moments in different [CdS<sub>4</sub>]<sub>o</sub>...[ZnS<sub>4</sub>]<sub>d</sub> clusters (intermediate range). The induction interaction occurs due to the polarization of [CdS<sub>4</sub>]<sub>o</sub> clusters by the permanent moment of another [ZnS<sub>4</sub>]<sub>d</sub> cluster (short range). The dispersion interaction arises from the motion correlation of electrons in neighboring of [CdS<sub>4</sub>]<sub>o</sub> and [ZnS<sub>4</sub>]<sub>d</sub> clusters (long range). Breaking symmetry process of these clusters, such as distortions, breathings and tilts, create a huge number of different structures and subsequently different materials

properties, and this phenomenon can be related to local (short), intermediate and long-range structural order–disorder [33].

Theoretical results point out that a breaking symmetry process in the structure of various semiconductor, associated to order–disorder effects, is a necessary condition for the presence of intermediate levels in the forbidden band gap [34]. These structural changes can be related to the charge polarization in different ranges that are, at least, manifestations of quantum confinement, when they occurs at short and intermediate range undependably of the particle size. The main point for quantum confinement occurs is the presences of discrete levels in the band gap, fact that are not possible with the crystal ore defect are periodic (dispersion interaction) [32].

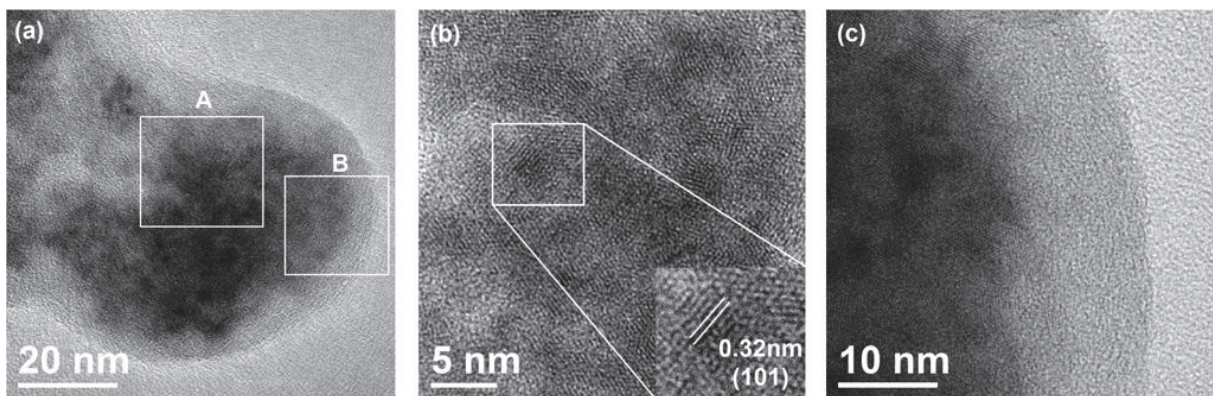


**Figure 1** – (a) TEM image of SAM03 (CdS@ZnS); (b) HRTEM image of region A; (c) HRTEM image of region B.

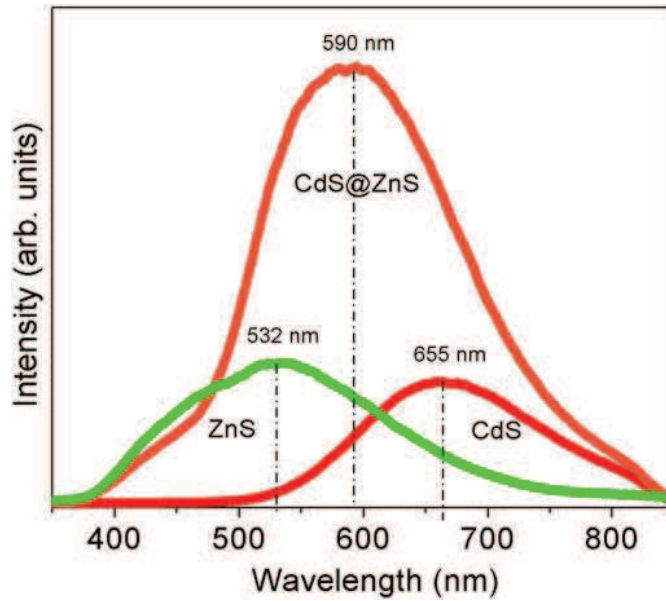


**Figure 2** – PL emission spectrum of ZnS, CdS and CdS@ZnS core-shell.

Table 1 depicts the experimental and theoretical calculated band gap and Fermi energy for the CdS and ZnS ordered and disordered models. The optical experimental band gap is related to the absorbance and the photon energy by the following Eq. (1):

$$h\nu\alpha \propto (h\nu - E_{gap})^{1/2} \quad (1)$$

where  $\alpha$  is the absorbance,  $h$  is the Planck constant,  $\nu$  is the frequency and  $E_{gap}$  is the optical band gap [35]. The band gap values of CdS, ZnS and CdS@ZnS were evaluated by extrapolating the linear portion of the curve ([Supplement material](#)). The entire sample presents a well defined inter-band transition with a quasi vertical absorption front which is typical of semiconductor crystalline materials. The CdS@ZnS core-shell system has two absorption regions, 2.4 and 3.8 eV, which are linked to CdS core and ZnS shell, respectively. The comparison with theoretical results shows a very good concordance between experimental and theoretical results.

Based on both experimental and theoretical findings, we propose a model where the driving force of this dynamic process is the order-disordered effects at intermediate range. In this way we are considering that the core and the shell are neutral and they have the same relevance in terms of electronic structure. This effect

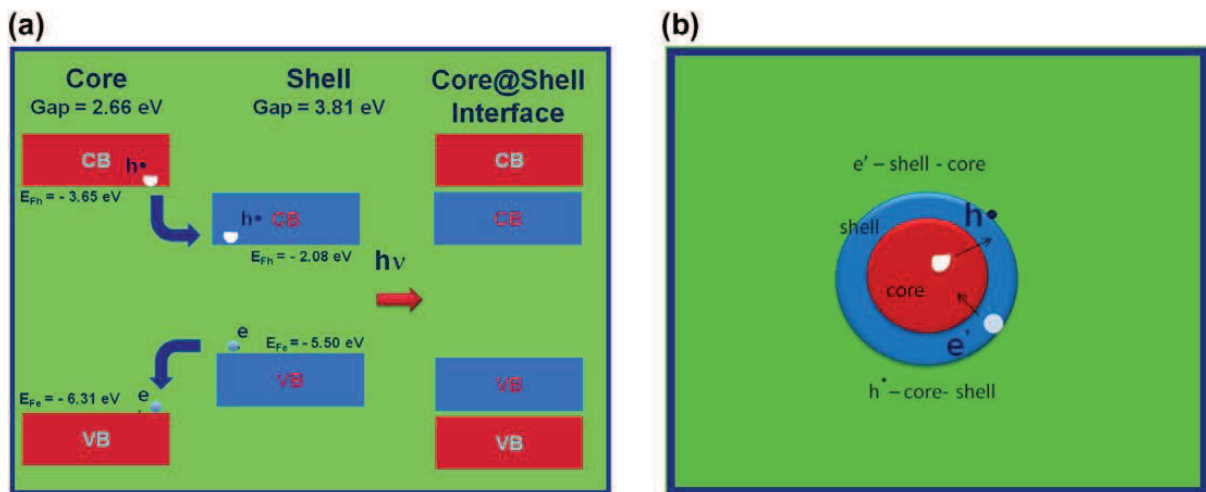
can only appear when the intermediate range order–disorder between interfaces, as in this case, core and shell are present.

Figure 3 illustrates an electronic model of CdS ordered core and ZnS disordered shell and CdS@ZnS core–shell interface before the photon arrival. The model is closely related to the alignment of energy levels of CdS ordered core and ZnS disordered shell. In a first step, electrons split from the electron shell Fermi level ( $E_{Fe}$ )<sub>S</sub> to the core electron Fermi level ( $E_{Fe}$ )<sub>C</sub> and holes split from the core-shell Fermi level ( $E_{Fh}$ )<sub>C</sub> to the hole shell Fermi level ( $E_{Fh}$ )<sub>S</sub>. These can also be termed dynamic Fermi levels and are a spontaneous process as the electronic core and shell structure has the electron and whole Fermi energy located at different Fermi energy but in the same Brillouin zone. The consequence of this dynamic process is the electron population of the valence band (VB) of CdS ordered core and holes migration to shell ZnS conduction band (CB). The final electronic configuration between CdS and ZnS interfaces is interconnected band structures where the core has more electrons and the shell more holes (see S.I.).

During the excitation process, there is a cluster to cluster charge transfer (CCCT) [32,33] of electrons from CdS electron populated clusters to ZnS holes populated clusters. The structural and electronic reconstruction of all the possible combinations of clusters in a crystal are essential for the understanding the CCCT process and at least the PL phenomenon.

**Table 1** – Experimental and Theoretical band Gap energy and Fermi energy of ordered (o) and disordered (d) CdS and ZnS periodic models.

	Theoretical				Experimental		
	CdS_o	CdS_d	ZnS_o	ZnS_d	CdS	ZnS	CdS@ZnS
Gap ( $\Gamma$ – $\Gamma$ ) (eV)	2.66	2.26	3.88	3.42	2.4	3.8	2.4 and 3.8
Fermi Energy (eV)	-6.31	-5.96	-5.84	-5.50			



**Figure 3** – (a) Electronic models of CdS@ZnS core-shell interface before the photon arrival (b) illustration of model of CdS@ZnS core-shell.

There exist such photo induced electron-transfer processes where an electron is promoted from an occupied level of the cluster donor to a vacant level of the cluster acceptor. The formation of isolated energy levels and the presence of  $[CdS_3.V^\bullet]$  or  $[ZnS_3.V^\bullet]$  disordered clusters leads to a substantial recombination between the photoexcited electron and hole during the excitation process. Probably, the ordered  $[ZnS_4]^x - [CdS_4]^x$  cluster activated during the excitation process changing their symmetry going to singlet or triplet excited states, as demonstrated by Gracia et al. [17,36] in perovskite and scheelite structures. In this way, similarly studies have to be done for wurtzite materials to confirm this fact.

## Conclusions

In summary, CdS@ZnS core-shell system was prepared by an efficient microwave-assisted solvothermal technique and their optical properties were carefully investigated. The XRD patterns and HRTEM images reveal a disordered ZnS layer in the shell and the polycrystalline CdS core. In the light of first principle calculations we propose a model where the unfused layers between core and shell interface renders the favorable condition that triggers PL emission in CdS@ZnS core-shell.

It is clear that controlling the particle size and morphology promotes modulation of advanced properties in heterostructured materials that can be used in future novel technologies. Such novel technologies can in principle explore



materials which are not available in the bulk single crystal form, but their figure of merit is dramatically dependent on the surface interface defect states. We believe that the strategy may also be applicable to other materials.

### Acknowledgements

The authors are thankful for the financial support of Brazilian research financing institutions: CAPES, CNPq and FAPESP. We also thank the Electron Microscopy Laboratory (LME) of the Brazilian National Synchrotron Light Laboratory (LNLS) for the use of its HRTEM microscopy facility.

### References

- [1] M.A. Malik, P. O'Brien, N. Revaprasadu, *Chem. Mater.* 14 (5) (2002) 2004.
- [2] P.V. Braun, P. Osenar, S.I. Stupp, *Nature* 380 (1996) 325.
- [3] V.L. Colvin, M.C. Schlamp, A.P. Alivisatos, *Nature* 370 (1994) 354.
- [4] W. Hoheisel, V.L. Colvin, C.S. Johnson, A.P. Alivisatos, *J. Chem. Phys.* 10 (1994) 8455.
- [5] J.S. Liu et al., *J. Alloy Compd.* 509 (2011) 9428.
- [6] A.V. Murugan, R.S. Sonawane, B.B. Kale, S.K. Apte, A.V. Kulkarni, *Mater. Chem. Phys.* 71 (2001) 98.
- [7] M.V. Limaye, S. Gokhale, S.A. Acharya, S.K. Kulkarni, *Nanotechnology* 19 (2008) 41.
- [8] L. Biadala, Y. Louyer, P. Tamarat, B. Lounis, *Phys. Rev. Lett.* 103 (2009). [9] S. Xu et al., *J. Phys. Chem. C* 115 (2011) 20876.
- [10] S.M. Liu, H.Q. Guo, Z.H. Zhang, R. Li, W. Chen, Z.G. Wang, *Physica E* 8 (2000) 174.
- [11] F. Li, Y. Jiang, L. Hu, L.Y. Liu, Z. Li, X.T. Huang, *J. Alloy Compd.* 474 (2009) 531. [12] D. Pergolesi et al., *Nat. Mater.* 9 (2010) 846.
- [13] L. Wang, H.W. Wei, Y.J. Fan, X.Z. Liu, J.H. Zhan, *Nanoscale Res. Lett.* 4 (2009) 558.
- [14] M.J.L. Santos, J. Ferreira, E. Radovanovic, R. Romano, O.L. Alves, E.M. Giroto, *Thin Solid Films* 517 (2009) 5523.
- [15] A. Ishizumi, Y. Kanemitsu, *Adv. Mater.* 18 (2006) 1083.
- [16] M.L. Moreira, J. Andres, V.M. Longo, M.S. Li, J.A. Varela, E. Longo, *Chem. Phys. Lett.* 473 (2009) 293.
- [17] L. Gracia et al., *J. Appl. Phys.* 110 (2011) 043501.
- [18] L.S. Cavalcante, M.F.C. Gurgel, A.Z. Simoes, E. Longo, J.A. Varela, M.R. Joya, P.S. Pizani, *Appl. Phys. Lett.* 90 (2007) 011901.
- [19] R.G. Xie, U. Kolb, J.X. Li, T. Basche, A. Mews, *J. Am. Chem. Soc.* 127 (2005) 7480.
- [20] J.F.A. Oliveira, T.M. Milao, V.D. Araujo, M.L. Moreira, E. Longo, M.I.B. Bernardi, *J. Alloy Compd.* 509 (2011) 6880.
- [21] E.H. Kisi, M.M. Elcombe, *Acta Crystallogr. C* 33 (1983) 1493. [22] C.T. Lee, W.T. Yang, R.G. Parr, *Phys. Rev. B* 37 (1988) 785.
- [23] R. Dovesi et al., *CRYSTAL09 User's Manual*, University of Torino, Torino, 2009.

- [24] J.E. Jaffe, A.C. Hess, Phys. Rev. B 48 (1993) 7903.
- [25] A. Lichanot, E. Apra, R. Dovesi, Phys. Status Solidi B 177 (1993) 157.
- [26] N. Godbout, D.R. Salahub, J. Andzelm, E. Wimmer, Can. J. Chem. 70 (1992) 560.
- [27] M.J.D. Powell, Siam Rev. 12 (1970) 79.
- [28] S. Wei, S.B. Zhang, Phys. Rev. B 62 (2000) 6944.
- [29] H.Z. Zhang, B. Gilbert, F. Huang, J.F. Banfield, Nature 424 (2003) 1025. [30] Y.J. Hsu, S.Y. Lu, Y.F. Lin, Adv. Func. Mater. 15 (2005) 1350.
- [31] S. Kalele, S.W. Gosavi, J. Urban, S.K. Kulkarni, Curr. Sci. 91 (2006) 1038.
- [32] L.S. Cavalcante et al., CrystEngComm 14 (2012) 853. [33] V.M. Longo et al., J. Phys. Chem. C 115 (2011) 5207.
- [34] E. Longo et al., Phys. Rev. B 69 (2004) 125115.
- [35] D.L. Wood, J. Tauc, Phys. Rev. B 5 (1972) 3144.
- [36] L. Gracia, J. Andres, V.M. Longo, J.A. Varela, E. Longo, Chem. Phys. Lett. 493 (2010) 141.

## 2.2. Artigo 2 – Dalton Transactions

DaltonTransactions

PAPER

### Photocatalytic activity of semiconductor sulfide heterostructures

Cristiane W. Raubach,<sup>\*a</sup> Yuri V. B. De Santana,<sup>a</sup>  
Mateus M. Ferrer,<sup>a</sup> Prescila G. C. Buzolin,<sup>b</sup> Júlio  
R. Sambrano<sup>b</sup> and Elson Longo<sup>c</sup>

Cite this: DOI:  
10.1039/c3dt50374g

<sup>a</sup> INCTMN-UFSCar, Universidade Federal de São Carlos, P.O. Box 676, 13565-905 São Carlos, SP, Brazil.

E-mail: [cristiane@liec.ufscar.br](mailto:cristiane@liec.ufscar.br)

<sup>b</sup> INCTMN-UNESP, Universidade Estadual Paulista, P.O. Box 473, 17033-360 Bauru, SP, Brazil.

<sup>c</sup> INCTMN-UNESP, Universidade Estadual Paulista, P.O. Box 355, 14801-907 Araraquara, SP, Brazil.

Received 6th  
February 2013,  
Accepted 29th May  
2013

DOI:  
10.1039/c3dt50374g  
[www.rsc.org/dalton](http://www.rsc.org/dalton)

This paper reports a theoretical and experimental study of the heterostructure photocatalytic activity in a CdS or ZnS and CdS@ZnS decorated system prepared by a microwave assisted solvothermal (MAS) method. A theoretical model of the decorated system was created in order to analyze the electronic transition mainly in their interface. The results show that CdS and ZnS interfaces produce an electron charge transfer from the CdS electron-populated clusters to the ZnS hole-populated clusters which helps to enhance the photocatalytic activity of the CdS@ZnS decorated system.

## Introduction

Photocatalytic materials use the photon energy of light to catalyze a chemical reaction. The applications of photocatalysts include the decomposition of water into hydrogen and oxygen and the complete oxidation of organic contaminant in aqueous environments. Advanced oxidation processes are of current interest for the effective oxidation of a wide variety of organics and dyes,<sup>1</sup> and semiconductor assisted photocatalytic degradation has high priority.<sup>1-3</sup> Most photocatalytic studies use either synthetic or commercial  $\text{TiO}_2$  as the photocatalyst.<sup>4-6</sup> Over the past few years, many catalysts such as  $\text{TiO}_2$ ,  $\text{ZnO}$ ,  $\text{WO}_3$ ,  $\text{SnO}_2$ ,  $\text{ZrO}_2$ ,  $\text{CeO}_2$ ,  $\text{CdS}$  and  $\text{ZnS}$  have been employed for photocatalytic oxidation of environmental water contaminants,<sup>1,3,5-9</sup> and recently metallic sulfides have attracted considerable interest due to their photocatalytic activity.<sup>8</sup>  $\text{ZnS}$  and  $\text{CdS}$  are wide band gap II-VI group semiconductor materials with a gap energy of 3.7 and 2.4 eV at 300 K, respectively.<sup>10</sup>  $\text{CdS}$  and  $\text{ZnS}$  are two of the initial semiconductors with promising applications in photochemical catalysis,<sup>11</sup> gas sensors<sup>12</sup> and optical materials.<sup>13-15</sup> Studies of surfaces and interfaces are expanding areas of scientific research and technological innovations. In this sense, the development of new heterostructures is still a challenging subject.<sup>16,17</sup> Research suggests that semiconductor/semiconductor (heterostructures) nanocrystals have a significant impact on photocatalytic, luminescence and conductive properties due to the elimination of surface non-radiative recombination defects.<sup>14,18,19</sup>

Theoretical calculations and computer simulations can complement experimental methods and have revealed new insights into medium-range order and dynamic changes in the local structure.<sup>20,21</sup> By these methods it is possible to obtain a better understanding of the relationship between the structural disorder in complex clusters with an intermediate-range interaction (interaction between two clusters) and the resulting electronic defects that are generated.<sup>22</sup>

In this paper we report a theoretical and experimental study of the photocatalytic activity of CdS or ZnS and CdS@ZnS decorated system prepared by the microwave-assisted solvothermal method. The origin of the photocatalytic activity was investigated by electronic structure calculations carried out within the framework of semi-empirical periodic quantum mechanical techniques and by comparing the measured degradation of Rhodamine B (RhB) under UV radiation. The results point out that CdS and ZnS interfaces produce an electron charge transfer from the CdS electron populated clusters to the ZnS hole populated clusters which helps to enhance the photocatalytic activity of the CdS@ZnS decorated system.

## Methods

### Synthesis of CdS@ZnS

The preparation of the CdS@ZnS decorated system was achieved via a two step solvothermal process. All reagents were of analytical grade and were used without further purification. The samples were synthesized using the MAS method as described previously.<sup>23,24</sup> Briefly the CdS@ZnS decorated system was synthesized using 0.017 mol of CdS powder dispersed in 25 mL of ethylene glycol (EG) (solution 1). Separately, 0.017 mol of zinc ions and 0.03 mol of thiourea were dissolved in 75 mL of EG (solution 2). Then solutions 1 and 2 were mixed in a 120 mL Teflon autoclave and put in a microwave system for 32 min at 453 K. The resulting solution was washed with ethanol several times to neutralize the solution pH ( $\approx 7$ ), and the precipitate was finally collected and dried at 373 K (5 h). Pure ZnS and pure CdS were also synthesized and used as the reference in the degradation test.

### Powder characterization

The powders obtained were characterized by XRD data from  $10^\circ$  to  $75^\circ$  in the  $2\theta$  range using Cu K $\alpha$  radiation (Rigaku-DMax/2500PC). UV-Vis spectra were taken using a Varian spectrophotometer (Model Cary 5G, USA) in the diffuse reflection mode. All measurements were taken at room temperature.

### Photocatalytic activity

The photocatalytic activity of samples for the oxidation of RhB dye with the molecular formula  $[C_{28}H_{31}ClN_2O_3]$  (99.5% purity, Mallinckrodt) in an aqueous solution was tested using UV-light illumination. 50 mg of catalyst crystals and 50 mL of an RhB solution ( $1 \times 10^{-4} \text{ mol L}^{-1}$ ) with  $\text{pH} = 4$  were placed in a 250 mL beaker. These suspensions were ultrasonicated for 10 min in a Branson (Model 1510) ultrasonic cleaner with a frequency of 42 kHz before illumination and were then stored in the dark for 10 min to facilitate saturated adsorption of RhB on the catalyst. Then the beaker was placed in a photoreactor at  $20^\circ\text{C}$  and illuminated by six UV lamps (TUV Philips) at 15 W with a maximum intensity at 254 nm. The power light was measured by a Coherent Power Max (Model N<sup>o</sup>. PM10); the optical energy density value was  $20 \text{ mW.cm}^{-2}$ . A 3 mL aliquot of these suspensions was removed and centrifuged at 30 min intervals at 9000 rpm for 5 min to remove suspended crystals. Finally, variations of the absorption band maximum of supernatant solutions were monitored by UV-Vis absorbance spectra measurements using a double-beam spectrophotometer with a double monochromator and a photomultiplier tube detector (JASCO, Model V-660, USA).

### Theoretical calculations

Periodic density function theory (DFT) calculations with the B3LYP hybrid functional<sup>25</sup> were taken using the CRYSTAL09 computer code.<sup>26</sup> Atomic centers have been described by an all electron basis set Zn\_86-411d31G<sup>27</sup> for Zn and S\_86-311G\*S.<sup>28</sup> For CdS, the atomic centers have been described by Gaussian basis sets of double zeta valence polarized (DZVP)<sup>29</sup> which were modified for use in the CRYSTAL09 code. As a first step, the optimization of the exponents for the outermost sp and d shells was carried out to minimize the total energy of the structure at experimental parameters. The optimized external exponents are  $\alpha_{\text{sp}}(\text{Zn}) = 0.14349998$ ,  $\alpha_{\text{d}}(\text{Zn}) = 0.73000001$  and  $\alpha_{\text{sp}}(\text{S}) = 0.38000002$ . The Powell algorithm<sup>30</sup> method was used to perform all basis sets of the optimization procedure. From these optimized exponents, a new optimization procedure of lattice parameters  $\mathbf{a}$ ,  $\mathbf{c}$  and  $\mathbf{u} = (1/3) \cdot (\mathbf{a}/\mathbf{c})^2 + (1/4)$  was

constructed. The calculated and experimental values (in parentheses) are  $a = 4.30$  (4.14) Å,  $c = 6.96$  (6.71) Å<sup>31</sup> and  $u = 0.377$  (0.376) for CdS and  $a = 3.84$  (3.85) Å,  $c = 6.26$  (6.29) Å and  $u = 0.379$  (0.375) for ZnS. Our results are in good agreement with other theoretical and experimental data.<sup>32</sup>

Two periodic models were built from these optimized parameters to represent the ordered ZnS<sub>o</sub> or CdS<sub>o</sub> models and disordered ZnS<sub>d</sub> or CdS<sub>d</sub> models, displacing the Zn or Cd atom, 0.3 Å, in the z-direction, respectively. These models can be useful in representing different degrees of order–disorder in the material as well as structural defects resulting from Zn to Cd displacements.

## Results and discussion

Fig. 1(a) illustrates XRD patterns and lattice parameter values of the ZnS, CdS and CdS@ZnS decorated system processed in a MAS system at 453 K for 32 min. The ZnS sample is crystalline with a hexagonal structure which is in agreement with the respective Joint Committee on Powder Diffraction Standards (JCPDS) card n°. 36-1450.<sup>33</sup> A cubic ZnS phase from XRD patterns alone cannot be excluded due to the large similarity between cubic and hexagonal ZnS structures.<sup>22</sup> CdS pure and CdS@ZnS samples can be indexed to the hexagonal structure with a space group of P63mc which is in agreement with the respective JCPDS card n°. 65-3414. Peaks related to the ZnS phase of the CdS@ZnS sample are not visible, but clearly there is a broadening of the peaks mainly in the (101) direction which verifies this phase.

The optical properties of the ZnS, CdS and CdS@ZnS decorated system were measured using UV-Vis absorption; UV-Vis absorption spectra of the samples are shown in Fig. 1(b). The optical experimental band gap is related to the absorbance and photon energy by equation (1):

$$hv\alpha \propto (hv - E_{gap})^{1/2} \quad (1)$$

where  $\alpha$  is the absorbance,  $h$  is Planck's constant,  $v$  is the frequency and  $E_{gap}$  is the optical band gap.<sup>34</sup> The band gap values of the CdS, ZnS and CdS@ZnS decorated system were evaluated by extrapolating the linear portion of the curve. The entire sample has a well defined interband transition with a quasi

vertical absorption front which is typical of semiconductor crystalline materials. For pure CdS and ZnS samples, the obtained band gaps were 2.5 and 3.8 eV, respectively. The CdS@ZnS decorated system has two absorption bands at 3.8 eV and at 2.4 eV which correspond to the ZnS and CdS phases, respectively. These results identify ZnS in the synthesized decorated system using the MAS method.

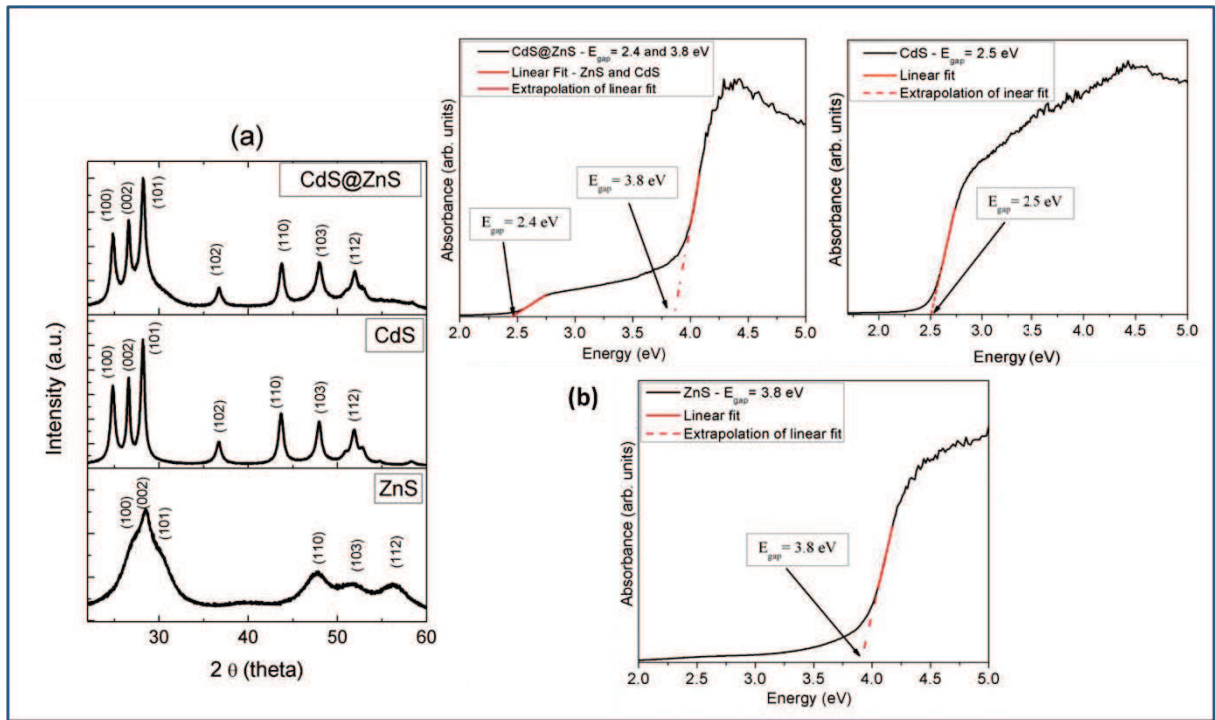


**FIG. 1** – (a) XRD patterns of sulfide samples and (b) UV-Vis spectrum of the CdS pure, ZnS pure and CdS@ZnS decorated system synthesized at 453 K for 32 min in MAS.



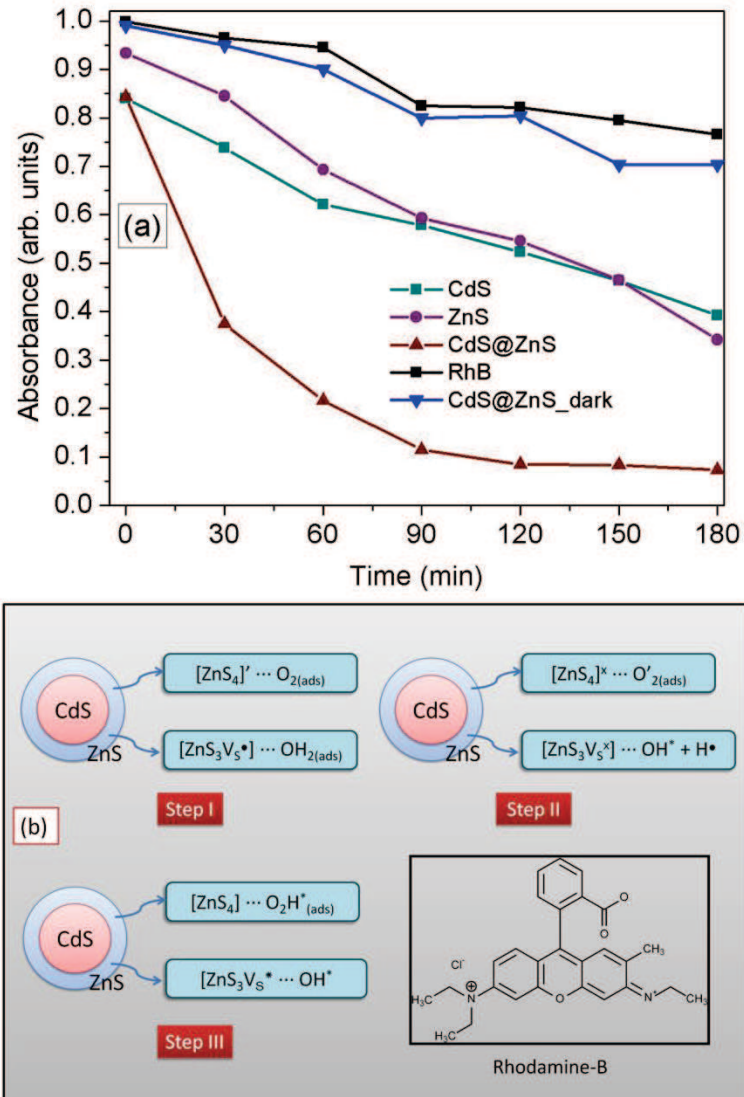


**FIG. 2** - (a) Kinetics of photocatalytic degradation of RhB with the synthesized CdS, ZnS pure and CdS@ZnS decorated system and (b) mechanism of the photodegradation for the CdS@ZnS sample.

Fig. 2(a) shows the RhB aqueous solution degradation rate by the ZnS, CdS and CdS@ZnS decorated system synthesized at 453 K for 32 min, which was obtained by monitoring UV-Vis absorbance spectra temporal changes in the aqueous dye solution. Blank experiments conducted in a RhB solution containing the dye and the sample verified the occurrence of negligible degradation of the dye upon UV photolysis. Experiments with the sample in the dark were also conducted. The photodegradation of RhB dye occurs due to an oxidative attack by one of the active oxygen species on the N-ethyl group.<sup>35</sup> Fig. 2(a) verifies the high efficiency of CdS@ZnS for the degradation of RhB dye in comparison with pure ZnS and pure CdS samples.

The Fig. 2(b) shows a possible mechanism for the photodegradation of the decorated system. The simplified mechanism consists of the formation of  $\text{OH}^*$  and  $\text{O}_2\text{H}^*$  radicals which react with the organic compound and promote their oxidation.

The physical and chemical properties of materials are strongly related to structural factors, mainly the structural order (o)–disorder (d) in the lattice. These materials can be identified in terms of the constituent cluster packing of the atoms as structural motifs. Effective charge separation requires an electric field (core) with the shell, and this interaction generates electron–hole ( $e^-$ – $h^+$ ) pairs which play a key role in the photocatalytic process.<sup>2,36</sup>

In a typical semiconductor, the intercluster (intermediary range) and intracluster (local range) interactions can occur as a consequence of three different sources: orientation, induction and dispersion interactions.<sup>2</sup> The orientation interaction results from the correlation between the rotation motion of the permanent moments in different  $[\text{CdS}_4]_o \dots [\text{ZnS}_3\text{V}_s]_d$  clusters (intermediate range). The induction interaction occurs due to the polarization of  $[\text{CdS}_4]_o$  clusters by the permanent moment of another  $[\text{ZnS}_3\text{V}^*]$  cluster (short range). The dispersion interaction arises from the motion correlation of electrons in neighboring  $[\text{CdS}_4]_o$  and  $[\text{ZnS}_3\text{V}^*]$  clusters (long range).<sup>37</sup> This phenomenon can be associated with an inter-band connection between the CdS core interface and the ZnS disordered shell where ZnS confines the photogenerated electron hole pairs to the CdS core interface. This interface is modified by the quantum confinement effect and results in the passivation of non-radiative transitions which thus enhance the photocatalytic process.<sup>19</sup>

Theoretical results show that a symmetry breaking process in the structure of various semiconductors associated with order–disorder effects is a necessary condition for intermediate levels in the forbidden gap.<sup>23,38</sup> These structural changes can be related to the charge polarization in different ranges that are (at the very least) manifestations of quantum confinement when they occur at short and intermediate ranges which are independent of the particle size. The main point of quantum confinement occurs at discrete levels in the band gap energy which is impossible when the crystal core

defect is periodic (a dispersion interaction).<sup>39</sup> Previous calculations showed that the band gaps for CdS<sub>o</sub> and ZnS<sub>d</sub> are in accordance with the experimental optically measured gaps of 2.4 eV and 3.8 eV, respectively.<sup>23</sup>

According to the proposed model, a decorated system with an organized CdS (CdS<sub>o</sub>) as the core and a disorganized ZnS (ZnS<sub>d</sub>) as the shell simulates the density of states (DOS) of both structures. For the CdS<sub>o</sub>, Fig. 3 shows the valence band (VB) derives from 3p<sub>x</sub>, 3p<sub>y</sub>, 3p<sub>z</sub> sulfur orbitals as well as a small contribution from transition-metal cadmium 5s, E<sub>g</sub> and T<sub>2g</sub> atomic orbitals. These orbitals are separated by a direct band gap from the conduction band (CB) which is composed of two different kinds of energy states: cadmium 5s atomic orbitals and 4p<sub>x</sub>, 4p<sub>y</sub>, 4p<sub>z</sub> cadmium orbitals. For the ZnS<sub>d</sub> (see Fig. 4), the VB is globally composed of S 3p<sub>x</sub>, 3p<sub>y</sub>, 3p<sub>z</sub> character states as well as a minor contribution from 4s orbitals of displaced zinc. The CB is composed of 4s zinc orbitals, 3p<sub>x</sub> and 3p<sub>y</sub> dislocated zinc orbitals and 3p<sub>z</sub> non-dislocated zinc orbitals in addition to a small contribution of 3p<sub>x</sub>, 3p<sub>y</sub>, 3p<sub>z</sub> sulfur orbitals.

Table 1 presents the Mulliken charges results of the simulation which verifies the interaction of structures.

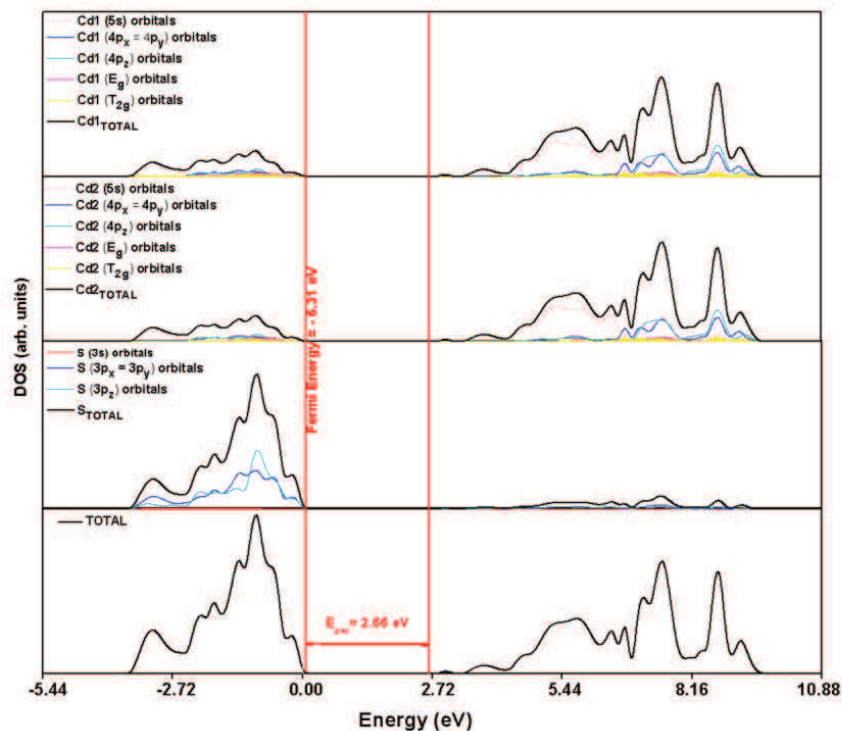


**FIG.3** – Density of states (DOS) for CdS<sub>o</sub>.

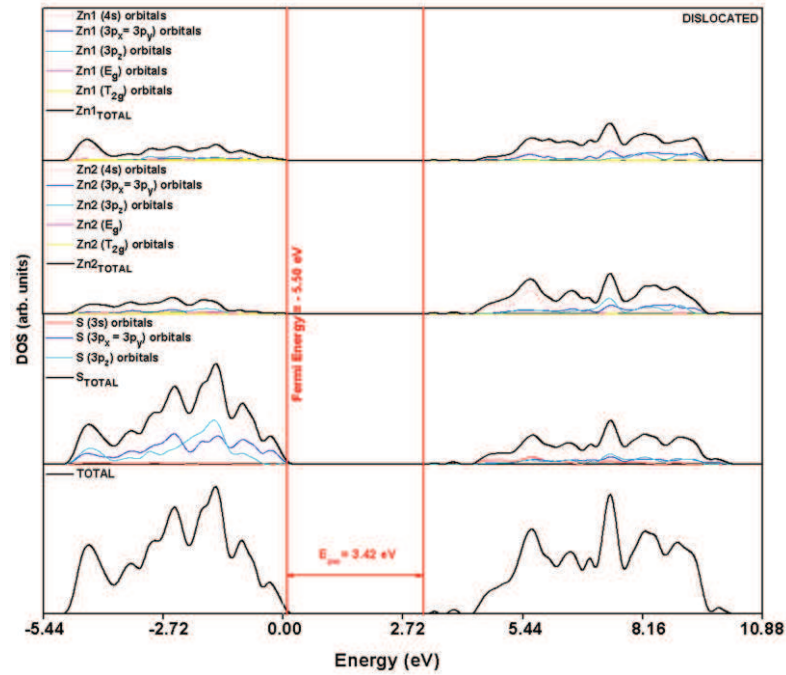


**FIG. 4** – Density of states (DOS) for ZnS\_d.

**Table 1** – Mulliken Charge Distribution ( $|e|$ ) for CdS\_o and ZnS\_d Models.<sup>a</sup>

	CdS_o	ZnS_d
Cd1	0.650	-
Cd2	0.650	-
Zn1	-	0.533
Zn2	-	0.531
S3	-0.650	-0.456
S4	-0.650	-0.608
[Cd1S <sub>4</sub> ]	-1.950	-
[Cd2S <sub>4</sub> ]	-1.950	-
[Zn1S <sub>4</sub> ]	-	-1.747
[Zn2S <sub>4</sub> ]	-	-1.445

<sup>a</sup> The charges for the clusters were calculated using the expressions: Charge for the clusters [Cd1S<sub>4</sub>] = Cd1 + S3 + 3.S4. Charge for the clusters [Cd2S<sub>4</sub>] = Cd2 + 3.S3 + S4. Charge for the clusters [Zn1S<sub>4</sub>] = Zn1 + S3 + 3.S4. Charge for the clusters [Zn2S<sub>4</sub>] = Zn2 + 3.S3 + S4.

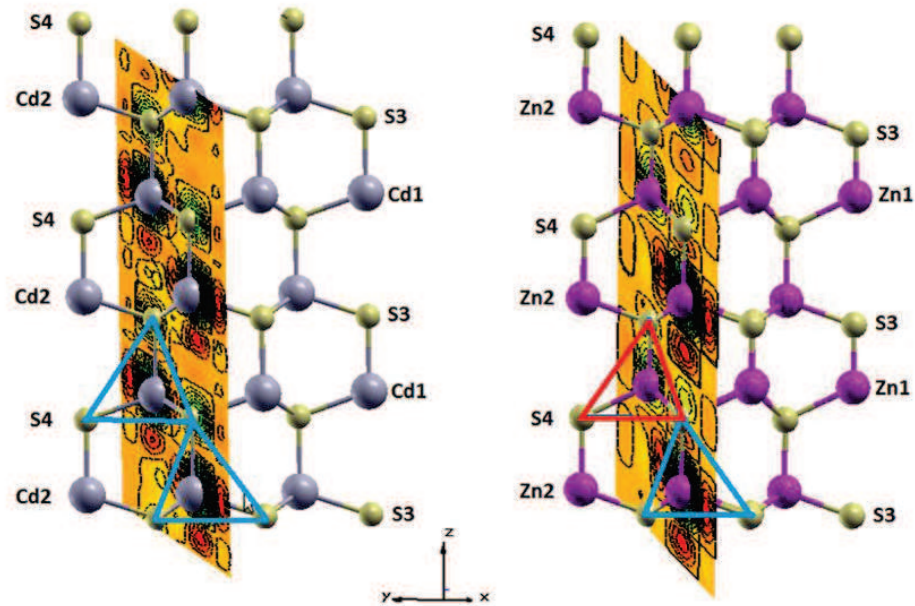


**FIG. 5** – Projected spin density map of the CdS ordered and ZnS disordered.

Regarding individual atom charges, it is impossible to find large differences in the electronic distribution; however, an analysis of the cluster charges for  $[\text{Cd1S}_4]$ ,  $[\text{Cd2S}_4]$ ,  $[\text{Zn1S}_4]$  and  $[\text{Zn2S}_4]$  reveals small changes. In general,  $[\text{Zn1S}_4]$  and  $[\text{Zn2S}_4]$  clusters have a lower charge in the ZnS<sub>d</sub> model.

With the displacement of the Zn1 atom, an alteration occurs in  $[\text{Zn1S}_4]$  and  $[\text{Zn2S}_4]$  cluster charges. Therefore, disordered structures have an asymmetry which results in a charge difference between these clusters and suggest a polarization which also may be apparent for the electron density map (see Fig. 5).

Based on both experimental and theoretical results, we propose a model where the driving force of this dynamic process is the ordered–disordered and quantum confinement effects at the intermediate range. Thus, the core and the shell are neutral and have the same relevance in terms of the electronic structure. However, the ordered and disordered core phase interface and shell generate an increase in the effect.

Fig. 6 illustrates an electronic model of the CdS ordered, the ZnS disordered and the CdS@ZnS decorated system interface before the  $\text{O}_2$  and  $\text{H}_2\text{O}$  interaction. The model is close to the energy level alignment of the ordered and disordered CdS. In the first step, electrons split from the  $[\text{ZnS}_4]'$  shell to the  $[\text{CdS}_4]^{1x}$  and holes split from the  $[\text{CdS}_3\text{V}_S^{\cdot}]$  to the  $[\text{ZnS}_3\text{V}_S^x]$ .

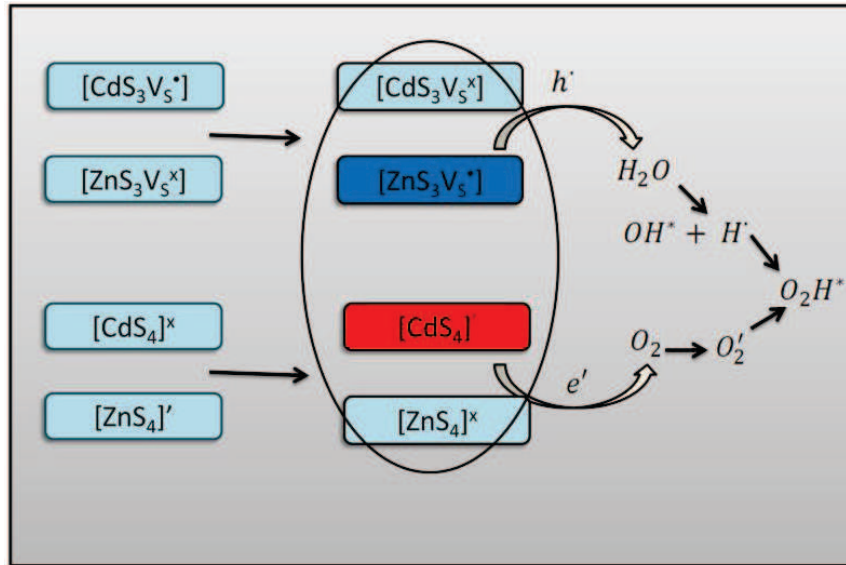
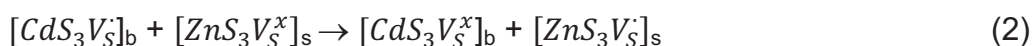


**FIG. 6** – Mechanism models of the CdS@ZnS decorated system interface in the photodegradation process.

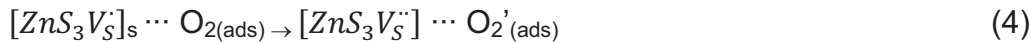
The consequence of this dynamic process is the electron population of the CdS ordered core VB and the hole migration to the ZnS disordered shell CB. The final electronic configuration between CdS and ZnS interfaces has an interconnected band structure where the core has more holes. The nature of the superoxide or hydroxyl radicals can be described using a complex cluster charge transfer (CCCT)<sup>2,37</sup> model where the electron or hole transfer from the surface to the adsorbed oxygen or water occurs.<sup>36,40,41</sup> During the photocatalytic process, a cluster-to-cluster charge transfer of electrons from the CdS electron-populated clusters to the ZnS hole-populated clusters occurs. The structural and electronic reconstruction of all possible combinations of clusters in a crystal is essential to understand the CCCT process and at least the photocatalytic phenomenon.

In fact, if they are not recombined,  $e^-h^+$  can be trapped as  $[ZnS_3V_5^*]$  or  $[ZnS_3V_5^{**}]$  defect sites of the CdS@ZnS with the oxidative species (e.g.,  $O_2$  or  $H_2O$ ). Due to their high oxidizing potential, these reactions generate  $OH^*$  or  $O_2H^*$  radicals which oxidize organic compounds until complete mineralization occurs. Consequently, the surface effect should be considered in terms of the following reactions:

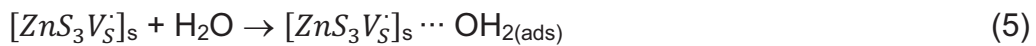


Where b= bulk and s= surface.

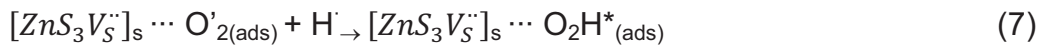
The molecular oxygen reactivity with n-type CdS@ZnS system results in the formation of a chemisorbed species and the subsequent oxygen incorporation into the decorated system:



The clusters formed by the complex interact with the water which separates into its hydroxyl radicals and hydrogen ion according to the following reactions:



The primary reaction (cathodic) is the formation of superoxide species  $[ZnS_3V_S^{\cdot\cdot}] \cdots O'_{2(ads)}$ . These species then react with hydrogen ion to produce the formation of hydrogen peroxide radicals ( $O_2H^*$ ), according the following reactions:



Studies of crystal samples confirm that structures of bulk and defective surfaces are well understood and reveal surfaces that contain large numbers of oxygen vacancies associated with higher optical properties. Most available experimental evidence from crystal studies suggests a higher activity associated with vacancy sites as compared with no vacancy sites (polarization). These reaction mechanisms involving oxygen and water adsorption, the formation of an active complex cluster, and its decomposition desorption of the final products and the electron-hole recombination process have an important role in photocatalytic effects [37, 43].

## Conclusions

In summary, the CdS@ZnS decorated system was prepared by an efficient MAS technique, and its photocatalytic properties were carefully investigated. The results indicate a considerable increase in the degradation rate in the decorated

system as compared with pure ZnS and CdS. We propose a model based on experimental and theoretical results to explain these alterations in their properties. CdS and ZnS interfaces produce an electron charge transfer from the CdS electron populated clusters to ZnS hole-populated clusters.

## ACKNOWLEDGMENT

The authors are thankful for the financial support of the Brazilian research financing institutions: CAPES, CNPq and FAPESP process n<sup>o</sup>: 2010/19484-0.

## References

1. K. Byrappa, A. K. Subramani, S. Ananda, K. M. L. Raj, R. Dinesh and M. Yoshimura, *Bulletin of Materials Science*, 2006, 29, 433-438.
2. L. S. Cavalcante, V. M. Longo, J. C. Sczancoski, M. A. P. Almeida, A. A. Batista, J. A. Varela, M. O. Orlandi, E. Longo and M. S. Li, *Crystengcomm*, 2012, 14, 853-868.
3. K. Maeda and K. Domen, *Journal of Physical Chemistry Letters*, 2010, 1, 2655-2661.
4. E. M. Saggioro, A. S. Oliveira, T. Pavesi, C. G. Maia, L. F. V. Ferreira and J. C. Moreira, *Molecules*, 2011, 16, 10370-10386.
5. J. Grzechulska and A. W. Morawski, *Applied Catalysis B: Environmental*, 2002, 36, 45-51.
6. V. R. de Mendonca and C. Ribeiro, *Applied Catalysis B-Environmental*, 2011, 105, 298-305.
7. H. Q. Wu, Y. Z. Yao, W. T. Li, L. L. Zhu, N. Ni and X. J. Zhang, *Journal of Nanoparticle Research*, 2011, 13, 2225-2234.
8. R. K. Upadhyay, M. Sharma, D. K. Singh, S. S. Amritphale and N. Chandra, *Separation and Purification Technology*, 2012, 88, 39-45.
9. B. Zielińska and A. W. Morawski, *Applied Catalysis B: Environmental*, 2005, 55, 221-226.
10. M. A. Malik, P. O'Brien and N. Revaprasadu, *Chemistry of Materials*, 2002, 14, 2004-2010.
11. P. V. Braun, P. Osenar and S. I. Stupp, *Nature*, 1996, 380, 325-328.
12. V. L. Colvin, M. C. Schlamp and A. P. Alivisatos, *Nature*, 1994, 370, 354-357.
13. W. Hoheisel, V. L. Colvin, C. S. Johnson and A. P. Alivisatos, *Journal of Chemical Physics*, 1994, 101, 8455-8460.
14. J. S. Liu, C. B. Zhao, Z. Q. Li, J. K. Chen, H. Z. Zhou, S. Q. Gu, Y. H. Zeng, Y. C. Li and Y. B. Huang, *Journal of Alloys and Compounds*, 2011, 509, 9428-9433.
15. F. A. La Porta, M. M. Ferrer, Y. V. B. de Santana, C. W. Raubach, V. M. Longo, J. R. Sambrano, E. Longo, J. Andres, M. S. Li and J. A. Varela, *Journal of Alloys and Compounds*, 2013, 556, 153-159.
16. D. Pergolesi, E. Fabbri, A. D'Epifanio, E. Di Bartolomeo, A. Tebano, S. Sanna, S. Licoccia, G. Balestrino and E. Traversa, *Nat. Mater.*, 2010, 9, 846-852.
17. C. W. Raubach, M. Z. Krolow, M. F. Mesko, S. Cava, M. L. Moreira, E. Longo and N. L. V. Carreno, *Crystengcomm*, 2012, 14, 393-396.
18. S. M. Liu, H. Q. Guo, Z. H. Zhang, R. Li, W. Chen and Z. G. Wang, *Physica E*, 2000, 8, 174-178.



19. L. Wang, H. W. Wei, Y. J. Fan, X. Z. Liu and J. H. Zhan, *Nanoscale Research Letters*, 2009, 4, 558-564.
20. E. Longo, E. Orhan, F. M. Pontes, C. D. Pinheiro, E. R. Leite, J. A. Varela, P. S. Pizani, T. M. Boschi, F. Lanciotti, A. Beltran and J. Andres, *Physical Review B*, 2004, 69.
21. V. M. Longo, L. S. Cavalcante, M. G. S. Costa, M. L. Moreira, A. T. de Figueiredo, J. Andres, J. A. Varela and E. Longo, *Theoretical Chemistry Accounts*, 2009, 124, 385-394.
22. Y. V. B. de Santana, C. W. Raubach, M. M. Ferrer, F. La Porta, J. R. Sambrano, V. M. Longo, E. R. Leite and E. Longo, *Journal of Applied Physics*, 2011, 110.
23. C. W. Raubach, Y. V. B. de Santana, M. M. Ferrer, V. M. Longo, J. A. Varela, W. Avansi, P. G. C. Buzolin, J. R. Sambrano and E. Longo, *Chemical Physics Letters*, 2012, 536, 96-99.
24. J. F. A. Oliveira, T. M. Milao, V. D. Araujo, M. L. Moreira, E. Longo and M. I. B. Bernardi, *Journal of Alloys and Compounds*, 2011, 509, 6880-6883.
25. C. Lee, W. Yang and R. G. Parr, *Physical Review B*, 1988, 37, 785-789.
26. R. S. Dovesi, V. R.; Roetti, C.; Orlando, R.; Zicovich-Wilson, C. M.; Pascale, F.; Civalieri, B.; Doll, K.; Harrison, N. M.; Bush, I. J.; D'Arco, P.; Llunell, M., University of Torino: Torino, 2009.
27. J. E. Jaffe and A. C. Hess, *Physical Review B*, 1993, 48, 7903-7909.
28. A. Lichanot, E. Aprà and R. Dovesi, *physica status solidi (b)*, 1993, 177, 157-163.
29. N. Godbout, D. R. Salahub, J. Andzelm and E. Wimmer, *Canadian Journal of Chemistry*, 1992, 70, 560-571.
30. M. J. D. Powell, *Siam Review*, 1970, 12, 79-86.
31. S.-H. Wei and S. B. Zhang, *Physical Review B*, 2000, 62, 6944-6947.
32. A. P. Finne, T. Araki, R. Blaauwgeers, V. B. Eltsov, N. B. Kopnin, M. Krusius, L. Skrbek, M. Tsubota and G. E. Volovik, *Nature*, 2003, 424, 1022-1025.
33. E. H Kisi and M. M. Elcombe, *Acta Crystallogr.*, 1983, 33C, 1493.
34. D. L. Wood and J. Tauc, *Physical Review B*, 1972, 5, 3144-&.
35. Y. Zhao, C. Z. Li, X. H. Liu and F. Gu, *J. Alloy. Compd.*, 2007, 440, 281-286.
36. R. Scotti, I. R. Bellobono, C. Canevali, C. Cannas, M. Catti, M. D'Arienzo, A. Musinu, S. Polizzi, M. Sommariva, A. Testino and F. Morazzoni, *Chemistry of Materials*, 2008, 20, 4051-4061.
37. V. M. Longo, L. S. Cavalcante, E. C. Paris, J. C. Sczancoski, P. S. Pizani, M. S. Li, J. Andres, E. Longo and J. A. Varela, *Journal of Physical Chemistry C*, 2011, 115, 5207-5219.
38. E. Longo, E. Orhan, F. M. Pontes, C. D. Pinheiro, E. R. Leite, J. A. Varela, P. S. Pizani, T. M. Boschi, F. Lanciotti, A. Beltran and J. Andres, *Phys. Rev. B*, 2004, 69, 125115.
39. L. S. Cavalcante, V. M. Longo, J. C. Sczancoski, M. A. P. Almeida, A. A. Batista, J. A. Varela, M. O. Orlandi, E. Longo and M. S. Li, *Crystengcomm*, 2011.
40. A. Testino, I. R. Bellobono, V. Buscaglia, C. Canevali, M. D'Arienzo, S. Polizzi, R. Scotti and F. Morazzoni, *Journal of the American Chemical Society*, 2007, 129, 3564-3575.
41. A. Sclafani and J. M. Herrmann, *Journal of Physical Chemistry*, 1996, 100, 13655-13661.
42. P. V. Kamat, *Journal of Physical Chemistry Letters*, 2012, 3, 663-672.

### 2.3. Paper 3 – Journal of applied physics



#### Experimental and theoretical studies on the enhanced photoluminescence activity of zinc sulfide with a capping agent

Yuri V. B. de Santana,<sup>1,a)</sup> Cristiane W. Raubach,<sup>1</sup> Mateus M. Ferrer,<sup>1</sup> Felipe La Porta,<sup>2</sup> Julio R. Sambrano,<sup>3</sup> Valéria M. Longo,<sup>2</sup> Edson R. Leite,<sup>1</sup> and Elson Longo<sup>2</sup>

<sup>1</sup>Universidade Federal de São Carlos, INCTMN, 13565-905, São Carlos, SP, Brazil

<sup>2</sup>São Paulo State University (UNESP), INCTMN, 14800-900, Araraquara, SP, Brazil

<sup>3</sup>Grupo de Modelagem e Simulação Molecular, INCTMN-UNESP, São Paulo State University, 17033-360, Bauru, SP, Brazil

(Received 13 September 2011; accepted 2 November 2011; published online 20 December 2011)

The photoluminescence (PL) emission from zinc sulfide (ZnS) synthesized by the microwave-assisted solvothermal method in the presence/absence of a capping agent was examined to understand the key role of its PL activity. In addition, we also investigated the electronic structure using a first-principle calculation based on density functional theory (DFT) applied to periodic models at B3LYP level. Two models were selected to simulate the effects of structural deformation on the electronic structure; the ordered o-ZnS model and the disordered d-ZnS model, dislocating the Zn atom, 0.1 Å, in the z-direction. The PL emission in the visible region showed different peak positions and intensities in capped and uncapped ZnS. The PL emission was linked to distinct distortions in lattices and the emission of two colors, green in the capped and blue in the uncapped, was also examined in the light of favorable structural and electronic conditions. The computational simulations indicate that the electronic behavior can be associated with the new electronic levels above the valence band.

© 2011 American Institute of Physics. [doi:10.1063/1.3666070]

## INTRODUCTION

Semiconductor nanostructures are a class of material that have been extensively investigated due to their significance in fundamental research and their high potential for technological applications.<sup>1</sup> Compound semiconductors such as ZnS, CdS, PbS, ZnSe, etc., are important materials for a variety of applications, and their versatility for their chemical tuning of composition and structure. Zinc sulfide (ZnS) is an important II-VI semiconductor material with a wide band gap (3.72 eV for the cubic zinc blende phase, and 3.77 eV for the wurtzite phase at 300 K in bulk materials).<sup>2</sup>

It has a wide range of applications for flat-panel displays, optical sensors, IR windows, catalysts, lasers, etc.<sup>3–5</sup> Shape and structure are crucial factors in determining the chemical, optical, and electrical properties of these materials.<sup>6,7</sup> Thus, one of the most important goals of modern materials research is the development of simple chemical methods for large scale synthesis of nanomaterials with full control of defects and morphology and, in this context, a considerable variety of methods has been reported for the synthesis of ZnS nanocrystals.<sup>8–14</sup> Some of these methods employ the use of capping agents for the passivation of these nanocrystals or to activate desired morphologies.<sup>15–17</sup> Several reports in the literature describe the conditions required for PL.<sup>18–21</sup> In this paper, we present a comparative study of an intense and broad PL at room temperature for ZnS nanocrystals synthesized by an efficient microwave-assisted solvothermal method,<sup>22–24</sup> for different times to clarify the roles capping agents play in the enhanced PL activity of ZnS. The origin of the intense PL bands was investigated by electronic structure calculations carried out within the framework of *ab initio* periodic quantum-mechanical techniques. Evolutions of order–disorder in the network former, Zn, and the different colors of PL emission, are also discussed in light of the complex cluster concept.

## EXPERIMENT

ZnS powders were synthesized by the efficient microwave assisted solvothermal method for different times. The typical procedure is described as follows: 3.67 mmol of anhydrous  $\text{ZnCl}_2$  was dissolved in 25 ml of ethylene glycol (EG), and subsequently 22.3 mmol of tetramethylammonium hydroxide (TMAH) was added (solution 1); 3.67 mmol of thiourea was separately dissolved into another 25 mL of EG (solution 2). Under vigorous magnetic stirring, solution 2 was then quickly injected into solution 1. The same procedure previously described was conducted without the use of TMAH. In this sequence, the solution was transferred into a Teflon autoclave, which was sealed and placed inside a domestic microwave-solvothermal system (2.45 GHz, maximum power of 800 W). The microwave-solvothermal processing was performed at 413 K for different times (1, 2, and 4 min). The resulting solution was washed with deionized water and ethanol several times to neutralize the solution pH ( $\cong 7$ ), and the precipitates were finally collected and dried at 333 K (24 h).

The powders obtained were characterized by X-ray diffraction (XRD) collected from  $10^\circ$  to  $110^\circ$  in the  $2\theta$  range using  $\text{Cu } K\alpha$  radiation (Rigaku-DMax/2500PC). Morphological characterizations were performed by field emission scanning electron microscopy (FEG-SEM) (Supra 35-VP, Carl Zeiss), and transmission electron microscopy (TEM) (Tecnai G2TF20, FEI). Ultraviolet–visible (UV–vis) spectroscopy for the optical reflectance spectra of ZnS powders was taken using Cary 5 G equipment. The PL spectra were collected with a Thermal Jarrell-Ash Monospec monochromator and a Hamamatsu R446 photomultiplier. The 350.7 nm (2.57 eV) exciting wavelength of a krypton ion laser (Coherent Innova) was used with the output of the laser kept at 200 mW. This excitation wavelength was chosen because it is on the order of the calculated band gap of the material and also to minimize the radioactive transitions near the conduction band. All measurements were taken at room temperature.

## THEORETICAL STUDIES

The thermodynamically stable phase wurtzite (under normal conditions) was studied. It belongs to the space group P6<sub>3</sub>mc, and each Zn atom is surrounded by four S atoms at the corners of the tetrahedron. Periodic DFT calculations with the B3LYP hybrid functional,<sup>25</sup> were performed using the CRYSTAL06 computer code,<sup>26</sup> which has been successfully employed for studies of the electronic and structural properties of diverse compounds.<sup>27–30</sup> The atomic centers have been described by an all electron basis set, Zn\_86-411d31 G,<sup>31</sup> for Zn and S\_86-311 G\* S,<sup>32</sup> atoms.

As a first step, the optimization of the exponents for the outermost sp and d shells was carried out to minimize the total energy of the structure at experimental parameters. The optimized external exponents are  $\alpha_{sp}(\text{Zn}) = 0.14349998$ ,  $\alpha_d(\text{Zn}) = 0.73000001$  and  $\alpha_{sp}(\text{S}) = 0.38000002$ . The Powel algorithm<sup>33</sup> method was used to perform all basis sets of the optimization procedure. From these optimized exponents, a new optimization procedure of lattice parameters **a**, **c**, and **u** was performed. The calculated and experimental values (given in parentheses) are **a** = 3.83 (3.84)Å, **c** = 6.26 (6.29)Å, and **u** = 0.379 (0.375). Our results are in good agreement with other theoretical and experimental data.<sup>34</sup>

Two periodic models were built from these optimized parameters to represent the ordered o-ZnS model and the disordered d-ZnS model, displacing the Zn atom, 0.1 Å, in the z-direction. These models can be useful to represent different degrees of order-disorder in the material, along with the structural defects resulting from Zn displacements. Band structures were obtained for 80 *K* points along appropriate high-symmetry paths of the adequate Brillouin zone. Diagrams of the density of states (DOS) were calculated for an analysis of the corresponding electronic structure. The XcrysDen program<sup>35</sup> was used for the design of a band structure diagram. It should be noted that our models are not meant to represent the exact reality of disordered structures but to offer a simple scheme serving to shed light on the effects of structural deformation on the network former and on the electronic structure without completely suppressing the geometry of the cell, which is useful for periodic calculations.

## RESULTS AND DISCUSSION

In Fig. 1, XRD patterns revealed that all diffraction peaks of ZnS powders can be indexed to the hexagonal structure in agreement with the respective JCPDS card 67–453.<sup>36</sup> The diffraction peaks are significantly broadened because of the very small crystallite size that is more evident in samples where TMAH is used (Fig. 1(b)).

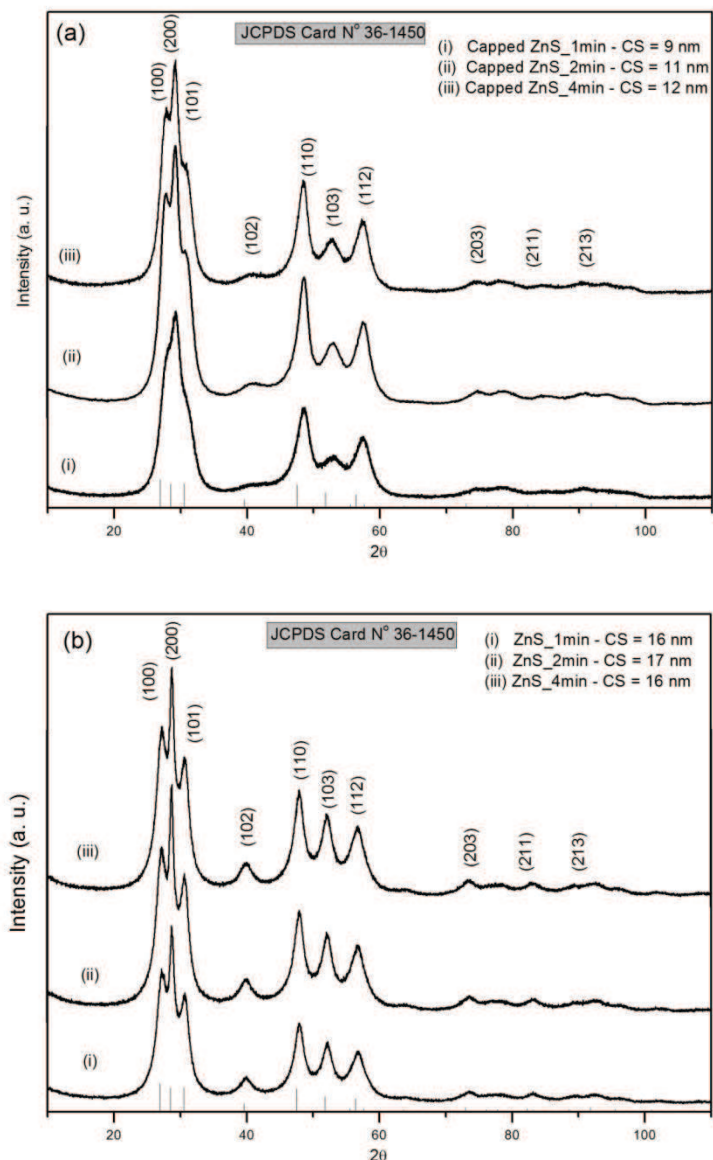


**FIG. 1** – The XRD patterns of ZnS powders processed in a microwave-solvothermal system at 413 K for different times; (a) capped ZnS, and (b) ZnS. The vertical dashed lines indicate the position and relative intensity of JCPDS card 36-1450.

The existence of a cubic ZnS phase from XRD patterns alone cannot be excluded due to the large similarity between the cubic and hexagonal ZnS structures. Thus, these results indicate that ZnS powders processed in a microwave-solvothermal system are crystalline, pure, and ordered at long range. These results are in very good agreement with other experimental studies.<sup>14</sup> Using the following Debye–Scherer formula,<sup>37</sup> the average crystallite size (CS) of the materials was calculated from the full width at half maximum (FWHM) of the diffraction peaks,

$$CS = k\lambda/\beta \cos \theta, \quad (1)$$

where,  $k$  = constant,  $\lambda$  = wavelength of the x-rays in nm,  $\beta$  = FWHM of the major peak in radians, as calculated from the data of the XRD peaks, and  $\theta$  = diffraction angle. By using the experimental values, the CS was calculated (Fig. 1).

It is important to note that we obtained pure crystalline powders in relatively low temperatures (413 K) in a short time (1 min) which proves the efficiency of the method employed. Table I shows a comparison of other researcher's solvothermal syntheses data, where the wurtzite phase was obtained.

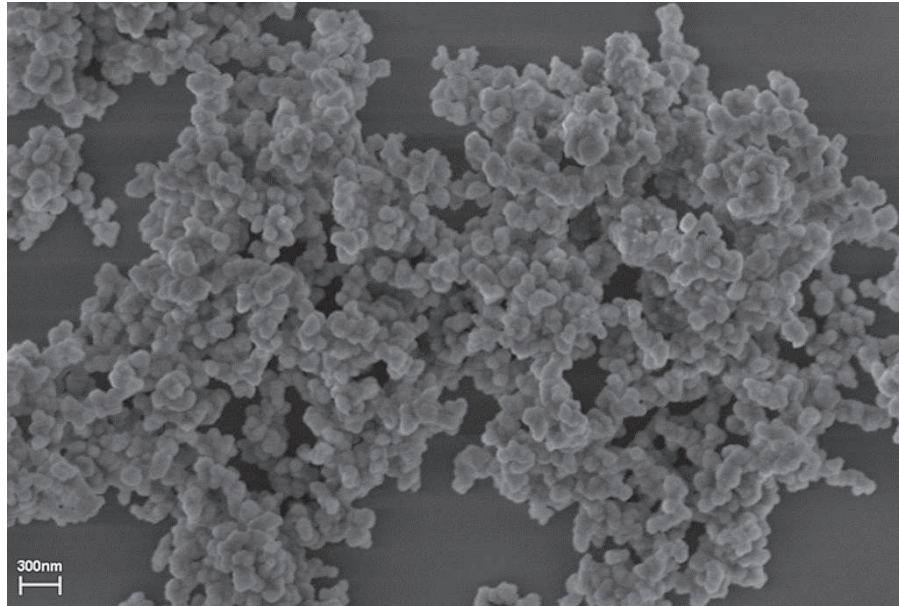
**TABLE I.** Comparison among synthesis methods.

Synthesis employed	Reaction time (min)	Temperature (K)
Hydrothermal <sup>a</sup>	300-1320	353-413
Hydrothermal <sup>b</sup>	60-600	433
Solvothermal <sup>c</sup>	5760	443
Solvothermal <sup>d</sup>	720	403-503
Microwave assisted single source method <sup>e</sup>	5	283
This work	1-4	413

<sup>a</sup>Reference 47. <sup>b</sup>Reference 48. <sup>c</sup>Reference 49. <sup>d</sup>Reference 50. <sup>e</sup>Reference 51.

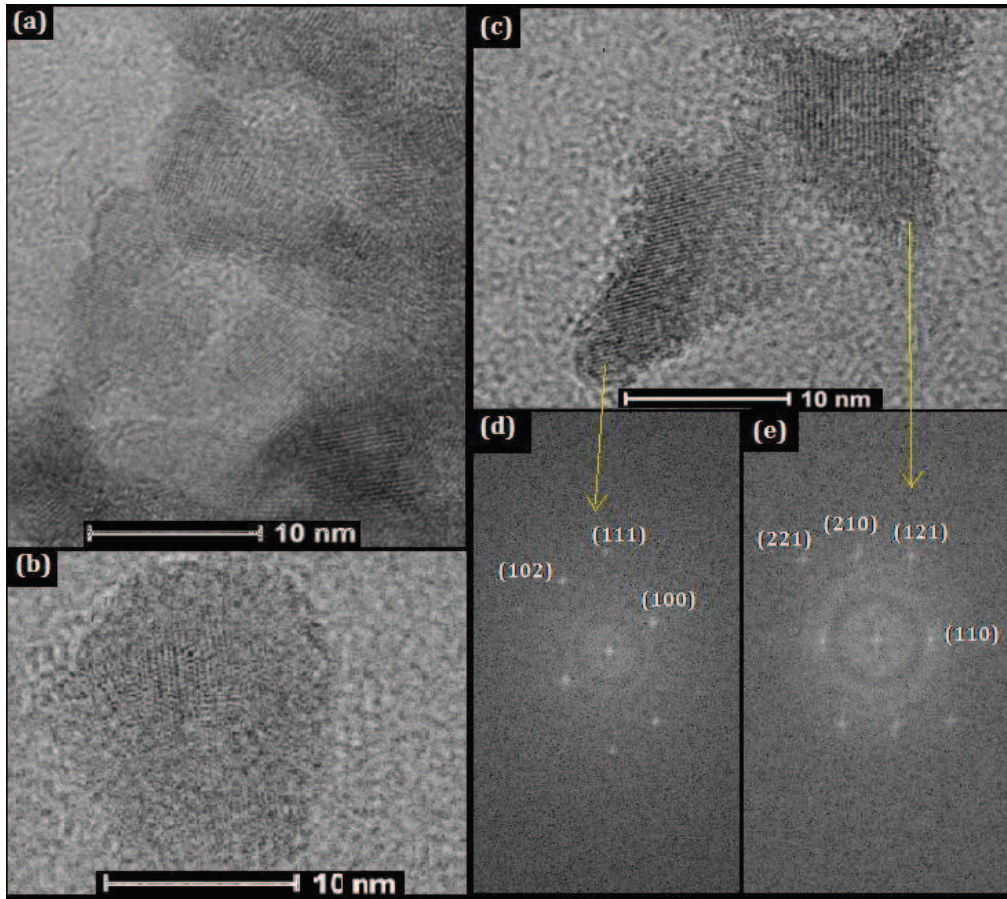
Figure 2 and 3 show FEG-SEM and TEM images for uncapped and capped ZnS nanocrystals, respectively. For uncapped nanocrystals, crystallites agglomerate and form particles with diameters of 110 nm for a synthesis of 1min, and there is a greater variation in size with increasing synthesis time (Fig. 2).

For capped samples, the crystallites do not show specific morphologies, and form small agglomerates (Fig. 3(a)). In these agglomerates it is difficult to define the crystallites edges and this is because it appears to be amorphous (Fig. 3(b)). Therefore, it is not possible to do a count- statistic on the size of the crystallites. Corresponding FFT images indicated the presence of hexagonal and cubic phases (Figs. 3(d) and 3(c), respectively), as was expected from the XRD diffraction.



**FIG. 2** – The FEG-SEM image of 1 min uncapped ZnS.





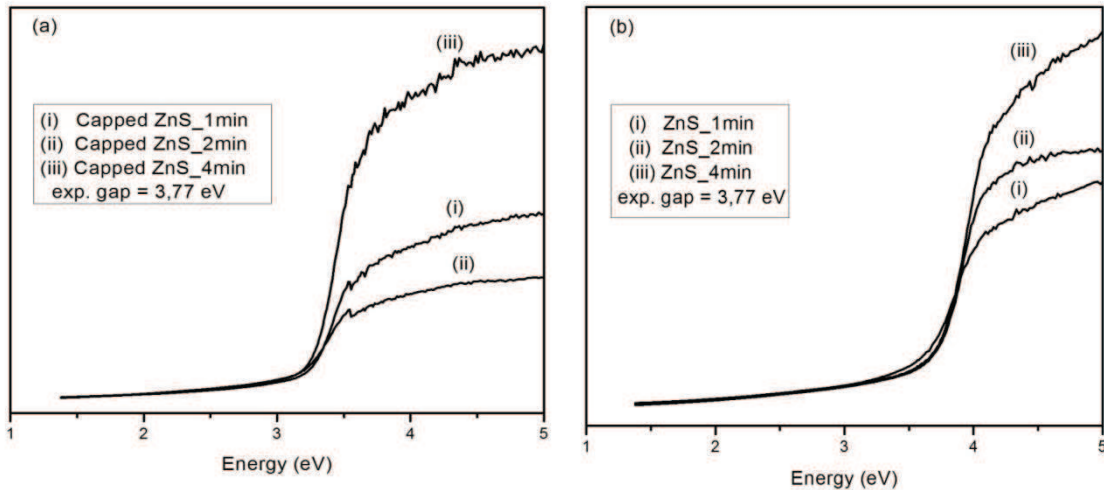
**FIG. 3** – The FEG-TEM images of 1 min capped ZnS. (a) The crystallites agglomerated, (b) crystallite with amorphous edges, (c) crystallites with cubic and hexagonal phases, (d) hexagonal phase FFT, and (e) cubic phase FFT.

Figure 4 shows the absorbance spectral dependence for the processed ZnS powders. The equation proposed by Wood and Tauc<sup>38</sup> was used to estimate the optical band gap. According to these authors, the optical band gap energy is related to the absorbance and photon energy by Eq. (2),

$$h\nu\alpha \propto (h\nu - E_g^{opt})^2, \quad (2)$$

where  $\alpha$  is the absorbance,  $h$  is Planck's constant,  $\nu$  is the frequency,  $E_g$  is the optical band gap, and  $n$  is a constant associated with the different types of electronic transitions ( $n = 1/2, 2, 3/2$  or  $3$  for direct allowed, indirect allowed, direct forbidden and indirect forbidden transitions, respectively). The literature<sup>39</sup> reports that the hexagonal ZnS have a typical optical absorption process governed by direct transitions. In fact, considering this information, the  $E_g$  values of the ZnS powders

were calculated using  $n = 2$  in Eq. (2) and extrapolating the linear portion of the curve or tail. The band gap in the materials is related to the absorbance and photon energy. Therefore, the combination of the absorbance and photoluminescence measurements allows for discovering the energy levels in the materials and the optical band gap value.



**FIG. 4** – The UV-vis spectrum of ZnS powders; (a) capped ZnS and (b) Uncapped ZnS.

The UV-vis measurements on the six samples showed a typical band gap value of approximately 3.1 and 3.6 eV for capped and uncapped nanocrystals, respectively (see Fig. 4). The exponential optical absorption edge and hence, the optical band gap are controlled by the degree of structural order disorder on the ZnS lattice. The decrease in the band gap can be directly related to the increase in defects in the ZnS lattice; in the present case, dislocations of the network former, Zn, raise the intermediary levels within the band gap region, reducing the optically measured band gap. The observed optical band gap indicates only the presence of defects; hence, localized electronic levels in the forbidden band gap, nevertheless, do not specifically indicate the structural defects that may be linked to them.

FIG. 5 exhibits the PL spectra of capped and uncapped ZnS nanoparticles measured at room temperature and excited at 350.7 nm.

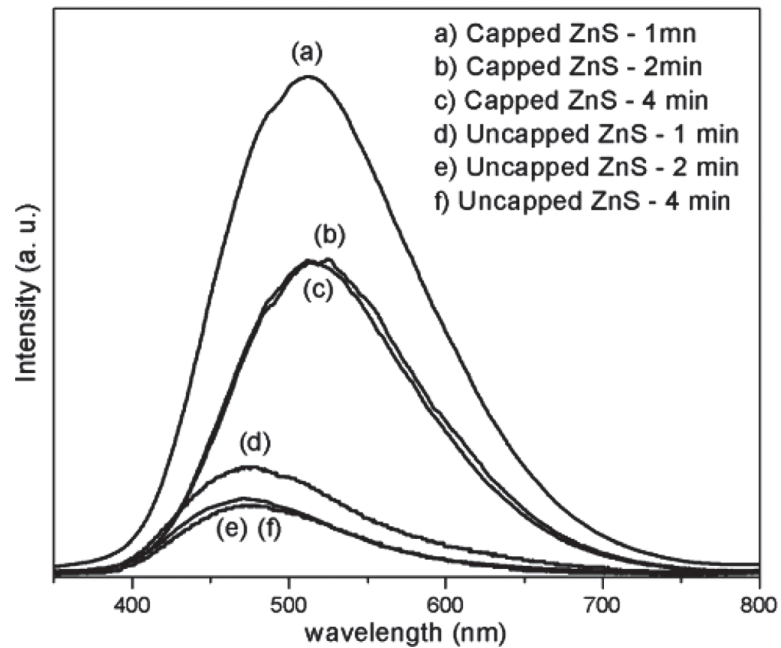


**FIG. 5** – The PL spectrum of ZnS powders at room temperature.

The profile of the emission band is typical of a multiphonon and multilevel process, i.e., a system in which relaxation occurs by several paths, involving the participation of numerous states within the *band gap* of the material. However, the origin of this PL emission has been quite controversial. Kasaii *et al.*<sup>40</sup> attributed the blue emission (430 and 450 nm) both to Zn and S vacancies. Uchida *et al.*<sup>41</sup> made the correlation with the off stoichiometry of the Zn and S, and concluded that samples with both zinc and sulfur excess emitted in the blue range. Murase *et al.*<sup>42</sup> conducted fluorescence and EPR studies of Mn doped ZnS, and the EPR measurements proved the existence of hole centers, such as Zn vacancies, and attributed the blue emission (450 nm) to Zn vacancies. Zhang *et al.*<sup>19</sup> attributed the blue emission to defects related to sulfur vacancies. Jun *et al.*<sup>18</sup> associated the blue emission (479 nm) in ZnS solid nanospheres to Zn vacancies. In addition, in hollow nanospheres they observed a strong green emission band centered at 509 nm and justified this emission to self-activated centers, vacancy states, or interstitial states associated with that peculiar nanostructure.

More recently, Chen *et al.*<sup>43</sup> explained the green emission of the ZnS nanostructures as being due to self-activated zinc vacancy points. Yunchao *et al.*<sup>44</sup> conducted a study comparing the PL of cubic and hexagonal ZnS structures. For cubic ones they attributed the peak at 322 nm to excitonic emission, the peak at 420 nm to Zn or S vacancies, and the 460 nm peak to the trapped surface states emission. For the hexagonal structure, they again attributed the 322 nm peak to excitonic emission and the peaks at 360 and 375 nm to interstitial sulfur emission and interstitial zinc emission, respectively. Theoretical results have shown that the symmetry break process (an effect of order-disorder) in the structure of various semiconductors is a condition necessary for the existence of intermediary energy levels within the forbidden band gap.<sup>45</sup> As shown in Figs. 5(a)–5(f), the evolution of the PL spectra was obviously different. During the growth of capped and uncapped ZnS, the peak correlating to the defect states was quenched in the initial 1 min (Figs. 5(a) and 5(d)). However, during the growth process, the peak correlating to the defect states slightly decreased and remained practically constant during the period from 2 to 4 min (Figs. 5(b), 5(c), 5(e), and 5(f)). The strong defect-induced luminescence of the initial particles could mainly be attributed to the internal lattice defects that arise from the fast deposition during the initial nucleation process. After 2 min, most of the internal defects from the nucleation process had disappeared. Thus, with the size increased the amount of internal defects and surface defects correspondingly decreased. Since the internal and surface defects are different during different synthetic periods, difficulties arise in the investigation of the relationship between the luminescence properties and the defects states.

This behavior is related to the structural disorder of ZnS and indicates the presence of additional electronic levels in the forbidden band gap of the material (see Fig. 6). The capped samples presented a maximum emission at 513 nm in the green region of the visible spectra, while the uncapped ones presented a maximum emission at 478 nm in the blue region of the visible spectra. The Stokes shift can be related to the difference between the excitation and the emission maximum and represents the strength of the electron-phonon interaction. For the uncapped samples the Stokes shift was 127.3 nm. The capped nanoparticles have a greater Stokes shift of 162.3 nm, indicating a dependence of the electron-phonon interaction on the excitation wavelength and the degree of disorder in the lattice.

This rearrangement of the lattice can be attributed to the crystallization process of the capped and uncapped nanoparticles.

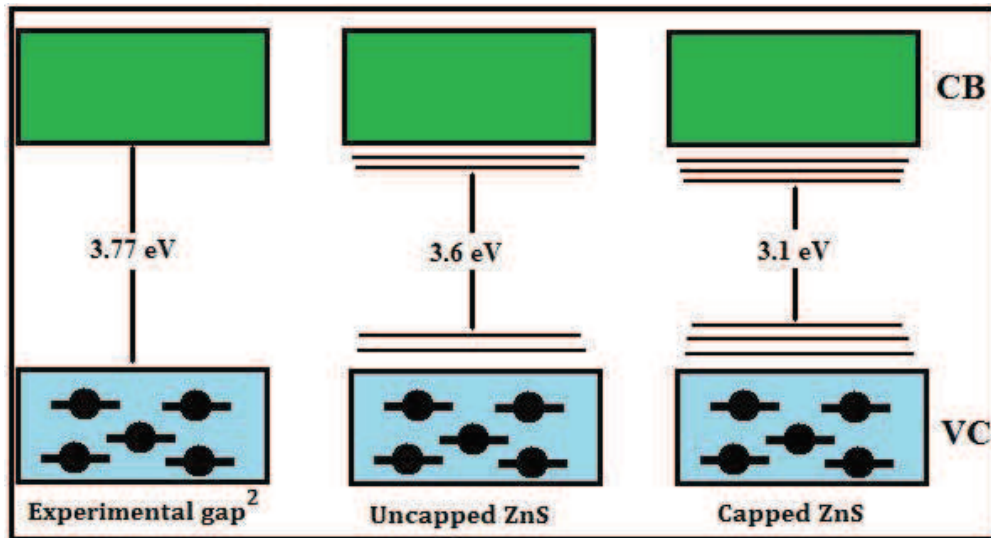


**FIG. 6** – Wide-band model, indicating the intermediary levels in the forbidden area.

Thus, we can understand the materials structures on a length scale. This understanding is relevant in shedding light on several outstanding issues in materials science, clarifying the relationships existing between local, intermediate, and long range structures and the properties of the materials. The theory allied to careful experiments, modeling, and simulations will be required to determine their origins. Experimental probes can provide more structural information on short- and long-range orders in materials; however, their structures over the intermediate range are still little understood. Theoretical calculations and computer simulations can complement experimental methods and have revealed new insights into medium-range order and dynamic changes in the local structure.<sup>46</sup> To understand the relationship between the structural disorder in complex clusters with an intermediate-range interaction (interaction between two clusters) and the resulting electronic defects that are generated, a detailed theoretical study was made of the electronic structure of the ordered o-ZnS model and of the disordered d-ZnS periodic models. To appreciate the differences in the electronic structure, it is important to make reference to quantities such as the band structures and density of states (DOS), which can be compared to each other independent of the crystalline space group.

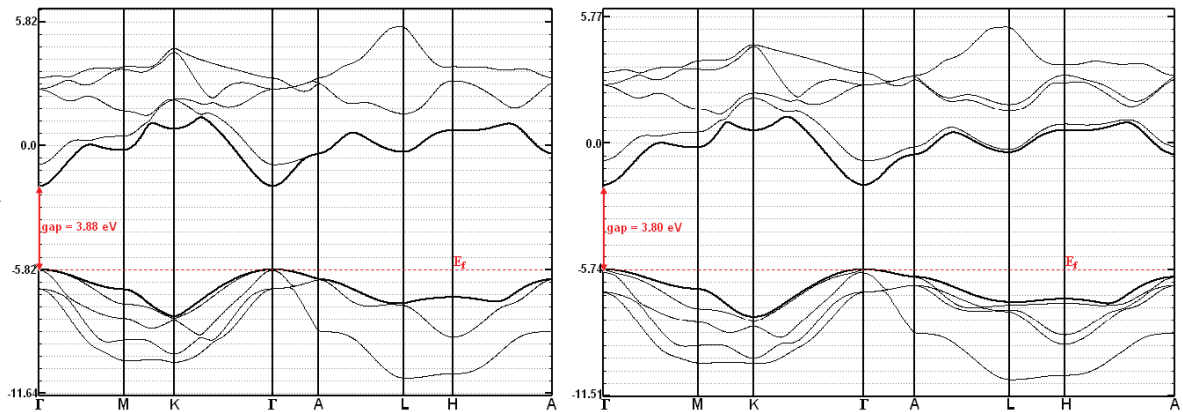


**FIG. 7** – Band structures for (a) o-ZnS, and (b) d-ZnS.

FIG. 7 represents the band structure of the bulk o-ZnS and d-ZnS models. For the o-ZnS and d-ZnS models the top of the valence band (VB), is located at the C point. The band gap is direct; 3.88 eV and 3.80 eV, respectively. The calculated band gap for o-ZnS is in accordance with the experimental optically measured gap (3.77 eV).<sup>2</sup> An analysis of the projected density of state (DOS-p) for the S atoms of the o-ZnS model, shown in Fig. 8 (a), indicate that the VB consists mainly of  $3p_x$ ,  $3p_y$ , and  $3p_z$  levels. The main contribution of conduction band (CB) comes from minor contributions of the  $3p_x$ ,  $3p_y$ , and  $3p_z$  levels with a lower contribution of  $3s$  levels of S atoms. The DOS-p for Zn atoms of the o-ZnS model, shown in Fig. 9(a), show that the VB is made from  $4p_x$ ,  $4p_y$ , and  $4p_z$  orbitals with a minor contribution of  $4s$  levels; the  $3d$  levels have a lower influence. The presences of the  $3d$  states in the VB in the two models reveal a strong bonding character between S and Zn. The same behavior is observed for the CB.

Quantum mechanical calculations of dislocated ZnS complex clusters indicate that localized states generated in the band gap reduce the gap energies. When the structural order increases, the gap energy increases. These findings confirm the fact that the PL is directly associated with the localized states existing in the band gap. Distorted clusters cause local lattice distortion that propagates throughout the material, pushing the surrounding clusters away from their ideal positions. Thus, distorted clusters must move for these properties to occur, changing the electronic distribution along the network of these polar clusters. This electronic structure dictates both optical and electrical transport properties and plays

a major role in determining reactivity and stability. However, these movements can be induced within the crystal lattice by the PL measurements and these anisotropic cooperative movements lead to these properties.

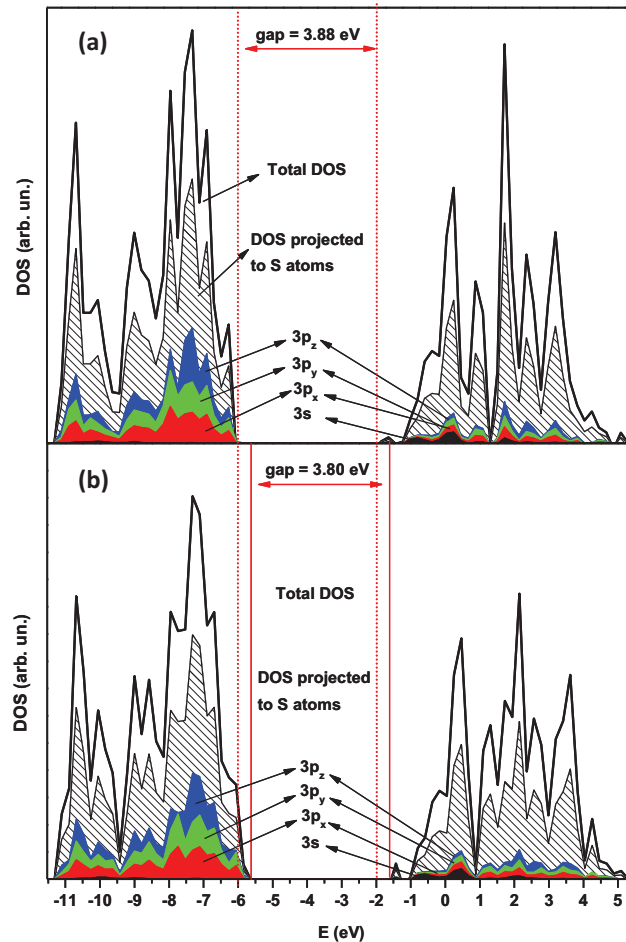


**FIG. 8** – Total and p-DOS calculation on S atoms for (a) o-ZnS, and (b) d-ZnS models.

The band gap of capped ZnS is comparatively smaller than that of uncapped ZnS. Therefore, the excitation wave-length of 350.7 nm is able to excite different populations of electrons in the band gap of the two structures. Here, each color represents a different type of electronic transition and is linked to a specific structural arrangement. In the case of capped ZnS, the recombination of electrons and holes gives rise to a strong green light emission and in the case of uncapped ZnS, to blue light emission. In our model, the wide-band model,<sup>45</sup> the most important events occur before excitation, i.e., before the photon arrives. The deep

and shallow defects generated by the complex clusters give rise to localized states in the band gap and inhomogeneous charge distribution in the cell, allowing electrons to become trapped. The localized levels are energetically distributed so that various energies are able to excite the trapped electrons. These structural changes can be related to the charge polarization in different ranges that are, at least, a manifestation of the quantum confinement, when they occur at short and intermediate range independent of the particle size.

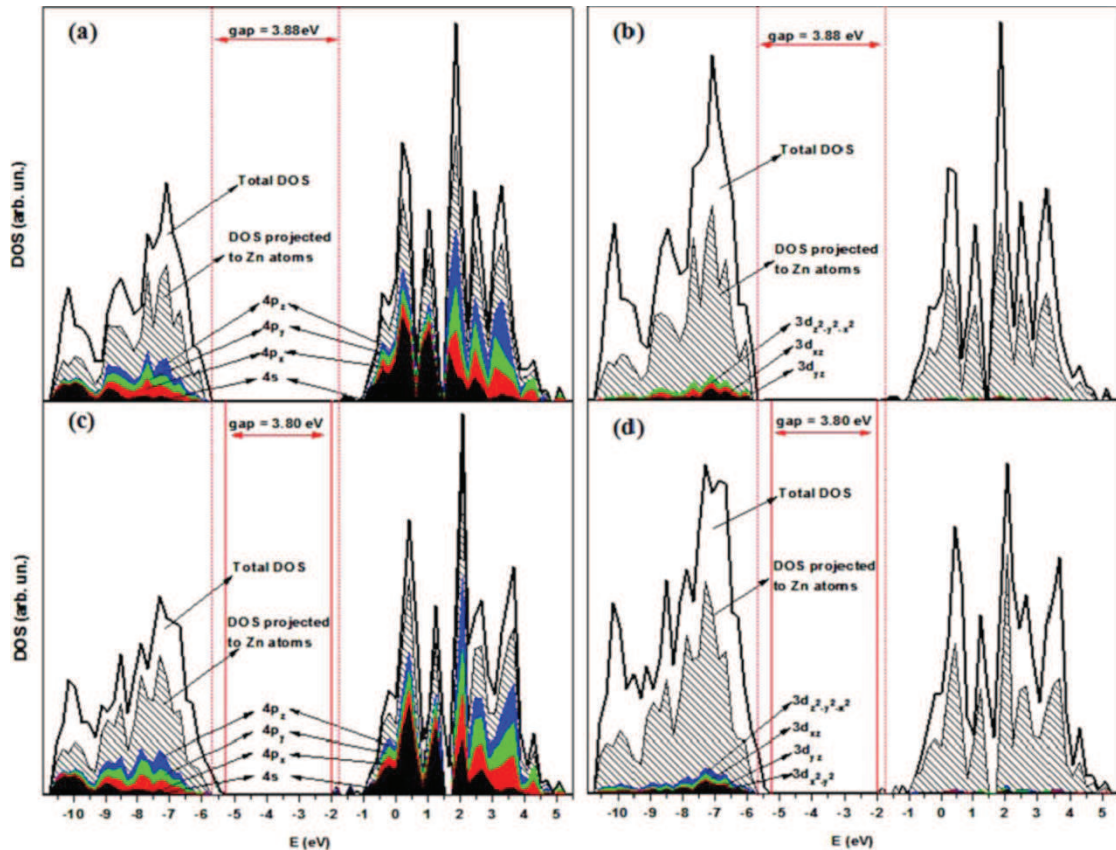


**FIG. 9** – Total and p-DOS calculation on Zn atoms for (a) and (b) o-ZnS and (c) and (d) d-ZnS models.

In this paper, we have shown that distinct structures and different orders/disorders in the lattice produce different types of PL emission. The complex clusters already existing in the ground state facilitate the emission process and lead to PL, i.e., radiative recombination. Thus, the distortions of complex clusters are crucial for an understanding of the properties of materials. The study presented here offers a conceptual framework to understand, discuss, and optimize electronic material properties on the basis of their lattice distortions. However, the mechanistic pathway of the PL emission is still not completely understood. Understanding it may provide information about how clustered molecules



“communicate” with one another in physical and chemical processes.

## CONCLUSION

The ZnS nanoparticles were successfully synthesized by the microwave-assisted solvothermal method in low temperature and short time synthesis (1 min). The PL measurements indicate an intense green light emission in capped ZnS and a less intense blue light emission in uncapped ZnS. The PL results can be attributed to distortions in the materials lattice. The different electronic levels appearing in the *band gap* of capped and uncapped ZnS are able to create different colors emissions in the visible spectra of light. This effect was confirmed by first-principles calculations based on the B3LYP density functional theory using disorder models of the lattice.

## ACKNOWLEDGMENTS

This work is supported by the Brazilian Funding Agencies FAPESP, CAPES, CNPq, and CEPID. We thank Ricardo Gonçalves and Rorivaldo Camargo for their help with the FEG-TEM and FEG-SEM images. The computational research supported by resources supplied by Laboratório de Simulação Molecular and the Center for Scientific Computing of the São Paulo State University are also acknowledged.

## REFERENCES

- <sup>1</sup>M. V. Limaye, S. Gokhale, S. A. Acharya, and S. K. Kulkarni, *Nanotechnology* 19, (2008).
- <sup>2</sup>S. Biswas and S. Kar, *Nanotechnology* 19, (2008).
- <sup>3</sup>M. Bredol and J. Merikhi, *J. Mater. Sci.* 33, 471 (1998).
- <sup>4</sup>P. Calandra, M. Goffredi, and V. T. Liveri, *Colloids Surf., A* 160, 9 (1999).
- <sup>5</sup>T. Yamamoto, S. Kishimoto, and S. Iida, *Physica B* 308, 916 (2001).
- <sup>6</sup>A. P. Alivisatos, *Science* 271, 933 (1996).
- <sup>7</sup>Z. F. Ding, B. M. Quinn, S. K. Haram, L. E. Pell, B. A. Korgel, and A. J. Bard, *Science* 296, 1293 (2002).
- <sup>8</sup>S. L. Lin, N. Pradhan, Y. J. Wang, and X. G. Peng, *Nano Lett.* 4, 2261 (2004).
- <sup>9</sup>W. Z. Wang, I. Germanenko, and M. S. El-Shall, *Chem. Mater.* 14, 3028 (2002).
- <sup>10</sup>H. F. Shao, X. F. Qian, and Z. K. Zhu, *J. Solid State Chem.* 178, 3522 (2005).
- <sup>11</sup>H. J. Liu, Y. H. Ni, M. Han, Q. Liu, Z. Xu, J. N. Hong, and X. Ma, *Nanotechnology* 16, 2908 (2005).

- 12L. Chai, J. Du, S. Xiong, H. Li, Y. Zhu, and Y. Qian, *J. Phys. Chem. C* 111, 12658 (2007).
- 13J. Y. Liu, Z. Guo, Y. Jia, F. L. Meng, T. Luo, and J. H. Liu, *J. Cryst. Growth* 311, 1423 (2009).
- 14Y. W. Zhao, Y. Zhang, H. Zhu, G. C. Hadjipianayis, and J. Q. Xiao, *J. Am. Chem. Soc.* 126, 6874 (2004).
- 15M. Sharma, S. Kumar, and O. P. Pandey, *J. Nanopart. Res.* 12, 2655 (2010).
- 16Motlan, G. Zhu, K. Drozdowicz-Tomsia, K. McBean, M. R. Phillips, and E. M. Goldys, *Opt. Mater.* 29, 1579 (2007).
- 17Y. Azizian-Kalandaragh and A. Khodayari, *Phys. Status Solidi A* 207, 2144 (2010).
- 18J. Geng, B. Liu, L. Xu, F.-N. Hu, and J.-J. Zhu, *Langmuir* 23, 10286 (2007).
- 19W. H. Zhang, J. L. Shi, H. R. Chen, Z. L. Hua, and D. S. Yan, *Chem. Mater.* 13, 648 (2001).
- 20S. K. Maji, N. Mukherjee, A. Mondal, B. Adhikary, B. Karmakar, and S. Dutta, *Inorg. Chim. Acta* 371, 20 (2011).
- 21W. G. Becker and A. J. Bard, *J. Phys. Chem.* 87, 4888 (1983).
- 22K. J. Rao, B. Vaidhyanathan, M. Ganguli, and P. A. Ramakrishnan, *Chem. Mater.* 11, 882 (1999).
- 23D. P. Volanti, D. Keyson, L. S. Cavalcante, A. Z. Simoes, M. R. Joya, E. Longo, J. A. Varela, P. S. Pizani, and A. G. Souza, *J. Alloys Compd.* 459, 537 (2008).
- 24S. Komarneni, R. Roy, and Q. H. Li, *Mater. Res. Bull.* 27, 1393 (1992).
- 25C. T. Lee, W. T. Yang, and R. G. Parr, *Phys. Rev. B* 37, 785 (1988).
- 26R. Dovesi, V. R. Saunders, C. Roetti, R. Orlando, C. M. Zicovich-Wilson, F. Pascale, B. Civalleri, K. Doll, N. M. Harrison, I. J. Bush, P. D'Arco, M. Llunell, *CRYSTAL06 User's Manual* (University of Torino, Torino), 2006.
- 27R. C. Lima, L. R. Macario, J. W. M. Espinosa, V. M. Longo, R. Erlo, N. L. Marana, J. R. Sambrano, M. L. dos Santos, A. P. Moura, P. S. Pizani, J. Andres, E. Longo, and J. A. Varela, *J. Phys. Chem. A* 112, 8970 (2008).
- 28M. L. Moreira, P. G. C. Buzolin, V. M. Longo, N. H. Nicoletti, J. R. Sambrano, M. S. Li, J. A. Varela, and E. Longo, *J. Phys. Chem. A* 115, 4482 (2011).
- 29N. L. Marana, V. M. Longo, E. Longo, J. B. L. Martins, and J. R. Sambrano, *J. Phys. Chem. A* 112, 8958 (2008).
- 30L. S. Cavalcante, J. C. Sczancoski, V. M. Longo, F. S. De Vicente, J. R. Sambrano, A. T. de Figueiredo, C. J. Dalmaschio, M. S. Li, J. A. Varela, and E. Longo, *Opt. Commun.* 281, 3715 (2008).
- 31J. E. Jaffe and A. C. Hess, *Phys. Rev. B* 48, 7903 (1993).
- 32A. Lichanot, E. Apra, and R. Dovesi, *Phys. Status Solid B* 177, 157 (1993).
- 33M. J. D. Powell, *SIAM Rev.* 12, 79 (1970).
- 34H. Z. Zhang, B. Gilbert, F. Huang, and J. F. Banfield, *Nature (London)* 424, 1025 (2003).
- 35See <http://www.crystal.unito.it/Basis-Sets> for the site where you can get the basis of atoms to perform calculation/simulation, at the program crystal.
- 36E. H. K. a. M. M. Elcombe, *Acta Crystallogr. C* 39, 1493 (1983).

- 37 L. A. H. Klug, X-Ray Diffraction Procedures (John Wiley and Sons, Inc., New York, 1962).
- 38 D. L. Wood and J. Tauc, Phys. Rev. B 5, 3144 (1972).
- 39 P. K. Ghosh, S. Jana, S. Nandy, and K. K. Chattopadhyay, Mater. Res. Bull. 42, 505 (2007).
- 40 P. H. Kasai and Y. Otomo, J. Chem. Phys. 37, 1263 (1962).
- 41 I. Uchida, J. Phys. Soc. Jpn. 19, 670 (1964).
- 42 N. Murase, R. Jagannathan, Y. Kanematsu, M. Watanabe, A. Kurita, K. Hirata, T. Yazawa, and T. Kushida, J. Phys. Chem. B 103, 754 (1999).
- 43 H. Chen, Y. Hu, and X. Zeng, J. Mater. Sci. 46, 2715 (2011).
- 44 Y. C. Li, X. H. Li, C. H. Yang, and Y. F. Li, J. Phys. Chem. B 108, 16002 (2004).
- 45 E. Longo, E. Orhan, F. M. Pontes, C. D. Pinheiro, E. R. Leite, J. A. Varela, P. S. Pizani, T. M. Boschi, F. Lanciotti, A. Beltran, and J. Andres, Phys. Rev. B 69, 25115 (2004).
- 46 V. M. Longo, L. S. Cavalcante, M. G. S. Costa, M. L. Moreira, A. T. de Figueiredo, J. Andres, J. A. Varela, and E. Longo, Theor. Chem. Acc. 124, 385 (2009).
- 47 M. Salavati-Niasari, M. R. Loghman-Estarki, and F. Davar, J. Alloys Compd. 475, 782 (2009).
- 48 L. Zhang and L. Yang, Cryst. Res. Technol. 43, 1022 (2008).
- 49 C. Cheng, G. Xu, H. Zhang, J. Cao, P. Jiao, and X. Wang, Mater. Lett. 60, 3561 (2006).
- 50 S. K. Panda and S. Chaudhuri, J. Colloid Interface Sci. 313, 338 (2007).
- 51 J. Q. Sun, X. P. Shen, K.-M. Chen, Q. Liu, and W. Liu, Solid State Commun. 147, 501 (2008).

## 2.4. Paper 4

### Blue shift of optical band gap in CaS prepared by solvothermal microwave method

Cristiane W. Raubach<sup>a,\*</sup>, Yuri V. B. de Santana<sup>a,b</sup>, José A. Varela<sup>b</sup>, Mateus M. Ferrer<sup>a</sup>, Amanda F. Gouveia<sup>a</sup>, Maximo S. Li<sup>c</sup>, and Elson Longo<sup>b</sup>

<sup>a</sup> INCTMN-UFSCar, Universidade Federal de São Carlos, Rod. Washington Luís Km 235, 13565-905, São Carlos, SP, Brazil

<sup>b</sup> INCTMN-UNESP, Universidade Estadual Paulista, P.O. Box 355, 14801-907, Araraquara, SP, Brazil

<sup>c</sup> IFSC-Universidade de São Paulo, P.O. Box 369, 13560 970, São Carlos, SP, Brazil

[\\*cristiane@liec.ufscar.br](mailto:cristiane@liec.ufscar.br)

#### Abstract

The shift in the photoluminescence (PL) emission in calcium sulfide (CaS) synthesized for the first time by the microwave-assisted solvothermal (MAS) method was examined to understand the key role of its PL activity. The PL emission in the visible region showed a blue shift with the variation of synthesis time. In addition, we also investigated the electronic structure using first-principle calculation based on density functional theory (DFT) applied to periodic models at B3LYP level. Two models were selected to simulate the effects of structural deformation on the electronic structure; the ordered *o*-CaS model and the disordered *d*-CaS model. This PL emission shift was linked to distortions and defects generate modifications in the electronic states and provide the possibility of numerous decay transactions to the valence band.

## Introduction

Alkaline earth sulfide (AES) has received an interesting amount of attention over the past decades [1-3]. Sulfide phosphors such as ZnS, SrS and CaS have interesting properties useful for practical application, i.e. television screens, fluorescence lamps, thermoluminescence dosimetry, X-ray imaging screens and high pressure mercury lamps [4-8]. Members of this group also are known as wide band-gap semiconductors (e.g., CaS 3.4 – 4.4 eV, MgS 5.27 – 5.47 eV and SrS 4.3 eV). Among these, CaS has been actively studied [9,10]. CaS is known as an afterglow phosphor with high luminescence efficiency and multiple luminescence centers. The CaS exhibits luminescence under irradiation at various wavelengths of light, X-rays, ultraviolet and visible light [11-13].

Calcium sulfide can crystallize in four different structures: NaCl-type (B1); CsCl-type (B2); zinc-blende (B3); and wurtzite (B4) [14-15]. At room temperature CaS crystallizes in NaCl structure, also called *rock-salt*. This structure is cubic (Fm-3m), which atoms occupy octahedral sites. Calcium cations are arranged in an FCC (face-centered cubic) pattern, and the sulfur anions reside in the octahedral holes, as shown in Figure 1. Each atom, calcium or sulfur, is surrounded by six of the opposite kind, resulting in a coordination expressed as (6:6).

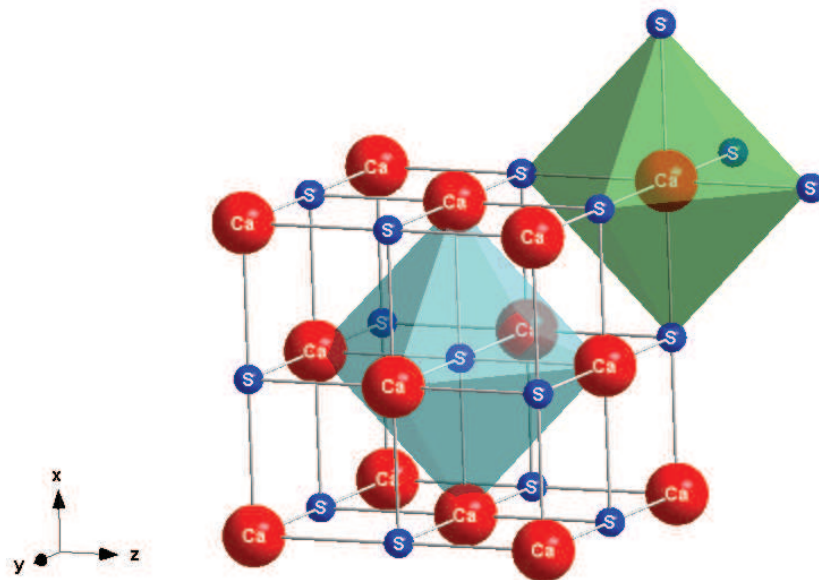


**Figure 1** – Arrangement of calcium and sulfur atoms in the CaS structure.

The structure, morphology and density of defects are crucial factors in determining the optical and electronic properties of these materials [16-17]. Thus, one of the most important goals in modern materials research is the development of simple and low cost methods for large scale synthesis, as well as understanding of the structure, shape and density of defects generated by the method employed.

In this scenario, a few of works have been reported on the preparation of CaS nanoparticles with and without dopants, such as co-precipitation for CaS:Eu<sup>2+</sup>, alkoxides method for CaS [2,18], solvothermal method for CaS and SrS [9] and microwave heating method for CaS [19]. Recently, an alternative method using microwave heating, the MAS method, has emerged in the field of powder preparation. Some benefits of this method are: kinetic enhancement, low reaction temperature and time reduction [20-22].

The present work focuses on links between the structure and the photoluminescent behavior of calcium sulfide. We investigate the role of microwave processing on the PL properties of CaS nanoparticles. The main objective is to investigate the impact of order–disorder on the PL emission. This research involves two steps: (1) synthesis of powders in different times and (2) revealing the relationships between structural disorder and the PL property. The purpose is to join both the experimental and theoretical results to explain the responses of PL emission at room temperature and de structure by using a structural disorder motif. To this end, we have used different experimental techniques and calculations based on the DFT to carry out a comprehensive investigation of the corresponding structures and electronic properties.

## **Methods**

### *Preparation of calcium sulfide crystals*

The 4mmol Na<sub>2</sub>S.9 H<sub>2</sub>O (99%, Synth) were dissolved in 75mL ethanol. The 300mL/min N<sub>2</sub> gas for 30 min was insufflated into this solution (solution 1). Separately CaCl<sub>2</sub> (99.90%, Synth) were dissolved in 75 mL of ethanol (solution 02). Then solutions 01 and 02 were mixture in a 120 mL Teflon autoclave and after 10 min the precipitate was put in the microwave system at 110°C under different times (4-64 min). The resulting solution was washed with tetrahydrofuran (THF) (99.5% Merck) several times to neutralize the solution pH (≈ 7), and the precipitates were finally collected, and dried at 70°C (5 h).

### Characterization

The powders obtained were structurally characterized by X-ray diffraction (XRD) patterns using a D/Max-2500PC diffractometer Rigaku (Japan) with Cu K $\alpha$  radiation ( $\lambda = 1.5406 \text{ \AA}$ ) in the  $2\theta$  range from  $20^\circ$  to  $75^\circ$  in the normal routine with a scanning velocity of  $2^\circ/\text{min}$  and from  $10^\circ$  to  $110^\circ$  with a scanning velocity of  $1^\circ/\text{min}$ . The shapes and sizes of these CaS crystals were observed with a field-emission scanning electron microscope (FE-SEM), Zeiss model Supra TM 35 operated at 10kV. UV-VIS spectra were taken using a Varian spectrophotometer (model Cary 5G) in a diffuse-reflectance mode. PL measurements were performed through a Monospec 27 monochromator (Thermal Jarrel Ash) coupled to a R446 photomultiplier (Hamamatsu Photonics, Japan). A Kr-ion laser (Coherent Innova 90K;  $\lambda = 350.0\text{nm}$ ) was used as the excitation source; with an output power maintained at 500mW. The laser beam was passed through an optical chopper and its maximum power on the sample was maintained at 40mW. All measurements were taken at room temperature.

### Computational method and periodic model of CaS crystals

The simulation was performed using a periodic approximation as implemented in the CRYSTAL09 computer code [23]. The computational method is based on DFT in conjunction with Becke's three-parameter hybrid non-local exchange functional [24], combined with the Lee Yang Parr gradient-corrected correlation functional, B3LYP [25]. The atomic centers for Ca and S atoms have been described by all electron basis sets Ca\_86-511d3G and S\_86-311G\*, respectively, provided by the CRYSTAL basis sets library [26].

As a first step, an optimization procedure of the lattice parameter  $a$  from the experimental value,  $5.65 \text{ \AA}$ , was carried out, yielding a value of  $5.76 \text{ \AA}$ . From these optimized parameters, periodic models with a 16-atoms supercell CaS ( $\text{Ca}_8\text{S}_8$ ) were built: 1) the orderly CaS ( $o$ -CaS) model and 2) the disorderly CaS ( $d$ -CaS) model where S atom was displaced, simulating some defects in the structure that can occur experimentally, for the purpose of explain observed differences in the band gap of experimental samples.

## **Results and discussion**

Figure 2 shows XRD patterns for CaS crystals prepared by MAS method for different times. In the Figure 2, XRD patterns indicate that all CaS

crystals have a cubic structure without any deleterious phases with a space group of  $Fm-3m$  (225). These crystals have sharp and well-defined diffraction peaks, which indicate a reasonable degree of structural order and crystallinity at long range. Moreover, all diffraction peaks are in good agreement with the respective Inorganic Crystal Structure Data (ICSD) base n° 41956 [27]. These results are in very good agreement with other experimental studies [6, 28].

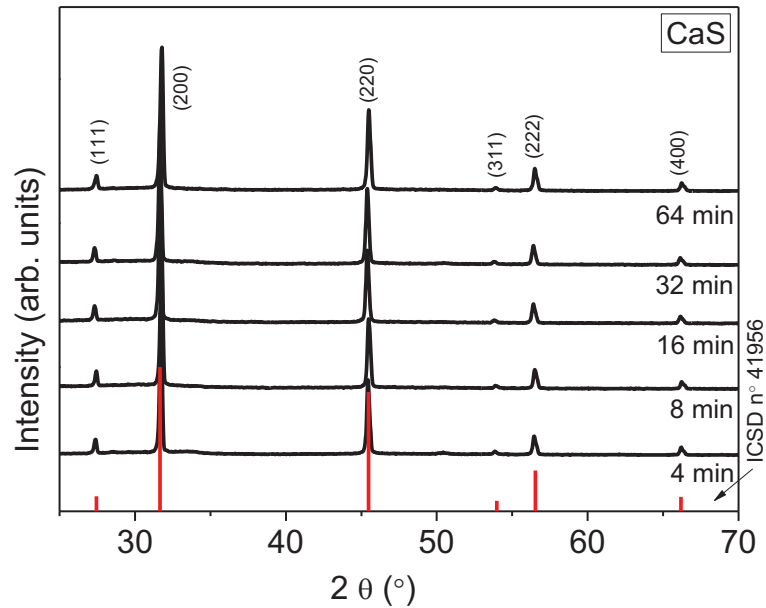


**Figure 2** – XRD patterns of CaS crystals synthesized by MAS method for different times. The vertical lines indicate the position and relative intensity of the ICSD card n° 41956 for the cubic CaS phase.

**Table 1** – Lattice parameters, Unit cell volume, R values obtained by Rietveld Refinement Data for the CaS crystals.

**Calcium Sulfide (CaS); space group  $Fm-3m$  (225) ICSD - 41956, cubic;  $z = 1$ ,  $a = b = c = 5.689 \text{ \AA}$ ,  $\alpha = \beta = \gamma = 90^\circ$  -  $V = 184.12 \text{ \AA}^3$**

Sample	Parameters					
	$a=b=c$ ( $\text{\AA}$ )	$V$ ( $\text{\AA}^3$ )	$\chi^2$	$R(F^{**2})$ (%)	$wRp$ (%)	$Rp$ (%)
CaS – 4 min	5.647	180.0	2.480	0.03	0.07	0.05
CaS – 8 min	5.648	180.1	3.162	0.04	0.09	0.06
CaS – 16 min	5.647	180.0	2.434	0.02	0.07	0.05
CaS – 32 min	5.646	179.9	3.811	0.04	0.09	0.06
CaS – 64 min	5.645	179.9	3.299	0.03	0.08	0.06



According to Chen [15], the CaS crystals can exhibit polymorphism: this sulfide can have different structure NaCl; CsCl, zinc blende; Wurtzite. NaCl structure is stable at ambient conditions; CsCl structure is stable above 45 GPa [27]. The structural refinement using the Rietveld Method [29] was performed to confirm the cubic structure for CaS crystals [27].

The Rietveld refinement was performed based on the CaS phase with a cubic structure using better approximation and indexing of the crystallographic information file (CIF) and employing CIF 41956. Figure 3 illustrate a good agreement between experimentally observed XRD patterns and theoretically fitted result, which indicates the success of the Rietveld refinement method (see Table 1).

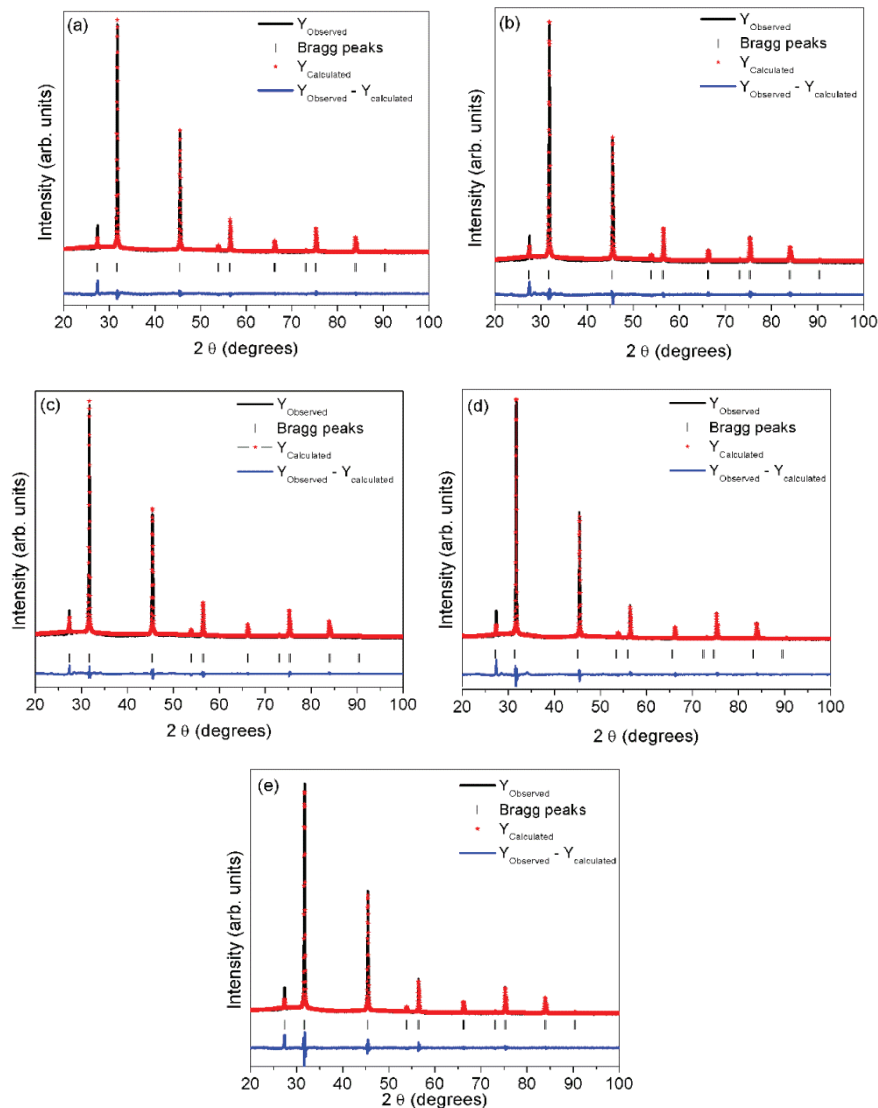


**Figure 3** – Rietveld refinement plot of CaS crystals prepared by MAS for (a) 4, (b) 8, (c) 16, (d) 32 and (e) 64 min.

The optical band-gap energy ( $E_{gap}$ ) was calculated by method proposed by Kubelka and Munk-Aussing [30]. This methodology is based on the transformation of diffuse-reflectance measurements to estimate  $E_{gap}$  values with good accuracy within the limits of assumptions when modeled in three dimensions [32]. The Kubelka-Munk equation for any wavelength is described as

$$F(R_{\infty}) = \frac{(1-R_{\infty})^2}{2R_{\infty}} = \frac{K}{s} \quad (1)$$

where  $F(R_{\infty})$  is the Kubelka-Munk function or the absolute reflectance of the sample.  $R_{\infty} = R_{sample}/R_{standard}$  ( $R_{\infty}$  is the reflectance when the sample is infinitely thick),  $\kappa$  is the molar absorption coefficient, and  $s$  is the scattering coefficient. In a parabolic band structure, the optical band gap and absorption coefficient of semiconductor [32] can be calculated by the following equation:

$$\alpha h\nu = C_1(h\nu - E_{gap})^n \quad (2)$$

where  $\alpha$  is the linear absorption coefficient of the material is,  $h\nu$  is the photon energy,  $C_1$  is a proportionality constant,  $E_{gap}$  is the optical band gap, and  $n$  is a constant associated with different kinds of electronic transitions ( $n = 0.5$  for a direct allowed and  $n = 2$  for an indirect allowed). Chen *et.al* [15] performed a theoretical study about the structural and electronic properties of CaS compound considering the four phase (B1, B2, B3 and B4). Their theoretical studies shown that B1 phase of CaS has an direct band gap. However, Kaneco et al [33] studies claim that the band gap of CaS B1 phases is governed by indirect transitions between the valence and conduction bands due to the lower transition energy with values of 4.4 eV. Our theoretical models, based on the experimental data, showed that CaS has a direct electronic transition occurring at the  $\Gamma$  point of Brillouin zone. Thus,  $E_{gap}$  values of CaS crystals were calculated using the eq. 2 for direct allowed transition.

Change carriers produced by MAS synthesis in the CaS form localized polaronic states, due to bond distortion, interface intrinsic defects and sulfur vacancies. These polarons can undergo different trapping or recombination process. This excited state favours the population of intermediary energy levels within band gap. The displacement of the sulfur related to the Ca, modulates these different species of trapped electron and holes.

Fig 4 shows the optical band gap values for the structure studied experimentally and theoretically: *o*-CaS and *d*-CaS with displacement in z-axis: 0.1, 0.3 and 0.5 Å. The increase of the defect caused by the displacement of sulfur atom in the axes decreases the  $E_{gap}$  values. The decrease in the  $E_{gap}$  values obtained experimentally can be explained according with the time that solution remained in the microwave system. Into the system, parts of the material can dissolve, crystallize and recrystallize several times. Therefore, the different time in microwave, occurs the modification of the structural order which is directly linked to electronic levels of the material. It is the reason in breaking the tendency of variation of estimated band gap after a long time in microwave (64 min).

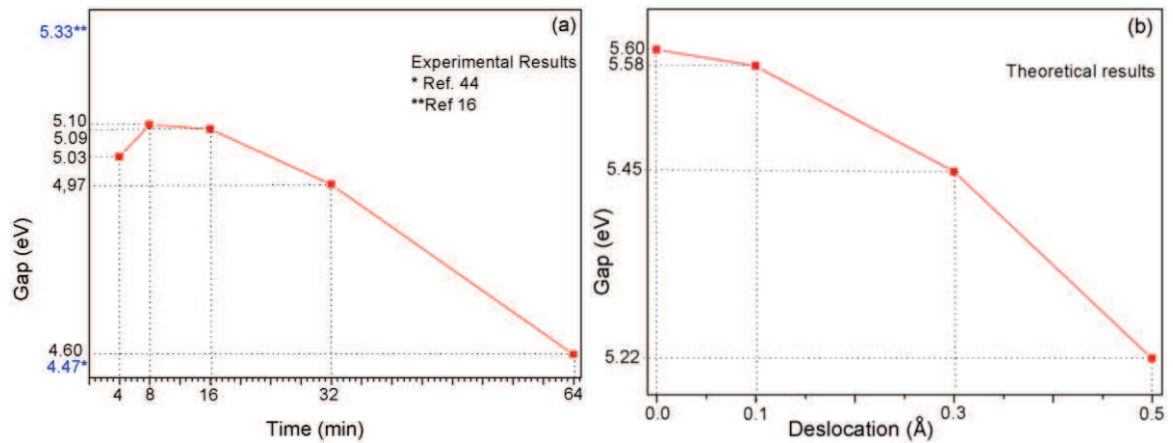
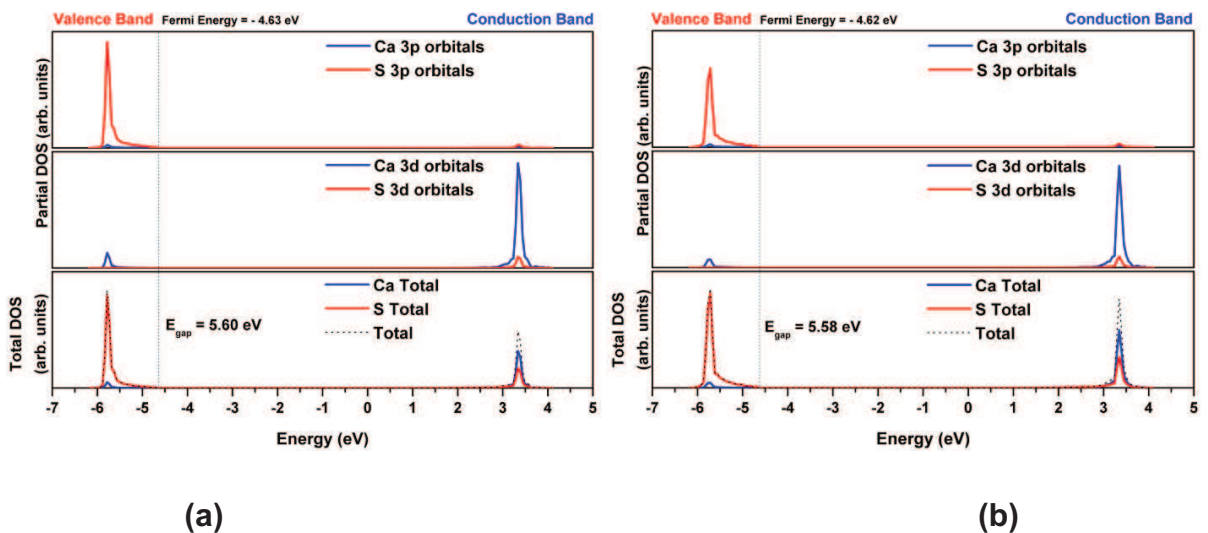


**Figure 4:** (a) Experimental and (b) theoretical band gap values (eV) for CaS.



(a)

(b)

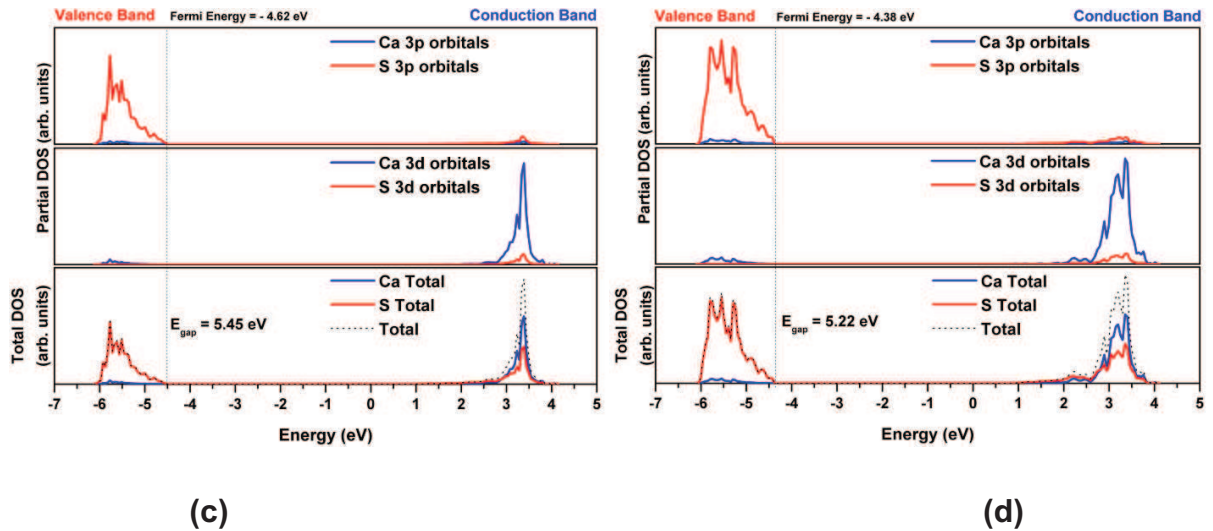


**Figure 5:** Partial DOS and Total DOS projected in: *o*-CaS (a), *d*-CaS: (b) (0.0 0.0 0.1), (c) (0.0 0.0 0.3) and (d) (0.0 0.0 0.5).

For CaS in B1 phases, we have found a direct band gap between the top of S 3p valence bands occurring at the  $\Gamma$  point and the bottom of the Ca 3d bands occurring at the same point, confirming the previously found results by Chen et al.[44], and in contradiction to the results obtained by others[45-46].

The total density of states (TDOS) and partial density of states (PDOS) obtained by first-principles calculations for the *o*-CaS and *d*-CaS, are shown in Fig. 5. The TDOS and PDOS are very useful to verify different transition levels locations and band compositions. Comparing the TDOS, the displacement of sulfur atom in the system generated a considerable modification of the profile.

Analysis of the PDOS projected on the atoms indicates that the valence band (VB) maximum is derived mainly from S (3p orbitals) with a minor contribution of Ca (3p orbitals). For the conduction band region (CB), the PDOS show that this band is predominant derived from Ca (3d orbitals) with a minor contribution of S (3d orbitals). Quantum-mechanical calculations of *d*-CaS indicate that localized states generated reduce the band gap energies. These findings confirm the disorganization of the lattice, which it's possible to note the news states in the PDOS. This displacement induces the structural distortions in the octahedron, which directly affect both the conduction and valence regions at the same time.

The FE-SEM image in Fig. 6 illustrated agglomerated CaS crystals in different forms and morphologies. When submitted to solvothermal processing at 110°C for different times, there is a change in the sample aspect. The more abrupt change occurs at 32 min (Fig. 6(d)) where looks like needles with different sizes forming a larger crystal.

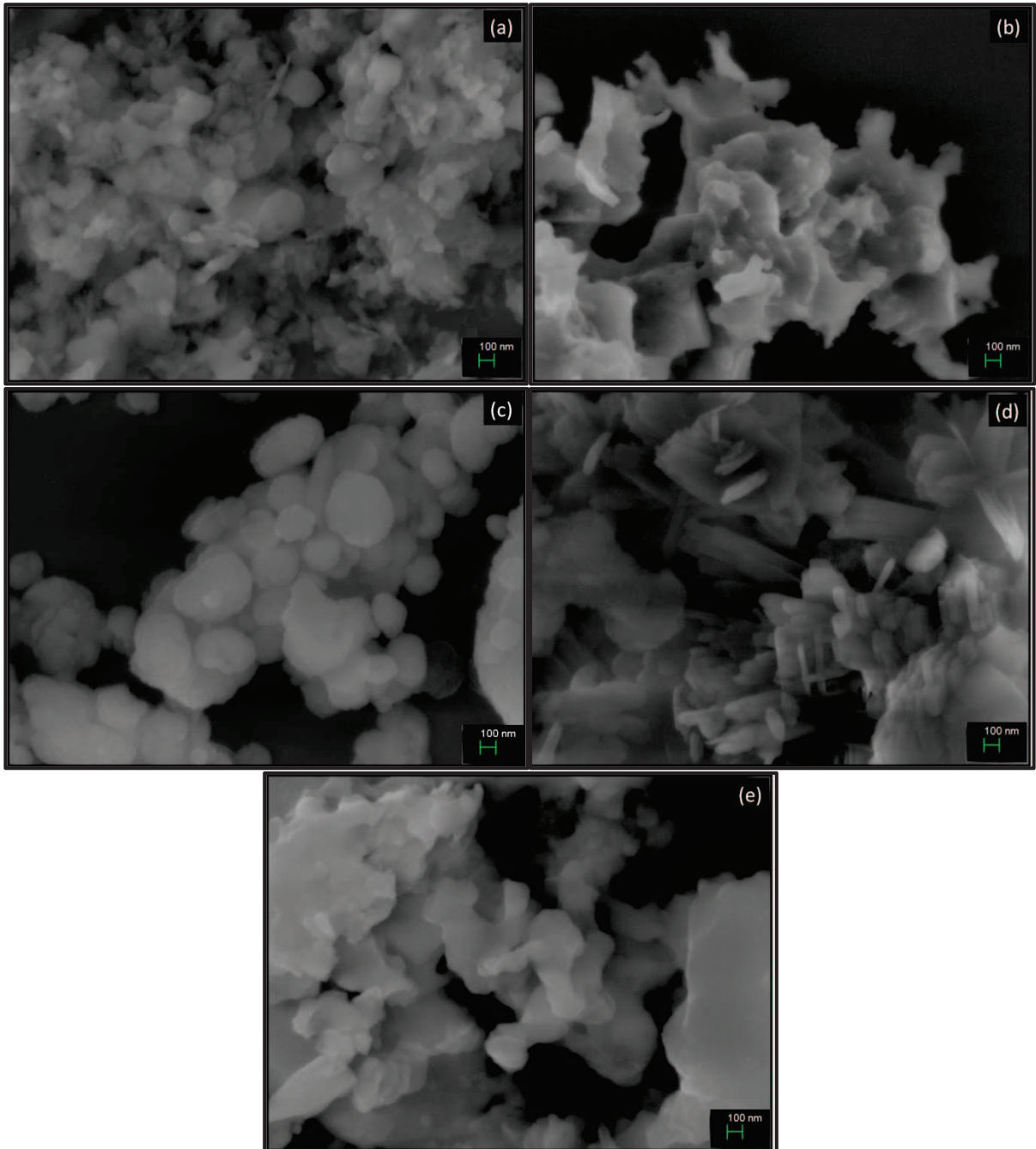


**Figure 6:** The FEG-SEM image of CaS synthesized by MAS of the (a) 4 (b) 8 (c) 16 (d) 32 and (e) 64 min.

Fig. 7 illustrates the PL evolutions of CaS samples synthesized by a MAS method under different times. The profiles have a typical behavior for multiphonon or multilevel process, i.e., a solid system where the relaxation occurs by several pathways, which involve the participation of numerous energy states within the band gap[12, 47] originating from intrinsic defects of the material. In the photoluminescence response for the CaS samples with a 350.7 nm excitation source, it can be seen that the luminescence behavior is composed of a broad luminescence band in the range of 350–650 nm which was centered around 450 nm in the blue-green region of visible spectra with two shoulders after and before the maximum emission. In general, PL emission spectra of calcium sulfide (CaS) is frequently decomposed into blue and green light components. In the literature, the blue, green or red shift is resultant of field splitting and the Stoke shift of the dopants and incorporation of the anion ( $\text{Cl}^-$ ,  $\text{Na}^+$ ) addition in the material [20, 48]. In this work, the PL behavior is explained by photogenerated electron-hole pair (excitons) processes and in terms of the electronic transition between the valence band (3p levels of S atoms) and the conduction band (3d levels of Ca atoms).

These results confirm that structural defects in the calcium sulfide nanocrystals lattice are responsible for the appearance of intermediate levels between the valence band and conduction bands, which are favorable to intense PL emission properties at room temperature. With crystallization evolution, the atomic crystalline design renders a better electronic configuration that promotes PL emission.

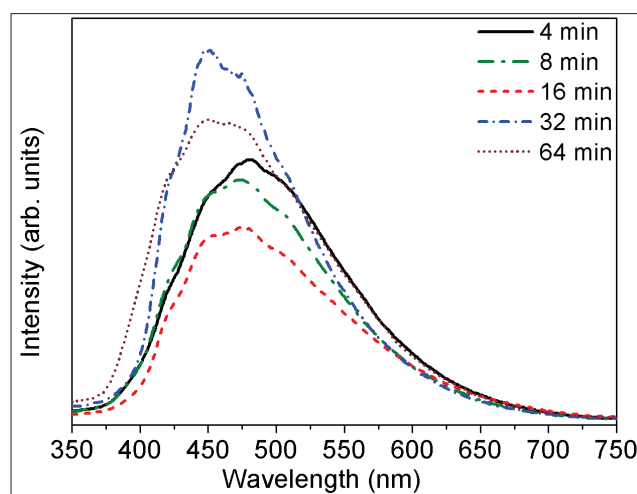
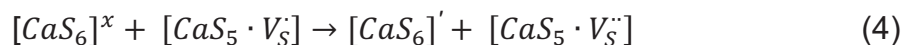
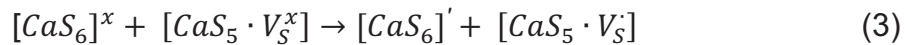


**Figure 7:** PL emission spectrum of CaS synthesized by MAS for different times.

First principles quantum mechanical calculations have shown that the break in lattice symmetry due to structural disorder is responsible for the presence of electronic states in the band gap and reveal that this disordered structure leads to local polarization and a charge gradient in the structure. New levels are formed above the valence band below the conduction band and are associated with specific CaS structural disorder [12-13, 47, 49].

The wide band model illustrated in Fig. 8(a) provides the three necessary steps for a PL emission to occur: (i) in the first step, the excitation source,  $h\nu$ , corresponds to the energy to promote a photon absorption from S 3p states at the valence up to Ca 3d states inside the forbidden band gap; (ii) after excitation, the recombination process occurs among the excited 3d states closer to the conduction band; and (iii) a wide band PL emission due to allowed 3d→3p transitions, associated with a multiple  $h\nu$  energy, can be measured.

During the excitation process, the cluster to cluster charge transfer in a crystal containing more than one kind of cluster is characterized by excitations involving electronic transitions from one cluster to another cluster. Here there are two types of coordination for Ca or S atoms. Sulfur vacancies in a disordered structure with  $[CaS_6']/[CaS_5V_S^Z]$  complex clusters are electron-trapping or hole trapping centers, according to the following equations:



where a  $[CaS_6]$  donor,  $[CaS_5 \cdot V_S']$  is a donor/acceptor and  $[CaS_5 \cdot V_S'']$  is an acceptor. It is assumed that charge redistribution may lead to electron-hole recombination of localized excitons. The structural and electronic reconstructions of all possible combinations of cluster belonging to a specific crystal are essential for the understanding of the complex cluster charge transfer (CCCT) process and its influences on the PL phenomenon [37]. This series of equations represents complex clusters in structural disordered solids and illustrates the sulfur vacancy occurrences that facilitate the interaction between interclusters.

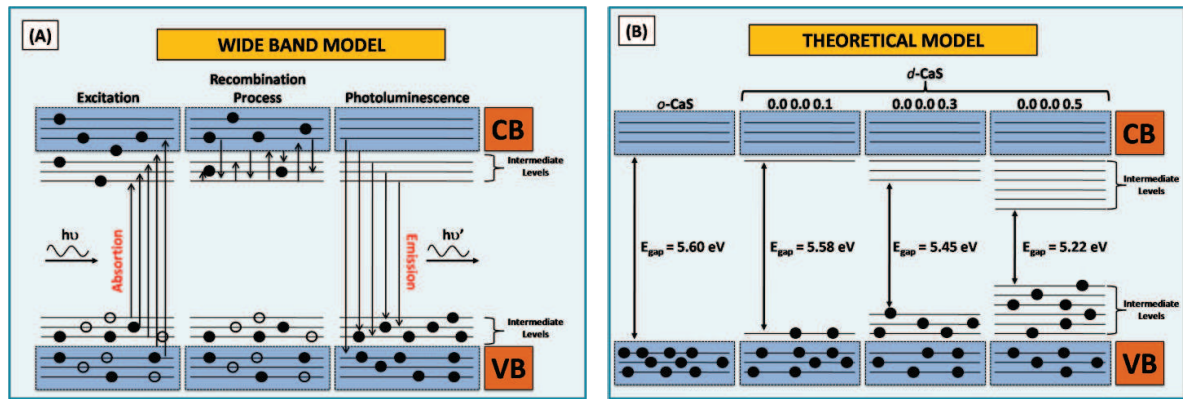


**Figure 8:** (a) Wide band model to illustrate the three steps of PL emissions and (b) theoretical model of CaS.

The theoretical model in Figure 7(b) it's based on wide band model to explain the creation of intermediate levels with decrease of band gap value. This model can be linked with the wide band model (Figure 7a) because the different kinds of defects changed the profile of the bands, creating new intermediate levels in the forbidden region.

Fig. 9 shows electron density maps for the CaS crystal along the exposed (100) plane. The contour plot reveals that bonding between Ca and S has an ionic bonding nature. It's observed that there is not isoline common between Ca and S atoms, namely, isoline that contour both atoms. The S atom displacement generated a difference in the charge density of the lattice as expected. By displacement of chemical bond CaS exists the formation of a hole-electron in the region surrounding the defect. The electron is self-trapped by sulfur and the hole is self-trapped by calcium, associated with the polaronic distortion. This fact it is pointed out when analyzing the atomic orbitals of the out when analyzing the atomic orbitals of the atoms localized in the region of the defect. These show that the electronic density is located in the X and Y orbitals (region of the electron) and the orbital w and x has lower density electronics (region of the hole). These displacements result in a kind of sulfur vacancies. Thus, more than one kind of cluster will exist in the structure, as  $[CaS_6]$  and  $[CaS_5 \cdot V_S^{\bullet\bullet}]$ .



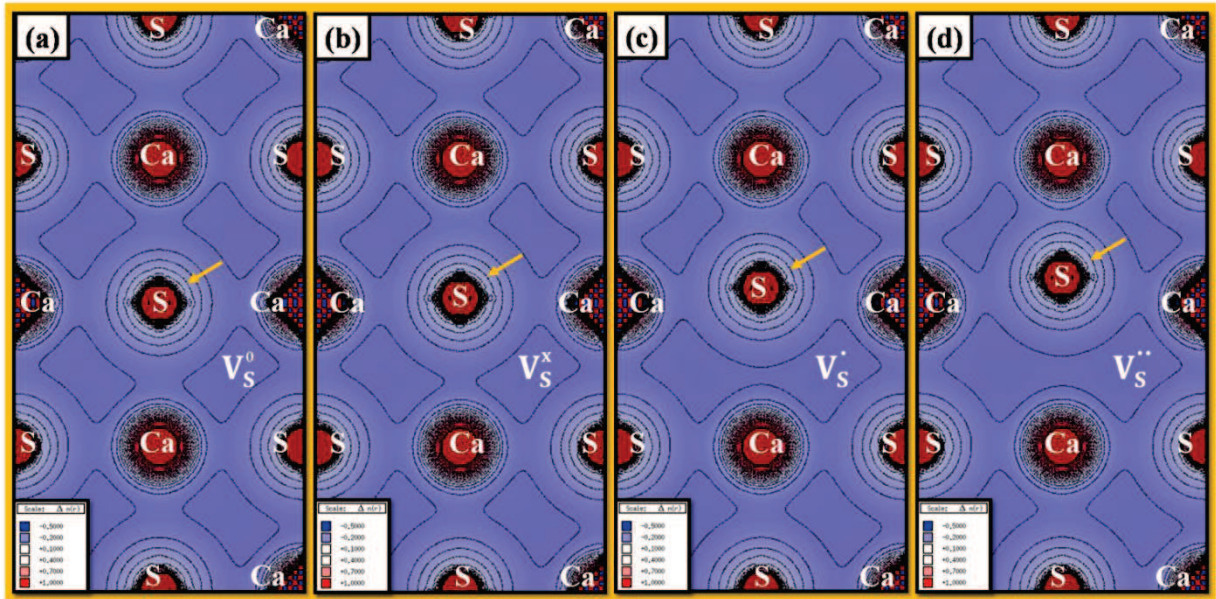


**Figure 9:** Electron density maps for the CaS crystal with vertical plane (100): *o*-CaS (a), *d*-CaS: (b) (0.0 0.0 0.1), (c) (0.0 0.0 0.3) and (d) (0.0 0.0 0.5).

It was found that annealing time and temperature played an important role in determining the photoluminescence properties of the nanoparticles. The nanoparticle prepared by microwave process has a high photoluminescence intensity achieved by annealing the nanoparticles. The better photoluminescence properties were obtained after 32 min of the synthesis. Varying annealing time the CaS nanoparticles some shifts in the photoluminescence spectra were observed, indicating that the emission wavelength of the nanoparticles could be adjusted by changing the time of the synthesis.

To discuss the PL profile of Fig. 7, the luminescence spectra are broken up into three peaks and each was fitted to a symmetric Gaussian function. Fig. 10 depicts the typical peak-resolution results, showing that three Gaussian curves constitute the overall luminescence in the visible region from approximately 350-650 nm.

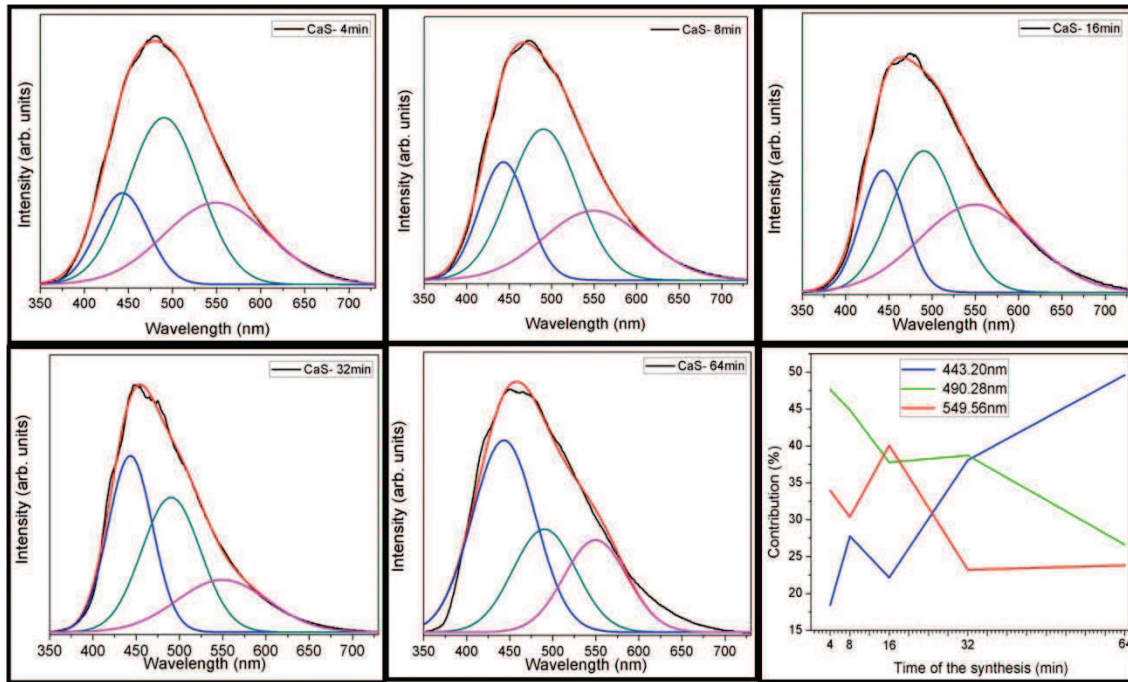


**Figure 10:** Deconvoluted PL bands in three curves, centered in 443 nm, 490 nm and 549 nm, and their contributions.

Fig. 10 shows the contribution of each deconvoluted curve and its variation. On deconvolution three curves were chosen to describe the emissions, 443 nm, 490 nm (blue components) and 549 nm (green component). In addition, in Fig. 10 the contribution of each of the above peaks as a function of time is presented. With the increase of time synthesis, the contribution of green region decreases and the blue region increases until 32 min. It was observed in the sample of 64 min a low shift to the red direction that can be related to the new defects created by the MAS method.

The contribution each peak measured by their corresponding area can be separated into three different behaviors. The peak correspondent for blue component (443 nm) increase from 18% to 50%, while the peak correspondent of the green component (549 nm) an opposite behavior is sensed, decreasing from 34% to 23%. The same behaviour occurs with the component blue (490 nm). Even that the estimated band gap by Wood-Tauc method did not show the same behavior in relation of the PL shift, it can not be used to explain all the electron transitions responsible by the wide luminescent band. As seen in the wide band theory, the distortions and defects generate modifications in the electronic states and provide the possibility of numerous decay transitions to the valence band. For this reason, the

result is a wide band of luminescence (contribution of a large amount of wavelengths) [37].

## Conclusions

In summary, CaS were successfully synthesized for the first time by the MAS method in low temperature and short time (4min). XRD patterns showed that the CaS crystals have a NaCl-type cubic structure with space group  $Fm\bar{3}m$ . FE-SEM images showed the formation of aggregated large crystal with different sizes and morphology. The different  $E_{gap}$  values were attributed to the existence of localized electronic levels within the forbidden band gap caused by defects in the structure. The theoretical calculation indicated that the band structures of all CaS models are characterized by direct electronic transitions. According to the TDOS and PDOS analyzes, the energy states in the VB is constituted from S (3p) orbitals, while in the CB is from Ca (3d) orbitals with a little contribution of S (3d) orbitals. Increasing time of synthesis until 32 min, there was a blue shift of the maximum PL emission that can be attributed to the structural organization. As seen in the theoretical results, the organized model (*o*-CaS) showed a higher band gap than the other (*d*-CaS) disorganized models that can be correlated with experimental results: increasing synthesis time there is an organization of the system.

## Acknowledgements

The authors are thankful for the financial support of Brazilian research financing institutions: CAPES, CNPq and FAPESP – 2010/19484-0, 2012/07967-1, 2012/22823-6 and 2012/14468-1.

## References

- (1) Lehmann, W.; Ryan, F. M. *Journal of the Electrochemical Society* **1971**, *118*, 477.
- (2) Sawada, N.; Chen, Y.; Isobe, T. *Journal of Alloys and Compounds* **2006**, *408*, 824.
- (3) Kumar, V.; Mishra, V.; Biggs, M. M.; Nagpure, I. M.; Ntwaeaborwa, O. M.; Terblans, J. J.; Swart, H. C. *Applied Surface Science* **2010**, *256*, 1720.
- (4) Bhatti, H. S.; Sharma, R.; Verma, N. K. *Journal of Modern Optics* **2006**, *53*, 2021.
- (5) Bhatti, H. S.; Sharma, R.; Verma, N. K. *Radiation Effects and Defects in Solids* **2006**, *161*, 113.
- (6) Adhikary, S.; Choubey, A.; Das, S.; Sharma, S. K.; Manam, J. *Journal of Alloys and Compounds* **2010**, *489*, 4.
- (7) Bhatti, H. S.; Singh, S.; Verma, N. K.; Kumar, S. *Indian Journal of Engineering and Materials Sciences* **2002**, *9*, 69.

- (8) Sweet, M. A. S.; Rennie, J. *Nuclear Instruments & Methods in Physics Research Section a-Accelerators Spectrometers Detectors and Associated Equipment* **1989**, 283, 330.
- (9) Wang, W. Z.; Germanenko, I.; El-Shall, M. S. *Chemistry of Materials* **2002**, 14, 3028.
- (10) Sharma, G.; Chawla, P.; Lochab, S. P.; Singh, N. *Chalcogenide Letters* **2009**, 6, 705.
- (11) Van Haecke, J. E.; Smet, P. F.; Poelman, D. *Journal of Luminescence* **2007**, 126, 508.
- (12) Kojima, Y.; Aoyagi, K.; Yasue, T. *Journal of Luminescence* **2007**, 126, 319.
- (13) Van Haecke, J. E.; Smet, P. F.; De Keyser, K.; Poelman, D. *Journal of the Electrochemical Society* **2007**, 154, J278.
- (14) Shaukat, A.; Saeed, Y.; Ikram, N.; Akbarzadeh, H. *The European Physical Journal B* **2008**, 62, 439.
- (15) Chen, Z. J.; Xiao, H. Y.; Zu, X. T. *Physica B: Condensed Matter* **2007**, 391, 193.
- (16) Yamamoto, T.; Kishimoto, S.; Iida, S. *Physica B-Condensed Matter* **2001**, 308, 916.
- (17) Ding, Z. F.; Quinn, B. M.; Haram, S. K.; Pell, L. E.; Korgel, B. A.; Bard, A. J. *Science* **2002**, 296, 1293.
- (18) Sun, B. Q.; Yi, G. S.; Chen, D. P.; Zhou, Y. X.; Cheng, J. *Journal of Materials Chemistry* **2002**, 12, 1194.
- (19) Liu, P. J.; Liu, Y. L. *Chinese Chemical Letters* **2000**, 11, 843.
- (20) Komarneni, S.; Roy, R.; Li, Q. H. *Materials Research Bulletin* **1992**, 27, 1393.
- (21) Volanti, D. P.; Keyson, D.; Cavalcante, L. S.; Simões, A. Z.; Joya, M. R.; Longo, E.; Varela, J. A.; Pizani, P. S.; Souza, A. G. *Journal of Alloys and Compounds* **2008**, 459, 537.
- (22) Moreira, M. r. L.; Andrés, J.; Varela, J. A.; Longo, E. *Crystal Growth & Design* **2008**, 9, 833.
- (23) Dovesi, R.; Saunders, V. R.; Roetti, C.; Orlando, R.; Zicovich-Wilson, C. M.; Pascale, F.; Civalleri, B.; Doll, K.; Harrison, N. M.; Bush, I. J.; D'Arco, P.; Llunell, M. *CRYSTAL09 User's Manual* Torino, 2009.
- (24) Beacke, A. D. *Journal of Chemical Physics* **1993**, 98, 5648.
- (25) Lee, C. T.; Yang, W. T.; Parr, R. G. *Physical Review B* **1988**, 37, 785.
- (26) Crystal [http://www.crystal.unito.it/Basis\\_Sets/Ptable.html](http://www.crystal.unito.it/Basis_Sets/Ptable.html).
- (27) Luo, H.; Greene, R. G.; Ghandehari, K.; Li, T.; Ruoff, A. L. *Physical Review B* **1994**, 50, 16232.
- (28) Wang, C. R.; Tang, K. B.; Yang, Q.; An, C. H.; Hai, B.; Shen, G. Z.; Qian, Y. T. *Chemical Physics Letters* **2002**, 351, 385.
- (29) Rietveld, H. M. *Journal of Applied Crystallography* **1969**, 2, 65.
- (30) Kubelka, P. *J. Opt. Soc. Am.* **1948**, 38, 448.
- (31) Myrick, M. L.; Simcock, M. N.; Baranowski, M.; Brooke, H.; Morgan, S. L.; McCutcheon, J. N. *Applied Spectroscopy Reviews* **2011**, 46, 140.
- (32) Smith, R. A. *Semiconductors* London, 1978.
- (33) Kaneko, Y.; Koda, T. *Journal of Crystal Growth* **1988**, 86, 72.
- (34) Jin, M. S.; Kim, N. O.; Kim, H. G.; Yoon, C. S.; Lee, C. I.; Kim, M. Y.; Kim, W. T. *Journal of the Korean Physical Society* **2001**, 39, 692.
- (35) de Santana, Y. V. B.; Raubach, C. W.; Ferrer, M. M.; La Porta, F.; Sambrano, J. R.; Longo, V. M.; Leite, E. R.; Longo, E. *Journal of Applied Physics* **2011**, 110.
- (36) Longo, V. M.; Gracia, L.; Stroppa, D. G.; Cavalcante, L. S.; Orlandi, M.; Ramirez, A. J.; Leite, E. R.; Andres, J.; Beltran, A.; Varela, J. A.; Longo, E. *Journal of Physical Chemistry C* **2011**, 115, 20113.

- (37) Jia, D. D.; Zhu, J.; Wu, B. Q. *Journal of the Electrochemical Society* **2000**, *147*, 386.
- (38) La Porta, F. A.; Ferrer, M. M.; de Santana, Y. V. B.; Raubach, C. W.; Longo, V. M.; Sambrano, J. R.; Longo, E.; Andres, J.; Li, M. S.; Varela, J. A. *Journal of Alloys and Compounds* **2013**, *556*, 153.
- (39) La Porta, F. A., Ferrer, M.M., Santana, Y.V.B., Raubach, C.W., Longo, V.M., ; Sambrano, J. R., Longo, E., Andrés, J., Li, M.S., Varela, J.A. *Current Phys. Chem.*, *in press*.

### 3. GENERAL CONCLUSIONS

The synthesis, characterization and application of the materials obtained are of great value in the framework of nanoscience. Control in obtaining the materials leads to huge variations in physical and chemical properties.

In summary, it was possible to obtain the CaS for the first time using the microwave-assisted solvothermal system, influencing the order and disorder of the system and creating intermediate states in the band gap, directly influencing the photoluminescent properties of this material. The same can be seen in obtaining zinc sulfide with capped and uncapped agent.

Studies have been performed on systems furnished by evaluating the surface and interface. Based on both experimental and theoretical findings, we propose a model where the driving force of this dynamic process is the order-disordered effects at intermediate range. In this way we are considering of the core and the shell are neutral and the same. They have relevance in terms of electronic structure. This effect can only appear when the intermediate range order-disorder between interfaces, as in this case, core and shell are present.

The theoretical model illustrates in a simple way as defect densities influence on the optical properties and Electronic, creating different intermediate levels in the band gap.

Particularly the case of the materials obtained. The system used in this work shows the range of possibilities for different synthetic materials, as well as the influence of this method in the photoluminescent properties and photocatalytic. Was possible through the system solvothermal assisted by microwave, control and optimize important parameters of synthesis, such as temperature and time.

## 4. REFERENCES

1. CUSHING, B. L.; KOLESNICHENKO, V.L., and O'CONNOR, C.J. "Recent advances in the liquid-phase syntheses of inorganic nanoparticles". Chem. Rev., **104**(9): 3893, 2004.
2. ROCO, M.C. "International strategy for nanotechnology research and development". J. Nanoparticle Res., **3**(5-6): 353, 2001.
3. ROCO, M.C. and BAINBRIDGE, W.S. "Societal implications of nanoscience and nanotechnology - Introduction. Societal Implications of Nanoscience and Nanotechnology", ed. M.C. Roco and W.S. Bainbridge, 2001.
4. CORMA, A.; REY, F.; RIUS, J. SABATER, M.J. and VALENCIA, S. "Supramolecular self-assembled molecules as organic directing agent for synthesis of zeolites". Nature, **431**(7006): 287, 2004.
5. MIZUTA, H. and ODA, S. "Bottom-up approach to silicon nanoelectronics". Microelectr. J. **39**(2): 171, 2008.
6. CALLISTER, W.D. "Materials science and engineering: an introduction". Ed. J.W. Sons., New York, 2007.
7. SINGH, J. "Electronic and optoelectronic properties of semiconductor structures". Ed. C. University, New York, 2003.
8. YANG, H.M.; HUANG, C.H.; LI, X.M.; SHI, R.R. and ZHANG, K. "Luminescent and photocatalytic properties of cadmium sulfide nanoparticles synthesized via microwave irradiation". Mater. Chem. Phys. **90**(1): 155, 2005.
9. JAYANTHI, K.C., S.; CHANDER, H. and HARANATH, D. "Structural, optical and Photoluminescence properties of ZnS: Cu nanoparticle thin films as a function of dopant concentration and quantum confinement effect". Cryst. Res. Technol. **42**(10): 976, 2007.
10. BISWAS, S.K. and KAR, S. "Fabrication of ZnS nanoparticles and nanorods with cubic and hexagonal crystal structures: a simple solvothermal approach". Nanotechnology **19**(4) 045710, 2008.
11. YAMAMOTO, T.; KISHIMOTO, S. and LIDA, S. "Control of valence states for ZnS by triple-codoping method". Phys. Rev. B. **308**: 916, 2001.
12. DE SANTANA, Y.V.B.; RAUBACH, C.R.; FERRER, M.M.; LA PORTA, F.; SAMBRANO, J.R.; LONGO, V.M.; LEITE, E.R. and LONGO, E. "Experimental and theoretical studies on the enhanced photoluminescence activity of zinc sulfide with a capping agent". J. Appl. Phys. **110**(12) 123507, 2011.
13. LA PORTA, F.A.; FERRER, M.M.; DE SANTANA, Y.V.B.; RAUBACH, C.R.; LONGO, V.M.; SAMBRANO, J.R.; ANDRES J.; LI, M.S.; VARELA, J.A.; LONGO, E. "Synthesis of wurtzite ZnS nanoparticles using the microwave assisted solvothermal method". J. Alloy. Compd. **556**: 153, 2013.
14. MURUGAN, A.V.; HENG, O.Y.; RAVI, V.; VISWANATH, A.K.; SAAMINATHAN, V. "Photoluminescence properties of nanocrystalline ZnS on nanoporous silicon". J. Mater. Sci. **41**(5) 1459, 2006.
15. CHEN, Z.J.; XIAO, H.Y. and ZU, X.T. "Structural and electronic properties of CaS Crystal: A density functional theory investigation". Phys. Rev. B **391**(1): 193, 2007.
16. JIN, M.S.; KIM, N.O.; KIM, H.G.; YOO, C.S.; LEE, C.I.; KIM, M.Y. and KIM, W.T. "Optical properties of undoped and Co<sup>2+</sup>-doped CaS, CaSe, BaS, and BaSe single crystals". J. Korean Phys. Soc. **39**(4) 692, 2001.

17. LUO, H.; GREENE, R.G.; GHANDEHARI, K.; LI, T. and RUOFF, A.L. "*Structural phase-transformations and the equations of state of calcium chalcogenides at high-pressure*". Phys. Rev. B, **50**(22): 16232, 1994.
18. KANEKO, Y.; MORIMOTO, K. and KODA, T. "*Optical properties of alkaline earth chalcogenides 2 vacuum ultraviolet reflection spectra in their synchrotron radiation region of 4-40 eV*". J. Phys. Soc. Jpn. **52**(12): 4385, 1983.
19. PHAMTHI, M. and RAVAUX, G. "*Calcium sulfide phosphors prepared by the flux method 1 growth parameters and luminescent efficiency*". J. Electrochem. Soc. **138**(4): 1103, 1991.
20. WANG, C.R.; TANG, K.B.; YANG, C.H.; AN, C.H.; HAI, B.; SHENG, G.Z. and QIAN, Y.T. "*Blue-light emission of nanocrystalline CaS and SrS synthesized via a solvothermal route*". Chem. Phys. Lett. **351**(5-6): 385, 2002.
21. SAWADA, N.; CHEN, Y. and ISOBE, T. "*Low-temperature synthesis and photoluminescence of IIA-VIB nano-phosphors doped with rare earth ions*". J. Alloy. Compd. **408**: 824, 2006.
22. GONG, X.; CHENG, W.J.; WU, P.F. and CHAN, W.K. "*Photoluminescence and upconversion optical properties of the CaS:Sm<sup>3+</sup> nanocrystallites*". Appl. Phys. Lett. **73**(20): 2875, 1998.
23. WU, S.Y.H.; TSENG, C.L. and LIN, F.H. "*A newly developed Fe-doped calcium sulfide nanoparticles with magnetic property for cancer hyperthermia*". J. Nanoparticle Res. **12**(4): 1173, 2010.
24. ADHIKARY, S.; CHOUBEY, A.; DAS, S.; SHARMA, S.K. and MANAM, J. "*Thermoluminescence investigations in X-ray irradiated CaS phosphor*". J. Alloy. Compd. **489**(1): 4, 2010.
25. SINEL'NIKOV, B.M.; KARGIN, N.I.; SAVEL'EV, V.A. and DANILOV, V.P. "*Thin film electroluminescent emitters based on calcium sulfide doped with cerium*". J. Appl. Spectrosc. **62**(3): 552, 1995.
26. BRADFORD, C.; O'DONNELL, C.B.; URBASZEK, B.; BALOCCHI, A.; PRIOR, K.A.; and CAVENETT, B.C. "*Growth of zinc blende MgS/ZnSe single quantum wells by molecular-beam epitaxy using ZnS as a sulphur source*". Appl. Phys. Lett. **76**(26): 3929, 2000.
27. PITALE, S.S.; SHARMA, S.K.; DUBEY, R.N.; QURESHI, M.S. and MALIK, M.M. "*TL and PL studies on defect assisted green luminescence from doped strontium sulfide phosphor*". J. Lumin. **128**(10): 1587, 2008.
28. FISCHER, L.B., "*Microwave Dissolution of Geologic Material - Application to Isotope-dilution Analysis*". Anal. Chem. **58**(1): 261, 1986.
29. KOMARNENI, S.; RAJHA, R.K. and KATSUKI, H. "*Microwave-hydrothermal processing of titanium dioxide*". Mater. Chem. Phys. **61**(1): 50, 1999.
30. HERRERO, M.A.; KREMSNER, J.M. and KAPPE, C.O. "*Nonthermal microwave effects revisited: On the importance of internal temperature monitoring and agitation in microwave chemistry*". J. Org. Chem. **73**(1): 36, 2008.
31. KAPPE, C.O. "*Controlled microwave heating in modern organic synthesis*". Angewandte Chemie-International Edition **43**(46): 6250, 2004.
32. DALLINGER, D. and KAPPE, C.O. "*Microwave-assisted synthesis in water as solvent*". Chem. Rev. **107**(6): 2563, 2007.
33. MILANEZ, K.D. "*Measurement of Photoluminescence*" New York: Academic Press, 1982.
34. SKOOG, D.A. HOLLER, F.J.; NIEMAN, T. A. "*Princípios de Análise Instrumental*". Bookman ed. Porto Alegre, 2002.



35. HU, B.; WU, L.H.; LIU, S.J.; YAO, H.J.; SHI, H.Y.; LI, G.P. and YU, S.H. "*Microwave-assisted synthesis of silver indium tungsten oxide mesocrystals and their selective photocatalytic properties*". Chem. Commun. **46**(13): 2277, 2010.
36. JING, P.T.; YUAN, X.; JI, W.Y.; IKEZAWA, M.; LIU, X.Y.; ZHANG, L.G.; ZHAO, J.L. and MASUMOTO, Y. "*Efficient energy transfer from hole transporting materials to CdSe-core CdS/ZnCdS/ZnS-multishell quantum dots in type II aligned blend films*". Appl. Phys. Lett. **99**(9) 093106 2011.
37. KAMAT, P.V. "*Manipulation of Charge Transfer Across Semiconductor Interface. A Criterion That Cannot Be Ignored in Photocatalyst Design*". J. Phys. Chem. Lett. **3**(5): 663, 2012.
38. WANG, L.; WEI, H.W.; FAN, Y.J.; LIU, X.Z. and ZHAN, J. H.; "*Synthesis, Optical Properties, and Photocatalytic Activity of One-Dimensional CdS@ZnS Core-Shell Nanocomposites*". Nanoscale Res. Lett. **4**(6): 558, 2009.
39. MA, R.; ZHOU, P.J.; ZHAN, H.J., CHEN, C. and HE, Y.N. "*Optimization of microwave-assisted synthesis of high-quality ZnSe/ZnS core/shell quantum dots using response surface methodology*". Opt. Commun. **291**: 476, 2013.
40. RAUBACH, C.W.; DE SANTANA, Y.V.B.; FERRER, M.M.; LONGO, V.M.; VARELA, J.A.; AVANSI, W.; BUZOLIN, P.G.C.; SAMBRANO, J.R. and LONGO, E "*Strutural and optical approach of CdS@ZnS core-shell system*". Chem. Phys. Lett. **536**: 96, 2012.
41. RAUBACH, C.W.; KROLOW, M.Z.; MESKO, M.F.; CAVA, S.; MOREIRA, M.L.; LONGO, E. and CARREÑO, N.L.V. "*Interfacial photoluminescence emission properties of core/shell Al<sub>2</sub>O<sub>3</sub>/ZrO<sub>2</sub>*". Crystengcomm **14**(2): 393, 2012.
42. SUN, A.K.; DONG, X.J.; WANG, X.Y.; DUAN, B. H. and WANG, D.Z. "*Synthesis of novel core-shell Cu@Mo nanoparticles with good sinterability*". J. Alloy. Compd. **555**: 6, 2013.
43. MAEDA, K. and DOMEN, K. "*Photocatalytic Water Splitting: Recent Progress and Future Challenges*". J. Phys. Chem. Lett. **1**(18): 2655, 2010.
44. CHEN, Z.J., XIAO, H.Y. and ZU, X.T. "*Structural and electronic properties of CaS Crystal: A density functional theory investigation*". Phys. B **391**(1): 193, 2007.